



Chair of Drilling and Completion Engineering

Master's Thesis



Conceptual Design of Drilling Cuttings  
Analysis System Based on Machine Learning  
Techniques

Pavel Iastrebov

July 2020



*Dedicated to my mother.*



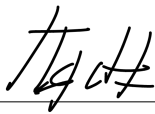
**AFFIDAVIT**

I declare on oath that I wrote this thesis independently, did not use other than the specified sources and aids, and did not otherwise use any unauthorized aids.

I declare that I have read, understood, and complied with the guidelines of the senate of the Montanuniversität Leoben for "Good Scientific Practice".

Furthermore, I declare that the electronic and printed version of the submitted thesis are identical, both, formally and with regard to content.

Date 08.07.2020



---

Signature Author  
Pavel, Iastrebov



# Abstract

Analyzing return cuttings during drilling is one of the opportunities, besides core analysis, to observe and characterize the drilled rock. It gives real time information needed for bit depth correction and lithology correlation, such as rock type, color, texture (grain size, shape and sorting), cement amount, fossils presence, porosity and permeability. Correct measurements of those parameters (shape and size distribution in particular) improves the drilling performance and anticipates possible problems and complications. Cuttings and cavings presence in annular space increase the Equivalent Circulating Density (ECD), which leads to higher pressure losses; they are also one of the causes of Rate of Penetration (ROP) reduction because of chip hold down effect. Their shape is the inference for probable causes of borehole instability and quality of the mud cake.

Several techniques have been used in last decades for obtaining the return cuttings parameters, such as their relative amount, particle size distribution (PSD), size and shape. They comprise state of the art technology based on computer vision techniques with machine learning algorithms as a software. A number of such techniques is already available on the market, and have their limitations and advantages. Basing on this principle, OMV is planning to build in house intelligent and cost-effective system which is capable of determining the cuttings parameters in real time. The built system should be feasible from the point of proactive problem prevention, reduction of Non-productive Time (NPT) by well complications mitigation and simplification of tedious mud-logger labor.

After carefully reviewing and studying the shortcomings of the recent techniques regarding cavings analysis, a conceptual design of automated cavings analysis technology is proposed in this thesis. The system is split into hardware and software parts. The first part includes circulation system for washing the cavings, as well as the camera and lightning facility. The camera is connected to the laptop with running software in the background, which is based on the Convolutional Neural Network (CNN). This algorithm analyzes the captured frames and delivers cavings' shape, size and lithology as an output. Furthermore, feasibility study is conducted, in which rough costs of the proposed system are estimated.





# Zusammenfassung

Die Analyse von Bohrschlamm während der Bohrung, abgesehen von der Kernanalyse, ist eine der Möglichkeiten, die gebohrte Gesteine zu beobachten und zu charakterisieren. Es liefert Echtzeitinformation, wie Gesteinstyp, Farbe, Textur (Korngröße, Form und Sortierung), Zementmenge, Vorhandensein von Fossilien, Porosität und Permeabilität, die für die Meißeltiefekorrektur und die Lithologiekorrelation benötigt wird. Die korrekte Parametermessung (bzw. Form und Größenverteilung) verbessert die Bohrleistung und vorbeugt mögliche Probleme und Komplikationen. Das Vorhandensein von Bohrschlamm und Auskesslungen im Ringraum erhöht die äquivalente Zirkulationsdichte, was zu höheren Druckverlusten führt. Sie sind auch eine der Ursachen für die Reduzierung der Bohrgeschwindigkeit wegen des Chip-Hold-Down-Effekts. Ihre Form ist die Voraussetzung für wahrscheinliche Ursachen der Bohrlochinstabilität und der Qualität der Filterkruste.

In den letzten Jahrzehnten verschiedene Techniken wurden verwendet, um die Bohrschlammparameter zu erhalten, wie z. B. ihre relative Menge, Partikelgrößenverteilung, Größe und Form. Sie umfassen modernste Technologien, die auf Computer-Vision-Technologie mit Algorithmen für maschinelles Lernen als Software basieren. Eine Reihe Anzahl solcher Techniken ist bereits auf dem Markt erhältlich und hat ihre Begrenzungen und Vorteile. Basierend auf diesem Prinzip, plant OMV den Bau eines eigenen intelligenten und kostengünstigen Systems, mit dem die Bohrschlammparameter in Echtzeit ermittelt werden können. Das gebaute System sollte unter dem Gesichtspunkt der proaktiven Problemverhütung, der Reduzierung der unproduktiven Zeit durch Verhinderung von Bohrlochkomplaktionen und der Vereinfachung mühevoller Arbeit des Feldgeologs machbar sein.

Nach sorgfältiger Prüfung und Untersuchung der Mängel der jüngsten Technologien in Bezug auf die Auskesslunganalyse, wird in dieser Arbeit ein Konzeptentwurf für die Technologie der automatisierten Auskesslunganalyse vorgeschlagen. Das System ist in Hardware- und Softwareteile unterteilt. Der erste Teil umfasst ein Zirkulationssystem zum Waschen der Auskesslungen sowie die Kamera- und Blitzeinrichtung. Die Kamera wird an den Laptop mit laufender Software im Hintergrund angeschlossen. Die Software ist auf dem Convolutional Neural Network (CNN) basiert. Dieser Algorithmus analysiert die erfassten Bilder und liefert die Form, Größe und Lithologie der Auskesslungen als Ausgabe. Darüber hinaus wird eine Machbarkeitsstudie durchgeführt, in der ein Etwapreis des vorgeschlagenen Systems geschätzt wird.



# Acknowledgements

I would firstly like to thank my university thesis advisors Dipl.-Ing. B.Sc. Asad Elmgerbi and Ass. Prof., Candidate of Technical Sciences, Alexey Arhipov for their invaluable help in my research and comprehensive guidance. In addition, Univ.-Prof. Mikhail Gelfgat faced the most of the difficulties in organizing our study and helped us to accomplish the double-degree program, what I am grateful for either.

I would like to thank OMV Exploration & Production GmbH including:

Senior Vice President Exploration, Development & Production OMV Upstream Christopher Veit for such great opportunity of getting a scholarship;

Drilling Engineer at OMV Exploration & Production, M.Sc. Richard Kucs for constant supervision during thesis writing and assistance in developing a concept;

Head of Exploration Ventures at OMV Exploration & Production, M.Sc. Ph.D., my mentor Peter Krois for directing me in a right way and exciting the curiosity of geology;

Sr Reservoir Engineer at OMV Exploration & Production, M.Eng. MBA Daniel Kunaver for showing the robustness of coding in Python;

Expert Talent Pipeline at OMV AG Bernhard Ebinger and Senior Expert Learning & Development at OMV AG Rafael Tomososchi for the help in my internship organization.

I would like to thank my friends who I studied with for their joy and fellowship: Timur Berdiev, Polina Gamayunova, Aleksandr Geraskin, Rostislav Gupalov, Shamkhal Mammadov, Aleksey Olkhovikov and Kseniia Frolova.

Special thanks to Anna, Daniil and Vladislav for helping me to land on my own moon.

Finally, I am expressing the appreciation to my parents for granting me the gift of life. You are the most valuable people to me.



# Contents

Chapter 1 Introduction .....	1
1.1 Overview .....	1
1.2 Motivation .....	2
1.3 Objectives .....	4
1.4 Thesis Structure .....	4
Chapter 2 Borehole Instability Signs During Drilling .....	7
2.1 Borehole Instability Mechanisms .....	7
2.2 Cavings Morphology .....	10
2.3 Cavings Comparative Matrix .....	14
Chapter 3 Cuttings Analysis Techniques .....	17
3.1 Standard Method .....	17
3.1.1 Cuttings Collection .....	17
3.1.2 Cleaning and Packing .....	19
3.1.3 Analysis .....	21
3.1.3.1 Sieve Analysis .....	21
3.1.3.2 Laser Diffraction .....	22
3.1.3.3 Optical Microscopy and Image Analysis .....	23
3.1.3.4 Focused Beam Reflectance Measurement .....	24
3.1.3.5 Ultrasonic Extinction .....	24
3.1.3.6 X-ray Fluorescence .....	25
3.1.3.7 X-ray Diffraction .....	26
3.1.4 Shortcomings (Standard Method) .....	27
3.2 Automated Measurement Tools .....	30
3.2.1 Cuttings Flow Meter .....	30
3.2.2 Computer-Based Techniques .....	31
3.2.2.1 2D Machine Vision .....	31
3.2.2.2 Stereo Vision .....	33
3.2.2.3 Structured Light .....	34
3.2.2.4 Time-of-Flight .....	35
3.2.3 Shortcomings (Automated Method) .....	37
3.3 Field Application of Automated Methods .....	38
3.3.1 Schlumberger CLEAR Service .....	38
3.3.2 Device for Measuring PSD and Cuttings Analysis .....	39
3.3.3 Intelligent System for Cuttings Concentration Analysis .....	40
3.3.4 Classifying Cuttings Volume via Video Streaming .....	42
3.3.5 Cuttings Shape Acquisition Using 3D Point Cloud Data .....	43
3.3.7 Rock Classification with a Deep Convolutional Network .....	47
3.3.8 Comparison Summary .....	49
Chapter 4 Convolutional Artificial Neural Network .....	53

4.1 Simplest Artificial Neural Network .....	53
4.2 Training, Validation, and Testing.....	55
4.2.1 Training.....	55
4.2.2 Validation.....	57
4.2.3 Testing and Splitting the Dataset .....	57
4.3 Convolutional Artificial Neural Network .....	58
4.3.1 Input Layer .....	58
4.3.2 Conv Layer .....	59
4.3.3 ReLU Layer.....	61
4.3.4 Pool Layer .....	62
4.3.5 FC and Softmax Layers .....	63
Chapter 5 Conceptual Design of the Proposed Technology .....	65
5.1 Overview .....	65
5.2 Hardware and equipment .....	66
5.2.1 Shale Shaker Modification.....	67
5.2.1.1 Tray.....	69
5.2.1.2 Collector Pipe and Hoses .....	69
5.2.1.3 Filter.....	69
5.2.1.4 Pump .....	69
5.2.1.5 Sprinkler Head.....	70
5.2.2 Camera Design And Placement.....	70
5.2.3 Light Source.....	77
5.2.4 Cover .....	79
5.3 Software.....	79
5.3.1 Network Building.....	79
5.3.2 Algorithm Workflow.....	80
5.3.3 Decision Support Matrix.....	82
5.4 Cost Estimation for Proposed System.....	83
5.5 Limitations .....	86
Chapter 6 Conclusion and Recommendations.....	89
6.1 Conclusion.....	89
6.2 Recommendations and Future Work .....	90
Appendix A Cuttings description parameters.....	91
A.1 Shape.....	91
A.2 Roundness and Sphericity .....	92
A.3 Colour .....	93

# Chapter 1 Introduction

## 1.1 Overview

Borehole stability issues are one of the main problems, which occur frequently during the well construction process. This happens due to mechanical failure of the rock, caused by stresses reorientation, as well as improper mud weight selection. Most of the time these complications are followed by rock cracking and moving towards the centre of the borehole or falling down the bottom hole. This might lead to a series of costly issues such as pipe sticking, low ROP, or poor cement job. In this context, drilling cuttings and cavings monitoring are crucial for proactive detection and mitigating wellbore instability, which is one of the main contributors in non-productive time. Cavings' size and shape basically demonstrate the circumstances, under which they were formed. It means that cuttings are the first piece of information, which gives the crew essential knowledge about what is actually happening during drilling. The main aim, which is to be achieved, is the reduction of NPT, caused by possible stuck pipe events, and consequent cost reduction by saving on fishing services and rig rent time.

The most widely spread method of cuttings analysis is the conventional technique, which is completely manual, utilizing human labour. As a rule, the cuttings are collected every hour, packed, and sent to the wellsite laboratory for the measurement and analysis. The resulting report contains the complete description of the collected sample, including rock type, size, and texture.

As long as the conventional analysis is time-consuming, a series of automated approaches have been invented. One of them is Cuttings Flow Meter (CFM), which determines the mass of incoming cuttings. The main benefit of this system is that it is fully automated and has very high accuracy due to its simplicity. However, it does not analyze any other parameters. Another well-known technique is image analysis. The overall concept resides in placing the camera at the shale shakers and utilizing software, which would analyze the video frames and deliver the desired properties. Related installations were designed to determine cuttings volume, Particle Size Distribution (PSD), and shape profile.

Unfortunately, the considered methods do not give evidence of possible complications. For that reason, there is a demand for another technique proposal, which could notify about possible borehole instability events, having cuttings information as an input.

Machine learning techniques, which are already available on the market, show their strength in comparison with other algorithms. Their benefit is a diversity of parameters, which could be extracted from the analysis. It is possible because such methods can not only conduct calculations but also classify the objects by referring them to a set of pre-determined classes. In this case, each of the objects is inspected individually. By assigning a number of classes within one category to the set of objects in advance (e.g. different kinds of shapes), the machine learns to extract certain features from it. Basing on the results of the learning phase, the machine can independently label the object

during the testing phase. In addition, the algorithm is able to determine the location of the object in a frame, giving the evidence of its accuracy.

## 1.2 Motivation

Statistics study related to the root causes of the NPT events faced by OMV during the year of 2019 was conducted. Such events were broken down depending on the root cause and illustrated with a pie chart in Figure 1.

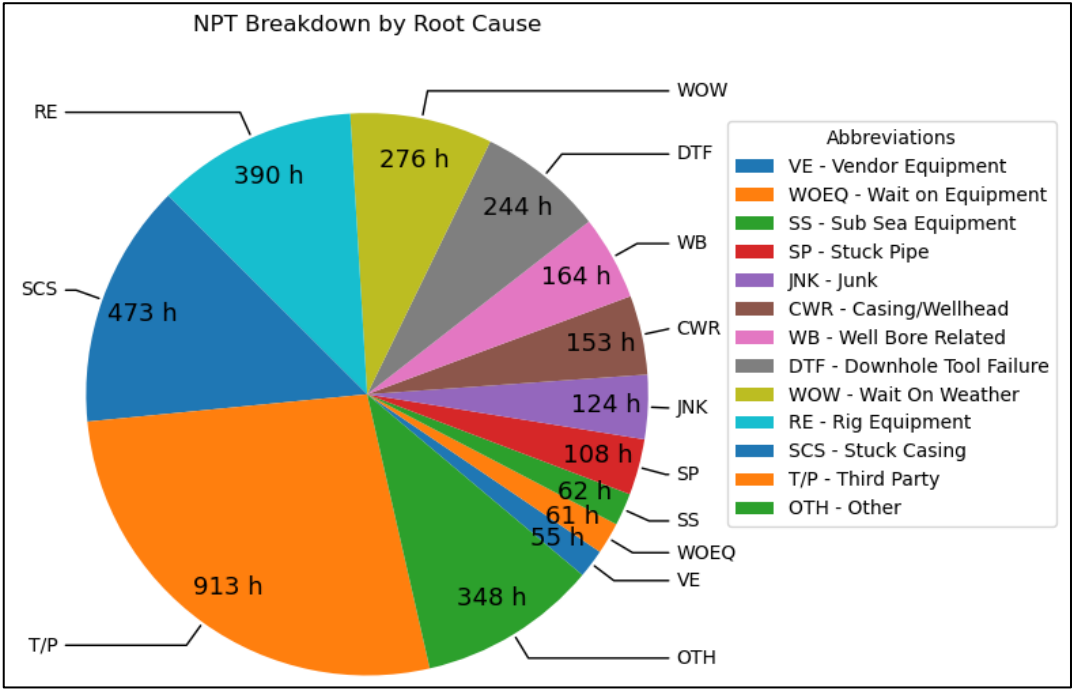


Figure 1: NPT Breakdown by Root Cause

Due to the fact that the scope of the thesis is focusing mainly on the NPT caused by borehole stability issues, the data concerning these problems was extracted for further analysis. These are (in codes): SCS, WB, and SP. The stuck casing is a special case, so it will be discussed separately. The total amount of NPT for these three cases is listed in Table 1. "Number of wells" column accommodates wells, which were reported to have specified complications.

Table 1: Total NPT For the Considered Cases

Case	NPT, hours	Number of wells
Stuck Casing (SCS)	473	1
Wellbore related	164	3
Stuck pipe	108	1

With regard to wellbore related issues, there was no information about the cause of each of the complications in the supplied data. So, it is very hard to infer, if the event was actually caused by borehole instability, which might be detected with the help of cuttings analysis, or by other causes. It is a complicated case with stuck pipes, as differential sticking or key seating can also contribute to the occurrence of this problem. Importantly,



stuck pipe and casing issues happened in the same well deep multi-lateral well with two completions. In one of the laterals, there were 108 hours of stuck pipe complications in total, followed by 330 hours of stuck casing events. In another lateral, there were 143 hours of total NPT dedicated to the stuck casing. As long as the well is specified as a deep well, there definitely should be narrow mud windows. That makes the mud program more sophisticated and more sensitive to pressure changes, which affects the likelihood of complications occurring. In addition, there were stuck pipe events only during drilling operations of the first lateral, while the second was safe.

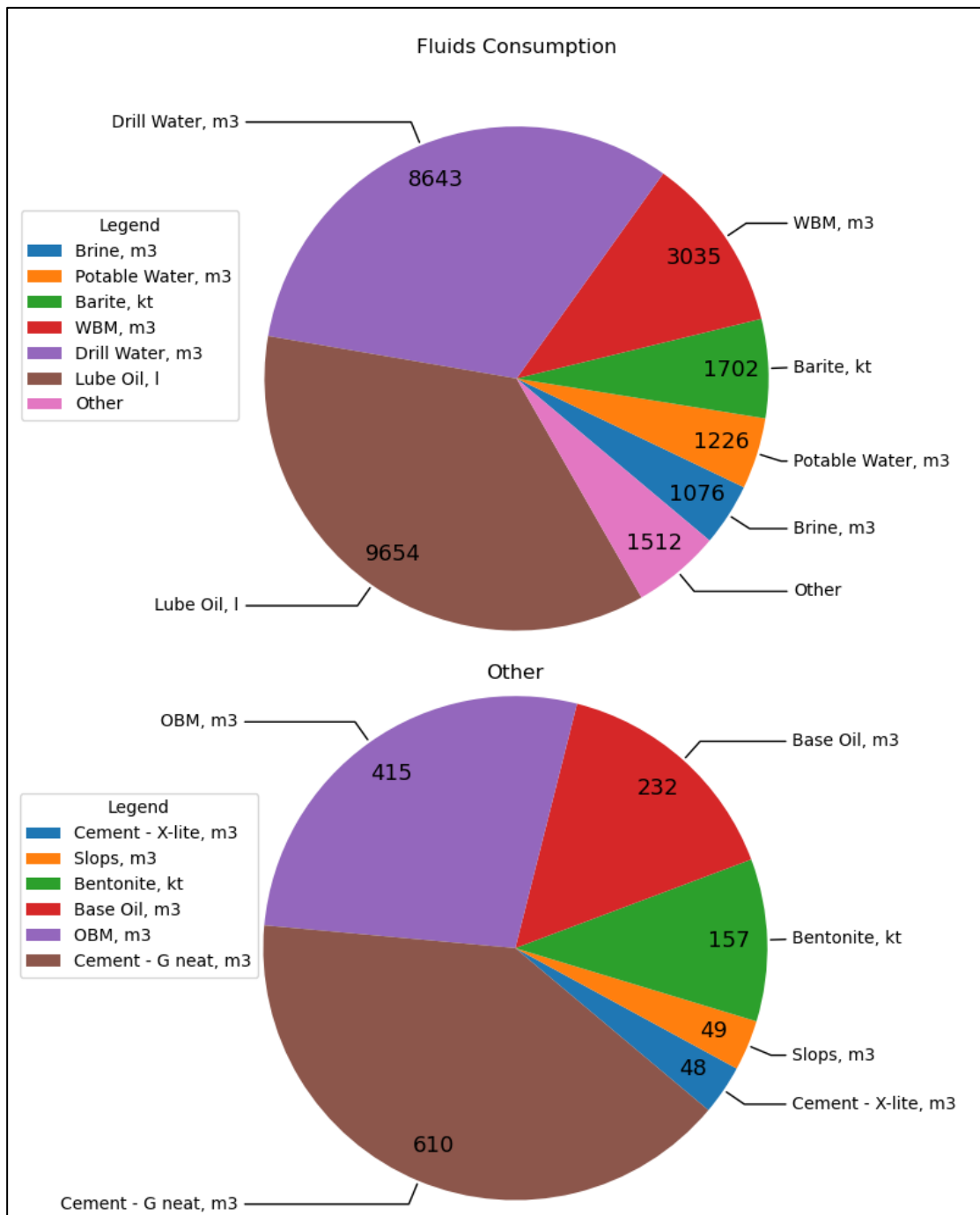


Figure 2: Reported Consumption of Fluids and Additives In 2019 By OMV

There was also another report supplied, which gives information on fluids and additives consumption (Figure 2). There are no fuels specified, as they are not the point of interest in this thesis. As it is seen, the amount of barite occupies a relatively large part after lube oil, drill water, and water-based mud, which makes it the most frequently used additive in the mud. The majority of bentonite was spent on drilling an offshore well in Norway. However, there was also a report for large bentonite consumption for deep multilateral well discussed earlier. If there was a need for mud weighing up, then there is a higher probability of borehole stability issues occurring.

Having the reported data considered, there is a certain need in designing a cost-effective system, which would give notifications and warnings about borehole instability event occurrence in order to avoid the mentioned complications, like stuck pipe or casing in particular.

### 1.3 Objectives

The prime goal of this thesis is to deliver a comprehensive methodology that covers the design of an integrated system that is capable of determining the cavings size and conducting the analysis in real-time.

In to reach this aim, the following objectives have to be achieved:

- To review all possible complications, occurring in the wellbore and provide a link to the formation of cavings in these conditions
- To study the conventional cuttings analysis workflow to find the existing weaknesses in the existing technique. This is intended to make a foundation for improvements
- To study the state of the art technologies of visual data recognition and select the best applicable one for the considered case
- To deliver an inexpensive, robust, and multitasking algorithm, which will not disturb an already established process of mud treatment and solids control. Apart from that, the algorithm is to work in real-time and with minimal delay, liberating the employee from the repetitive and tedious job

### 1.4 Thesis Structure

A literature review of borehole instability issues was conducted, the cavings are described according to their shapes and sizes. A link between cavings and actual complications is provided. This establishes a base for the suggested recommendation system, which would give the mud logger sequence of actions to be taken.

The general workflow for cuttings and cavings acquisition and analysis is discussed, giving the foundation for automated system development. Several approaches were discussed: conventional and automated. Manual techniques include a wide range of tools for cuttings and particle analysis. Automated technologies are discussed not only from the drilling perspective but also from an automation point of view in general. These mostly include computer vision systems. All the techniques were summed up and considered from their strong points and disadvantages. This helped to choose a single

technology to focus on. This chosen technique was two-dimensional computer vision thanks to inexpensiveness, simplicity, and a variety of possible parameters to determine.

The essence of artificial neural networks was discussed, as well as their features, architecture, and working principle. Convolutional neural networks are used as a central part of the proposed software system, which will take video frames as an input, filtering them out, and taking out features like colour patterns, edges, etc.

The proposed solution based on state-of-the-art technology is described. The description is split into two parts: describing hardware devices and equipment, which actually acquire data from shaker screens. In addition, software workflow is also suggested and discussed, giving the blueprint for the developers to write the code and link the software with the camera. Apart from that, the cost assessment study is conducted, giving the estimation of technology costs using a probabilistic approach.



# Chapter 2 Borehole Instability Signs During Drilling

Borehole instability is a notable example of how to yield the drilling process into dire straits. Such complications account for up to 40% of rig downtime and for nearly 25% of drilling costs (Gallant, et al. 2007). Having such high percentages of time and budget losses, instability-related NPT seriously jeopardizes the project economics and therefore is desired to be reduced or avoided.

Borehole instabilities occur due to the creation of a wellbore by collapsing some portion of the rock in the formation. As a result, the existing stresses are being reoriented, and a stable formation loses its support. If the stability is not maintained, the stresses might overcome rock strength and cause the borehole collapse or fracturing, these events are often followed by the formation of crushed rock in the zones of excessive stress. As long as the rock loses its integrity, it is broken off the borehole wall easily, either falling down in the wellbore or being transported to the surface. Depending on the issue, these rocks (or cavings) might have different shapes, which provide a link between the caving morphology and the mechanism of its generation.

In this case, cavings, which are the first physical and valid material information, allow us to relatively quickly analyze the current state of the wellbore condition and react proactively on possible complications. Cavings are typically produced due to several causes, such as underbalanced drilling, stress relief, pre-existing planes of weakness, or as a response to an action of drilling tools (Kumar, et al. 2012).

In this chapter various types of borehole instabilities are discussed, the cavings are described according to their shapes and sizes and a link between them is provided, establishing causal relationships for recommending remedial actions to be taken.

## 2.1 Borehole Instability Mechanisms

Encountered wellbore instability events could be classified depending on the existing conditions as following:

- Hole closure
- Hole enlargement
- Fracturing

Each of the mechanisms will be described thereunder considering associated consequences and resulting problems.

**Hole closure** is a time-dependent process, which is referred to as swelling shale layers and creeping salt formations. Shales lose their stability because of acquiring water from the drilling mud, resulting in an increase of the rock volume. At some point, shales cannot hold more water, so that their strength decreases, and they begin to slough, falling inside the borehole. Salts, in contrast, creep under other circumstances. This rock cannot withstand shear stresses (on a reservoir scale) and are similar to a very viscous

## Borehole Instability Signs During Drilling

liquid. Under the overburden stress, such mobile formations behave in a plastic manner, establishing deformation under pressure. In both cases, unstable rock might either decrease the cross-section of the wellbore or fall inside the well. It happens, as the mud weight is not high enough to withstand the formation squeezing into the wellbore (Bowes and Procter 1997). The associated problems are:

- Torque and drag increase
- Stuck pipe events
- Troubles running casing

**Hole enlargement** issues could be separated into two categories: **breakouts** and **washouts**. **Breakouts** are the result of surrounding the wellbore stresses exceeding the rock strength. In this case, the wellbore wall is subjected to shear failure, which forms zones of crushed rock in the direction of the least horizontal stress (in a vertical wellbore). Breakouts might grow during the good drilling process, but they only deepen into the formation, as illustrated in Figure 3. **Washouts** are a possible consequence of breakouts due to incorrectly selected mud weight. Drilling fluid would leak into pre-existing or drilling-induced cracks and cause further propagation of shear failure. As a result, the formation produces extra cavings around the wellbore, increasing cross-section. Therefore, mud velocity in the annulus decreases and the mud system is unable to circulate the excessive amount of cavings. The difference between breakout and washout is schematically drawn in Figure 4.

As a rule, this type of instability usually occurs in unconsolidated formations, overpressured shales, and naturally fractured rock. This results in:

- Cavings sticking to the BHA
- Cuttings bed
- Mechanical erosion
- An increased volume of required cement and the overall difficulty of cementing job
- The necessity of changing mud weight

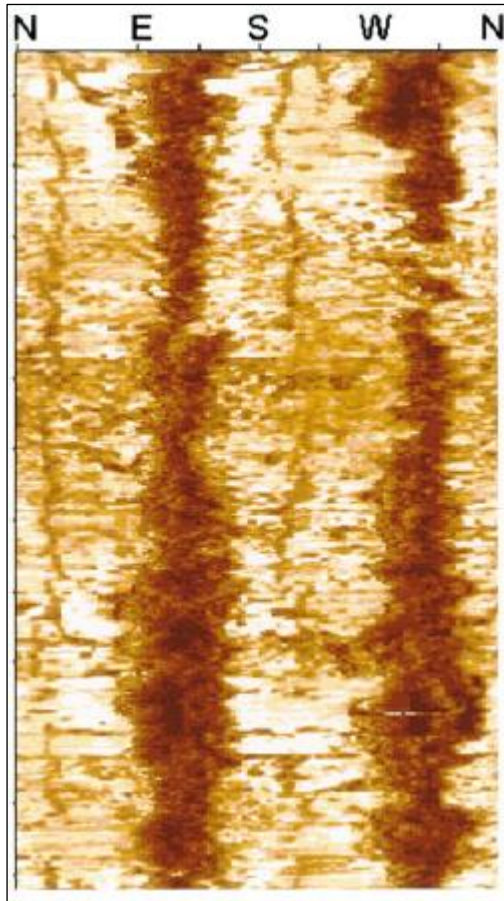


Figure 3: Televiwer Image Logs of a Well With Wellbore Breakouts (Dark Paths in South-East and North-West Directions) (Zoback, Barton, et al. 2003)

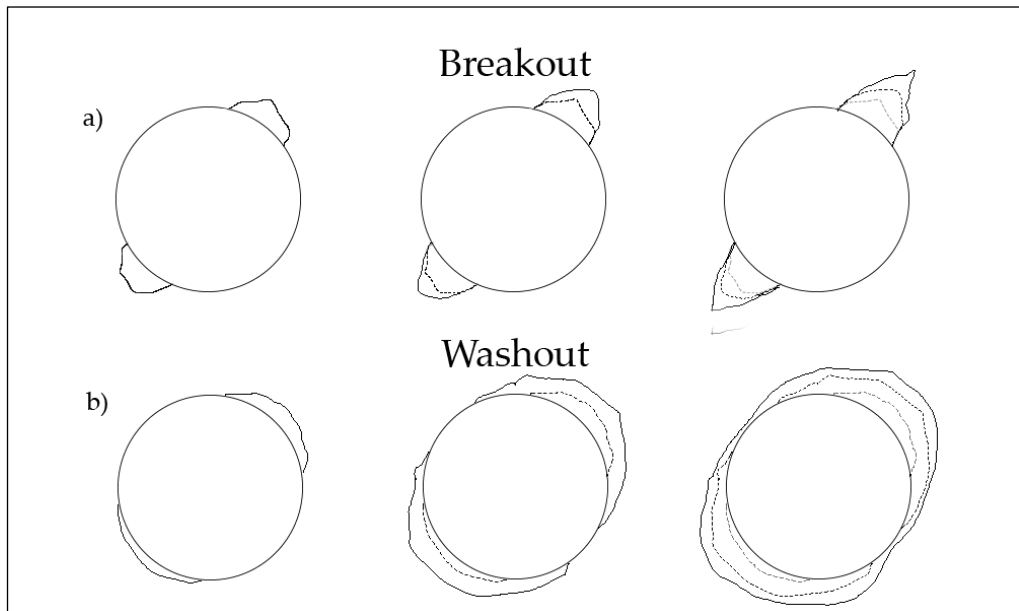


Figure 4: (a) Breakout, Showing Growth Deeper Inside the Formation. (b) Washout Grows All Around the Wellbore, Increasing Its Instability (modified after M. Zoback 2007)

**Fracturing** occurs when the wellbore hydrostatic pressure exceeds the least principal stress at a certain depth, developing either in a form of consistent fracture or echelons of fractures. Being the result of the tensile failure, those fractures are different from those, which are formed during shear failure. The main feature of fracturing by exceeding the least principal stress is the absence of cavings in the return flow. This leads to:

- Wellbore ballooning effects
- Lost circulation

In the scope of this thesis, only the first two of the complications will be considered. For that purpose, it is needed to focus on different cavings types, shapes, and sizes.

## 2.2 Cavings Morphology

Cavings, unlike cuttings, are the fragments of the rock, which appear on the shale shaker screens, and are usually two to three times larger, having odd shapes. They are produced not from the destroyed rock by the bit action, but from the borehole wall. It is important that cavings have practically no value in lithology understanding, as the borehole instability might occur at any time during drilling. Thus, cuttings are mainly analyzed for formation evaluation and hydrocarbon content estimation, whereas cavings are crucial for shape and size determination. Here is to define, which cavings shapes generally exist, and what are their size ranges.

Cavings morphology exhibits several types of them, depending on their shape, size and lithology. Depending on their origin, they can be split into the following types (Skea, et al. 2018):

- Angular
- Tabular
- Splintery
- Blocky

**Angular** cavings form by using a low-density mud by combination with low compressive strength and high hoop stress, creating a shear failure in the wellbore. These cavings could be described as arrowhead or triangular-shaped with a rough surface. Such caving is shown in Figure 5.





Figure 5: Example of an Angular Caving (Bradford, et al. 2000)

**Tabular** cavings are produced by the invasion of the drilling mud into the fractured formation or rock bedding surfaces, which results in mud losses, borehole enlargement, and possible stuck pipe events. In wells with  $15^{\circ}$ - $20^{\circ}$  deviation from bedding planes such cavings are formed as a result of low mud weight selection (Bradford, et al. 2000). A picture of tabular caving is in Figure 6. If the inclination angle is low relative to the dip angle of bedding planes, large tabular cavings (up to 20 cm) might be seen, as presented in Figure 7.



Figure 6: Example of a Tabular Caving. The Flat Surface of Bedding Plane Is Visible (Kristiansen 2004)



Figure 7: Large Tabular Caving Formed as a Result of Failure Along the Bedding Plane (Gallant, et al. 2007)

**Blocky** cavings are quite similar to tabular ones, as they are produced from weak bedding or fracture environments. However, blocky cavings tend to be formed in vertical wells with spread fracture network by mud invasion. This is usually the deal when drilling is executed in the faulting environment. One of the effects is lost circulation. Not lowering the mud weight would result in opening the fractures' aperture, liberating blocky cavings from the fault zone (Kristiansen 2004). An example is in Figure 8.

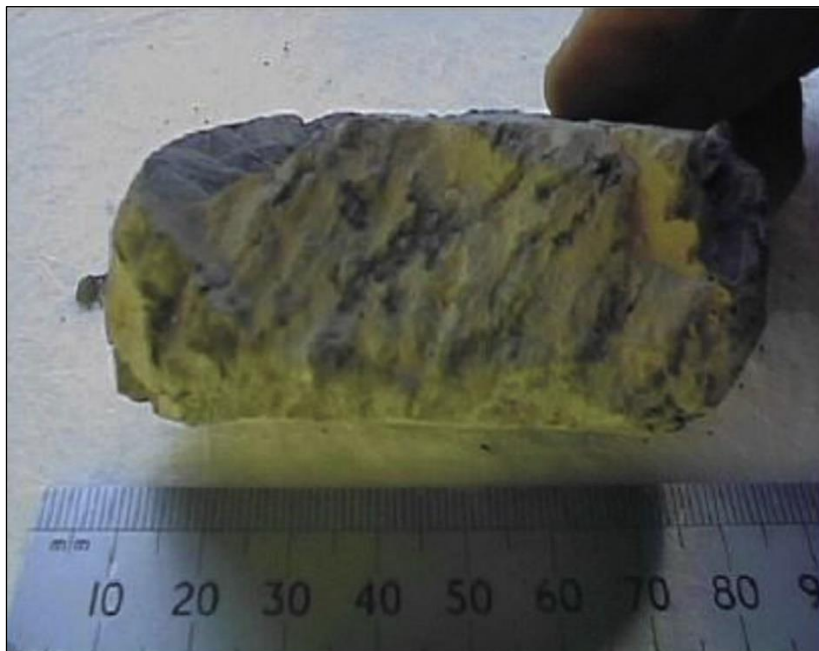


Figure 8: Example of a Blocky Caving from a Naturally Fractured Reservoir (Aldred, et al. 1999)

**Splintery** cavings are produced from the overpressured zones, where tensile fractures tend to form (Figure 9). They usually occur in tectonically active regions, where significant stresses are present. Here the rock is being compressed or stretched due to movement of the Earth's crust (Pašić, Gaurina-Međimurec and Matanović 2007). When a hole is drilled in an area of high tectonic stresses the rock around the wellbore will collapse into the wellbore and produce splintery cavings. In high-stress concentration cases, the pressure required to stabilize the wellbore might be higher than the fracture gradient. This usually occurs near mountainous regions. In this case, the formation is to be cased as quickly as possible (Bowes and Procter 1997).



Figure 9: Example of a Splintery Caving (Kumar, et al. 2012)

Borehole instabilities are often followed by cuttings and cavings accumulation in the well, especially if the well is inclined. In the last case, this leads to a cuttings bed, which is one of the evidence of borehole enlargement. In order to mitigate this issue, the well is usually circulated, transporting the rocks to the surface and solids control equipment. As a consequence, an event called mud overflow occurs. At this point, it is practically impossible to recognize the individual cavings during their travel along with the screens. The first reason is the amount of mud and rocks being poured onto the shaker. The cavings cannot be separated right after the weir, as the mud velocity is very high, and a too large amount of fluid is dropped. In addition, the amount of cavings is very high, and the screens are literally overloaded with rocks (Figure 10). Another reason is the appearance of cuttings stuck together because of the excessive amount of clay particles. As a result, drilled particles are grouped in large drops of dilatant fluid. Thanks to constantly vibrating the screens' surface, the viscosity increases, not allowing the remaining fluid to seep through the screens (Figure 11). Therefore, it is not possible to separate the cavings, as in the first case there is a large amount of fluid already, and impossibility to separate the solid particles in the second case.



Figure 10: Mud Overflow After Addition of the Fibrous Material to Suspend Cuttings and Clean the Well (Forta Corporation 1997)



Figure 11: Excessive Clay Appearance on the Screens (TR Solids Control 2016)

### 2.3 Cavings Comparative Matrix

Basing on the cavings classification and the circumstances under which they are formed, an advisory matrix is suggested (Table 2). This table contains all possible borehole complications causes, consequences, and treatment operations gathered from the mentioned literature. It should be considered as part of the workflow in the intelligent cuttings analysis system in a form of the automated advisory algorithm. It is assumed to be the helping hand for the mud logger or wellsite geologist, proposing the actions to be taken. The main disadvantage of this matrix is its ambiguity and uncertainty. In order to include this methodology into the workflow, it should be more specific and work

similarly to a conditional flowchart, having a specific response to every single condition (e.g. cavings appearance and description, known stratigraphy or change in drilling parameters). The evolution of this matrix is presented in Chapter 5, where the actual flowchart is built, giving the recommendations for the crew, which action to take under specific circumstances.

Table 2: Cavings Description, Causes, Consequences and Their Treatment (Kristiansen 2004) (Bowes and Procter 1997) (Gallant, et al. 2007) (Kumar, et al. 2012)

Shape	Size	Causes	Consequences	Treatment
Angular	<8 cm	Low mud weight and insufficient viscosity in a near-vertical well. Formed in low strength formations perpendicular to bedding planes.	Further enlargement of breakouts, bad hole cleaning, stuck pipe and improper cementing	Mud weight increase. Increase flowrate to ensure hole cleaning.
Tabular	2-25 cm	Wellbore with 15°-20° deviation from bedding planes and invasion of low mud weight into the weak bedding planes. Also seen in ERD wells	Mud losses, stuck pipe events, and high caving rates. Increase in torque and drag.	Lowering ROP with small adjustments in the mud weight. Minimizing surge and swab. LCM introduction.
Blocky	<9 cm	Invasion of the drilling mud into pre-existing fractures. Drilling through the fault zones. A high exposure time of mud penetration.	Lost circulation, destabilizing the well, cuttings bed. Cavings settle down with turned off pumps.	Lowering the mud weight. Lower the inclination angle, especially when drilling through faults. Avoiding the faults, when possible. Limit the exposure time. LCM introduction.
Splintery	<8 cm	Underbalanced drilling through tectonically stressed and overpressure areas. Having high ROP when drilling through low permeable rocks.	Hole collapse, torque and drag increase, pack-offs, and bridges.	Increasing the mud weight, or reducing the ROP. Casing the hole as quickly as possible.

The sizes of individual categories of cavings shapes listed in this table are taken from the reviewed literature. It was not possible to inspect an actual set of cavings, as this

## Borehole Instability Signs During Drilling

information was not submitted. Therefore, these values have an approximate nature and correspond to the typical sizes of return cavings, which appear on the shaker screens. In addition, in the “Causes” column all the possible causes are mentioned, which actually makes the introduced matrix so uncertain. It is actually not possible to link all the listed causes to the cavings shape, as cavings are the result of a certain instability type, which is actually can be drawn by different actions. As long as the same action performed by a crew leads to different complications in dependence from the drilling environment, the causes for the formation of different cavings’ shapes might interfere.



# Chapter 3 Cuttings Analysis Techniques

As it was discussed in the previous chapter, cavings (their shape in particular) appear as evidence of complicating borehole conditions. Unfortunately, there are no other means, except visual inspection of the cavings, to assume the state of the borehole wall in real-time. There is a number of logging tools, like acoustic imagers, which provide the graphical representation of the wellbore wall. However, it is impossible to conduct measurements during drilling, because such tools are mounted on the drill string at a fixed distance from the bit. It means that such tools will only take a snapshot at a current depth over time. On the other hand, borehole instability could occur at any depth of the borehole at any time. The situation is even more complicated with inclined and appraisal wells, as there is a lack of input data to conduct the geomechanical study. It makes drilling operations riskier and more unpredictable.

For this reason, cuttings analysis is conducted from the perspective of cavings shape, size, and lithology determination. Having known these parameters for a set of cavings appeared at the screens, it is possible to infer about the borehole wall conditions. Shape basically indicates on borehole stability issue, as it was discussed in Chapter 2. Size might indicate the presence of existing planes of weakness, rock integrity, and the stresses magnitude. Consequently, lithology should indicate the interval of possible instability. The cuttings and cavings, which appear on the screens, are likely to have different lithology and colour, as the cuttings are produced by bit action, while cavings are broken off the walls.

There are two main methods, which are used for the cuttings analysis. These are:

- Standard, when the mud engineer conducts the analysis manually. This way the samples are collected directly from the shakers, dried and sent to the laboratory, where the rock fragments are described depending on their sizes and shapes. There is a series of tools that allow us to classify the cuttings in batches, not each rock sample separately, which decreases the time for analysis. These methods still require the presence of a mud engineer to acquire the rock material
- Automated, combining both the tools for cavings acquisition (like various ramps, gutters, etc.), as well as the equipment for measurement and analysis, like sensors or cameras. These techniques leave the mud engineer controlling the process and taking actions instead of executing routine operations

## 3.1 Standard Method

### 3.1.1 Cuttings Collection

The workflow begins with rock destruction by the bit action, which results in the appearance of cuttings in the backflow of the annulus. It is not only the cuttings in the stream of drilling mud but also cavings, which actually slough or break off the borehole

wall and appear in the flow together with cuttings. When the slurry is fed into the shale shaker, it is collected in a feeder tank or “possum belly” (Figure 12).

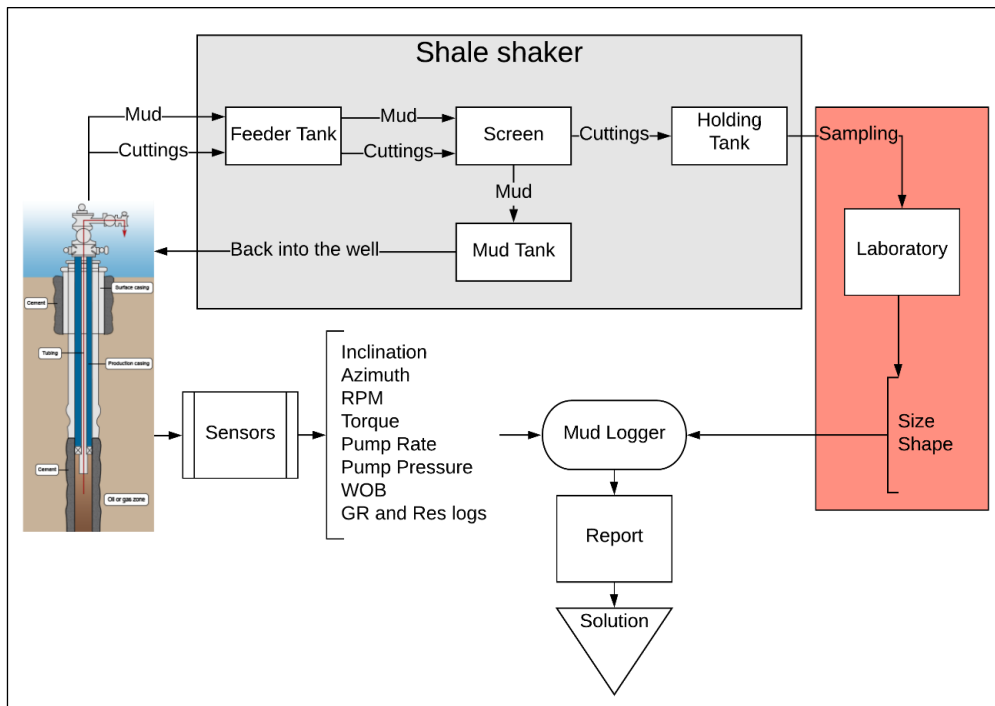


Figure 12: Conventional Cuttings Analysis Workflow

The client decides the sampling intervals, from which the cuttings are to be taken. The intervals vary from 5 to 30 feet. Generally speaking, the intervals selected are such that the mud logger is able to take four samples every hour (International Logging, Inc. 2001). It can be shortened due to the following factors:

- Drilling through areas of geological interest
- Changes in drilling parameters
- Changes in mud properties
- Changes in gas content

It depends, where to take the cuttings from: either from the possum belly or at the end of the screens. It is illustrated in Figure 13. Cuttings taken from the possum belly appear to be more representative, as the sample from the shaker outlet exhibits cuttings sticking together in large sumps. This becomes critical when determining the particle size distribution (PSD). It also matters, from which depth and location in the feeder tank to take the samples, as there is an uncertain gradient of cuttings concentration in the possum belly space. In addition, different designs of feeder tanks exist, and additional research is to be done (Karimi 2013). However, the most common way to collect the samples is the sample catcher at the end of the shakers (Figure 14). The most representative sample is taken and either washed or placed in the cloth bags, depending on the purpose. Afterwards, the catching board is cleaned from the remaining cuttings in order to accumulate a new portion of rock material.





Figure 13: Cuttings Taken From the Possum Belly (Left) and at the End of the Shaker Screens (Right) (Karimi 2013)



Figure 14: Taking the Cuttings from the Sample Catcher (International Logging, Inc. 2001)

### 3.1.2 Cleaning and Packing

The main objective of bagging the unwashed sample is to preserve the rocks for storage and future analysis. Another portion is washed especially for the proximate analysis (International Logging, Inc. 2001). It is needed to remind there that not all cuttings are collected there, as it is almost impossible to analyze all of them in such short time intervals. And, of course, the representivity is judged only by the mud logger, which brings in the subjectivity in the observations. This is not critical in cuttings analysis only, as their number is large enough to give significant enough errors on the analysis output.

## Cuttings Analysis Techniques

However, cavings should be observed in their full mass to present the whole information about borehole walls conditions.

When the samples are to be analyzed, they need to be washed. To save the cuttings characteristics the samples are washed in the base fluid of the drilling mud. Initially, they are placed in an 8-mesh sieve (meaning that particles greater than 2,38 mm will not be separated). Finer sieve is placed underneath to collect finer rocks during washing. After the procedure, the rocks which are left on the 8-mesh sieve are considered as cavings (Figure 15).



Figure 15: Cavings Collected in a Coarse Sieve (International Logging, Inc. 2001)

If the percentage of cavings is significant, the pressure engineer shall be informed about it to take measures. At first instance, this information is needed for pore pressure estimation (International Logging, Inc. 2001). Afterwards, the rocks are scooped on a metal tray and tagged to distinguish between samples. Finally, they are observed using the microscope or the UV box (as well as other tools). The cuttings and cavings are inspected for the following parameters:

- Rock type
- Colour
- Texture
  - Shape
  - Grain size
  - Sorting
  - Hardness
  - Lustre
  - Slaking and swelling

- Cementation and matrix
- Fossils presence
- Sedimentary structure
- Visual porosity
- Oil show

As long as the scope of the thesis is to describe the cavings according to their shape, size, and colour, only these parameters explanation is listed in Appendix A.

### 3.1.3 Analysis

In this subsection, the majority of tools and instruments for measuring the particle sizes, shapes, morphology, and mineralogical content are discussed. It is important to mention that not all existing equipment is intended to analyze drilling cuttings and cavings, but it was designed for measuring solids content in the drilling mud (laser diffraction, image analysis or FBRM methods), but it would be useful to focus on the technology, as the principle stays the same, and this concept could be used for measuring cavings size, shape and morphology.

Apart from that, to give a discussion of advantages and disadvantages of the methods in terms of automation possibilities and time consumption, it is needed to give an introduction to several ways of measuring the cuttings parameters (after Karimi 2013)

- In-Line Measurement: the instrument is inserted inside the pipe and conducts measurement during circulation
- At-Line Measurement: sample is taken manually or automatically and analyzed on-site
- On-Line Measurement: sample is collected and tested via the bypass line
- Off-Line Measurement: sample is collected and tested manually in the laboratory

It is worthy to mention that On-Line measurement has nothing in common with sending the information in real-time. It is called so, as the device is attached directly on the streaming line, which is called a bypass line, as written.

#### 3.1.3.1 Sieve Analysis

This simple method is used for determining the PSD. Measurement is done by shaking a sample through a set of the sieves until the rocks are distributed. The sieves are placed in a descending order& from coarse to fine (Figure 16). When the shaking is completed, the weight of each portion of rock left on the sieves is weighted, which gives information about the PSD. This analysis is two-dimensional, however, which gives the information of each cutting width and lacks the height (for flaky or platy pieces of rock).

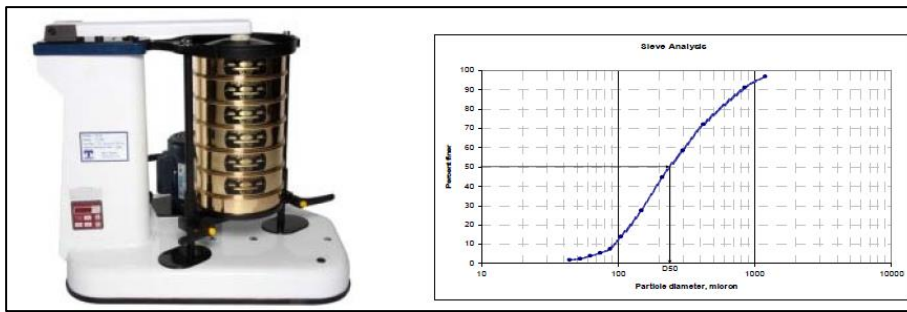


Figure 16: Sieve Analysis Procedure (Left) and Cumulative Curve of PSD (Right)  
(Karimi 2013)

### 3.1.3.2 Laser Diffraction

The essence of this technique is projecting a laser beam through a sample cell that contains a stream of moving particles suspended in a solvent, usually water, air, or alcohol (Karimi 2013). The concentration of particles has to be adjusted in order to allow the light to pass through the sample. When a beam hits the particle, it is scattered. This pattern, formed by scattered light, is registered by a number of detectors. Afterwardss, the software compares the scattered pattern with a model. As the output, a histogram of volume-weighted PSD is generated. the device is quite popular for PSD analysis because of its fast operation and reliable results (van Oort and Buranaj Hoxha 2016).

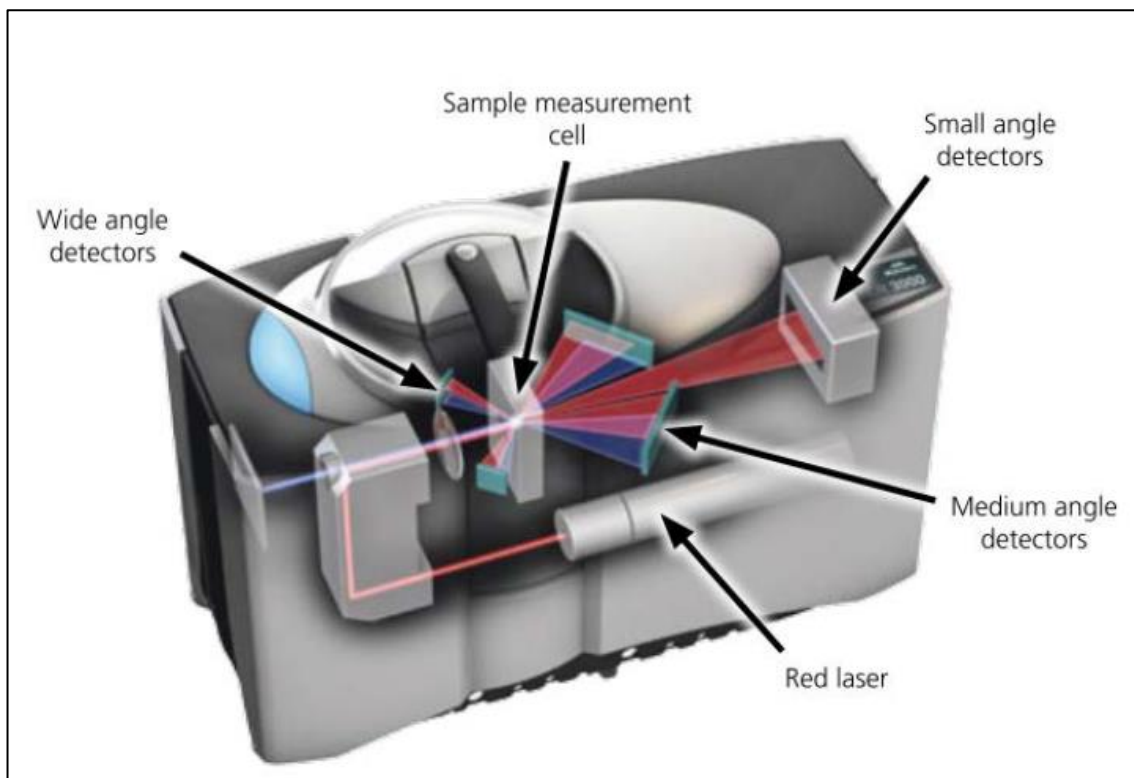


Figure 17: Laser Diffraction Device (courtesy of Malvern Instruments)

### 3.1.3.3 Optical Microscopy and Image Analysis

Image analysis technology is relatively distinct from the previously described tools, as here it is needed to process the image of the rocks itself, and not the reflected signal and its patterns. Individual images are captured from dispersed rocks, and Afterwards one receives the information about particle size, shape, and other parameters. There is also a possibility of particle thickness measurement (Karimi 2013). The lower particle size limit of image analysis is usually taken as  $0,8 \mu\text{m}$ . The procedure is quite simple: the camera captures an image of the sample, dispersed in a liquid, and applies imaging algorithms, which derive the particle size and shape. This is the only technique, which delivers a full batch of parameters, such as the longest and shortest diameter, perimeter, projected area, equivalent spherical diameter, aspect ratio, and circularity. This is very important for characterizing irregular particles, which take the majority of the input material (van Oort and Buranaj Hoxha 2016). The Liquid Particle Analyzer (LPA) is the device used for this purpose (Figure 18). In this image, LPA is used for drilling fluid analysis. A sampling system takes a fixed volume of drilling fluid and mixes it with a diluter in a mixing tank. Then the mixture is fed down the flow cell. The images are captured with a camera placed opposite the flow cell. The light source is located below the camera. To obtain the three-dimensional image, the particles are rotated (Saasen, et al. 2009).

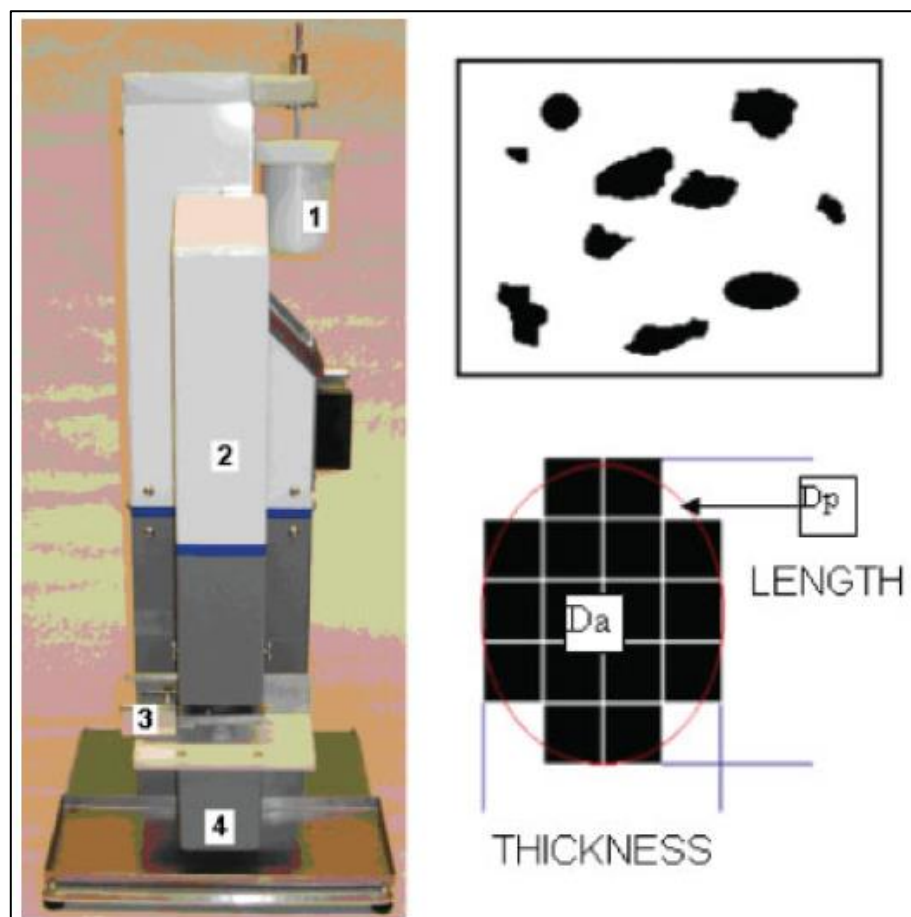


Figure 18: LPA and Examples of Images; 1 – Sample Mixing Tank, 2 – Camera, 3 – Flow Cell, 4 – Light Source (Saasen, et al. 2009)



### 3.1.3.4 Focused Beam Reflectance Measurement

Focused Beam Reflectance Measurement (FBRM) also utilizes a laser to obtain particle size. This is achieved by focusing the beam very precisely and passing it through the sample. The scattered and reflected light forms a return signal, and it is analyzed by the system, which tells how long the particle was in contact with the beam. The output of this procedure is the chord length, which is a line segment, connecting any two points on the particle boundary (van Oort and Buranaj Hoxha 2016). There is a possibility of obtaining the chord length distribution.

The tool illustrated in Figure 19 is used not only for the mud measurements but also for medicine and food industry. In the actual device, the laser beam is passed through the set of optics and focused on the sapphire window in a form of a beam spot. The optics are rotating with the frequency of 400 rpm, allowing the beam to pass through all the particles, as they flow near the window. The particles, as it was written earlier, scatter the light in a form of pulses, which are registered and counted as the duration. Knowing the speed of rotation, it is possible to calculate the distance, which was already mentioned as the chord length.

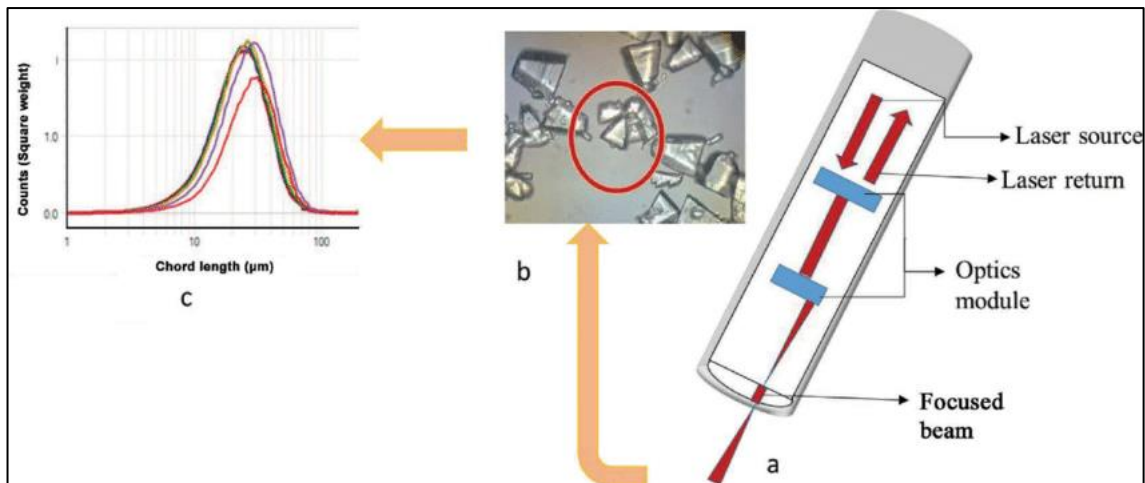


Figure 19: FBRM Measurement Workflow (Pandalaneni 2016)

### 3.1.3.5 Ultrasonic Extinction

In contrast with previously reviewed techniques, Ultrasonic Extinction (USE) method utilizes sound waves and not the light emission, which gives such devices a certain advantage, as it can operate independently of light conditions (Karimi 2013).

The working principle is relatively simple (Figure 20). An electrical high-frequency generator is connected to a piezoelectric ultrasonic transducer, which is generating the ultrasonic waves. The signal is passed through the media and is received by an ultrasonic detector, which converts mechanical waves into an electric signal. During travel through the measurement zone, the signal is scattered only by those particles, which are equal to or greater than the wavelength. During scattering the intensity of the signal decreases, which is seen on the detector. This extinction is calculated from the ratio of amplitudes on the generator and detector (Pankewitz and Geers 2020).

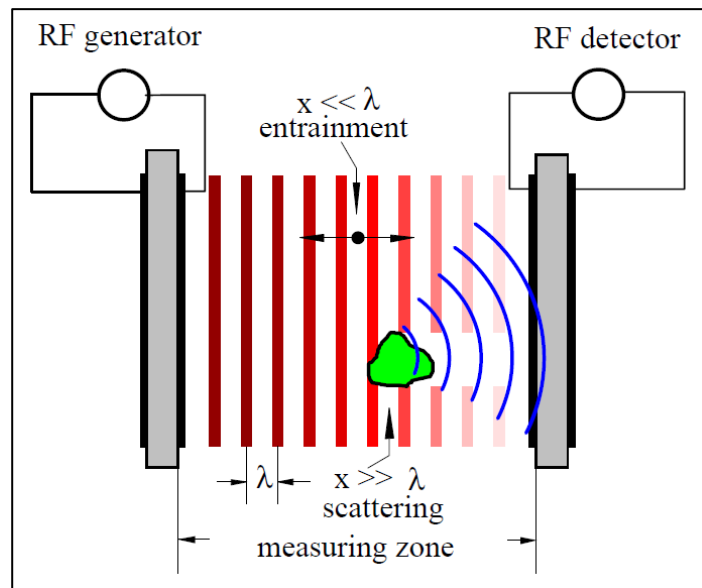


Figure 20: Measurement Principle of USE (Pankewitz and Geers 2020)

### 3.1.3.6 X-ray Fluorescence

The X-ray fluorescence (XRF) is used for determining the cuttings and cavings composition from the major and trace elements. It works for both organic and inorganic fingerprinting. In addition, it is used for identifying the mineralogy of the complex lithologies (Schumberger 2019). This technique has a low limit in the low ppm range, which is intended to give very precise results.

To conduct the measurement, the cuttings samples are to be cleaned, washed, and dried. Afterwards, they are ground with a grain size of approximately 80  $\mu\text{m}$ . The sample is placed into plastic cups, which are used further for analysis.

During the analysis, the sample is irradiated with an X-ray beam, which excites the electrons from the elements, of which the sample consists. When the electrons go back to their energy level, they emit light in a form of a fluorescence signal with a specific wavelength, which corresponds to the element type. This signal is amplified, measured, and compared to a standards sample used as a reference (Carr, et al. 2014).

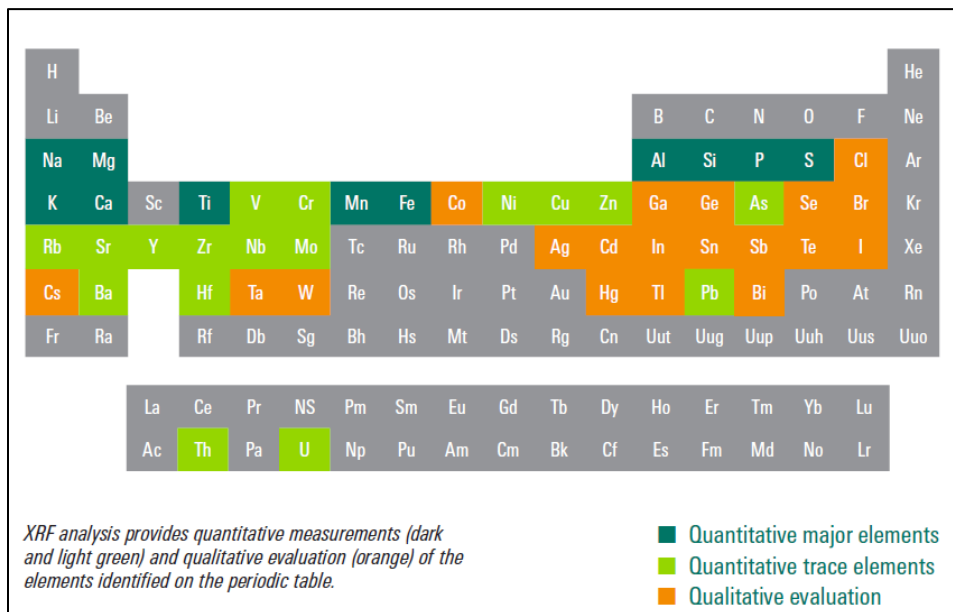


Figure 21: The Elements, Which Might Be Quantified From the X-Ray Fluorescence Analysis (Schumberger 2019)

### 3.1.3.7 X-ray Diffraction

In contrast to X-ray fluorescence, X-ray diffraction (XRD) is used not for identifying separate periodical elements from the sample, but its mineralogical composition. The procedure is relatively similar: the taken samples are washed, dried, and crushed to a grain size of less than 150  $\mu\text{g}$  (Schlumberger 2019). It is also recommended to have a particle size of at least 10 microns. The particles with smaller dimensions exhibit the decreased intensity of the X-ray resulting in lower detectability limits. This is one reason, why such analysis is relatively poor for the clays identification because of the small particle size (Ruessink and Harville 1992). The powder is also placed under a beam, which is scattered and diffracted by each crystal. The scattered light produces a unique diffractogram pattern, which has to be analyzed. There are several types of minerals, which can be analyzed with XRD, such as:

- Quartz
- Carbonates
- Feldspars
- Illite/smectite
- Chlorite
- Kaolinite, etc.

There is a certain difficulty in identifying clay minerals, as they have to be separated from the sandstone grains with centrifugation, for example. It is needed, because the granular minerals, like quartz, feldspar, and carbonates are randomly oriented. As long as the XRD analysis is severely dependent on the particle orientation because the X-ray beam will reflect from the grains surface.



### 3.1.4 Shortcomings (Standard Method)

The summary of conventional analysis considers only cavings size, shape, and lithology measurements, and the strengths and weaknesses are collected in Table 3.

Table 3: Advantages and Disadvantages of Conventional Cavings Analysis

Advantages	Disadvantages
Low cost of particle size and shape analysis	Time-consuming
No necessity of equipment except sieves	A requirement of personnel presence
Accuracy	Subjectivity of observations
Individual analysis of cavings	Not proactive

During the automation process, its strong points and advantages have to be preserved. The strong points are definitely accuracy and individual approach when analyzing each particle.

Furthermore, in order to automate the process of cuttings analysis and cavings detection, in particular, it is needed to overcome the mentioned disadvantages. In order to improve already existing technology, one has to split the workflow into separate operations and search for those which may be removed or executed in parallel. In addition, it is needed to specify the operations to be automated.

First of all, this technology requires a human presence to be executed. As it was described in the corresponding section, the employee shall be present during the following steps:

- Sample acquisition
- Washing of the sample in the 8-mesh sieve
- Packaging the samples depending on the purpose of analysis
- Manual measurement with sieves or other tools
- Comparison with the colour palette
- Writing the report

These procedures are subsequent, and all of them are part of the conventional workflow cycle. An important moment in this sequence of procedures is washing the samples. Only when the samples are collected with the 8-mesh sieve and washed, mud logger notifies the crew about the cavings presence. If not specified, the frequency of the cavings presence reporting is equal to one hour. This part makes the workflow non-proactive, as a certain amount of time is lost for the cuttings collection and separation. In addition, not all of the recovered cuttings are collected, but only a certain portion of them, which was collected subjectively. These factors make their contribution to the lost time, which could be used for decision making.

It was also mentioned, that the cuttings are to be washed intentionally for the analysis e.g. colour identification. As long as washing is not critical for shape and size determination because the mud layer is not thick enough to introduce large errors, it becomes essential for the colour identification, which would give premises for

distinguishing between different types of lithology. In this case, an automatic circulation system is required.

Having the analysis conducted at the time of the cavings' appearance on the shakers, all the steps are automatically illuminated, which is followed by the acquisition and washing operations. In addition, everything, which passes through the measurement device, will be analyzed, excluding the selectivity of sample collection and subjectivity in measurement.

Consequently, the proposed technology has to have the following features:

- It has to eliminate all the points discussed above, leaving the human as the operator or supervisor, not the executor
- The presence of cavings should be noticed right at the moment of acquisition. If the cuttings are stuck together, leaving no possibility of automatic caving detection, they have to be washed and sieved automatically in advance
- The measurement device should exclude all the steps, which are to be done after confirmation of cavings presence, so that not only cavings detection is executed, but also their measurement and report generation is done
- The analysis should not be time-consuming and deliver the results within a relatively short time range

In order to select the tool for capturing cavings information, all the methods and tools discussed above are coupled in Table 4. The best matching technique will be selected for the cavings' shape, size, and colour determination with regards to the demands mentioned above.

As long as the proposed system should be automated so that the tool should be chosen depending on the type of measurement: In-line, At-line, or On-line in particular. In the case of the At-line system, the measurement should be also done automatically, not manually. Here the list is narrowed down to four methods: Laser diffraction, Image analysis, FBRM, and USE. Focusing on the measurement technique itself, all the mentioned above, except Image Analysis and USE, definitely have the upper particle size limitation, as they are based on the scattering of the laser beam, which is too narrow to detect larger particles on a scale of centimetres. The USE method could be the simplest, in this case, to choose, however it has two main disadvantages: the existing tools for ultrasonic measurements have a fixed limit of particle size of 3000  $\mu\text{m}$  (Sympatec GmbH 2017). In addition, a shaking sieves' surface may introduce errors in the measurements. Since the design of the new tool is not the aim of this thesis, here only on the image analysis techniques will be considered. For the considered case, it is not necessary to disperse the cavings in a liquid in order to obtain images. As long as the imaging algorithms are robust and fast enough to process the image in real-time, this is the best matching technique. The strong side of this method is that it is able to calculate most of particle parameters and dimensions by conducting measurement individually for each particle, in contrast to other tools, which focus on capturing the scattered pattern.

Table 4: Comparison of Manual Measurement Tools (after Karimi 2013)

Parameters	Sieve analysis	Laser Diffraction	Image Analysis	FBRM	USE	XRF	XRD
Type	Off-line At-line	Off-line At-line	On-line At-line Off-line	In-line	Off-line On-line In-line	Off-line At-line	Off-line At-line
Min size, $\mu\text{m}$	~20	0,04	20	1	0,01	<80	>10
Max size, $\mu\text{m}$	6730	2000	Unlimited	2000	<80	80	150
Output	PSD	PSD	PSD	PSD	PSD	Elemental composition	Mineralogy
Test frequency	1 hour	10 min	< 3 min	1 second	30 seconds	12 min	2 min – 1 hour
Advantage	No upper size limitation	Lab availability	Identifies each particle individually	Measurement frequency	Volumetric solids concentration	Repeatable readings	Eliminates subjectivity
Limitations	Lower size limitation	Upper size limitation	The fixed spatial range of analysis	Upper size limitation	Might be sensitive to vibrating surfaces	Necessity of grinding	Necessity of grinding

With regard to colour detection for lithology determination, optical cameras can also transmit such information, but only if it acquires a colourful image. It is necessary to mention, that cuttings sent for the analysis are washed in a base fluid in advance, implying that the cuttings have to be washed prior to being photographed. This will require the installation of the circulation system to pump the base fluid for cleaning the drilled rocks. XRD and XRF methods are very specific and deliver results of high accuracy, however, there are two main limitations: necessity of grinding and length of the test, as one needs to take snapshots of the entire specimen, and the visible range is in order of  $0,01^\circ$  and the speed of moving the detector is  $0,05^\circ/\text{min}$ . There are also at-line XRD and XRF measurement tools, but they still require human presence, as the sample has to be ground and placed into a device as well (Olympus 2019).

To sum up, the most flexible technique is Image Analysis, as it has the following advantages:

- No limitation for the upper size of cuttings
- Identification of such parameters as the longest and shortest diameter, perimeter, projected area, equivalent spherical diameter, aspect ratio, and circularity by considering each particle individually
- Relatively low analysis time
- Inexpensiveness
- Absence of direct interaction with cuttings

## 3.2 Automated Measurement Tools

In this section, all the possible methods, which are used for determining the solids content were collected, as well as describing the particles individually. There are two different automated methods: physical and computer-based. The first technique utilizes a direct measurement of cuttings mass within specified time intervals. The second method comprises a wide range of techniques with various working principles. A classification for these approaches was built, and the strengths and weaknesses were discussed here.

### 3.2.1 Cuttings Flow Meter

Cuttings Flow Meter (CFM) continuously measures and records the cuttings flow at the outlet of the shakers. Since the cuttings flow rate is often small relative to the mudflow rate, measurement within the mudflow would not be accurate enough. Therefore, the measurement is likely to be done at the outlet of the shale shakers. As long as this area accommodates large and heavy equipment, there is little space left for another mechanical system installation and for cleaning, maintenance, and screen's check. In addition, severe conditions are present in this zone, as the shakers are exposed to the gas, high vibrations, and high-pressure cleaning jets. Being a simple mechanism, CFM doesn't disturb the operations and deliver its functions (Naegel, et al. 1998).

Figure 22 describes CFM construction. The device is located in front of each shale shaker and collects cuttings in a tray. While the cuttings are being collected, the gutter is prevented from rotating. At this period a strain gauge continuously measures the increase in weight. On fixed time intervals, the gutter is flipped downwards, discharging the collected cuttings. Then the tray stays in this state for a few seconds to ensure its emptiness and flips back to the original position.

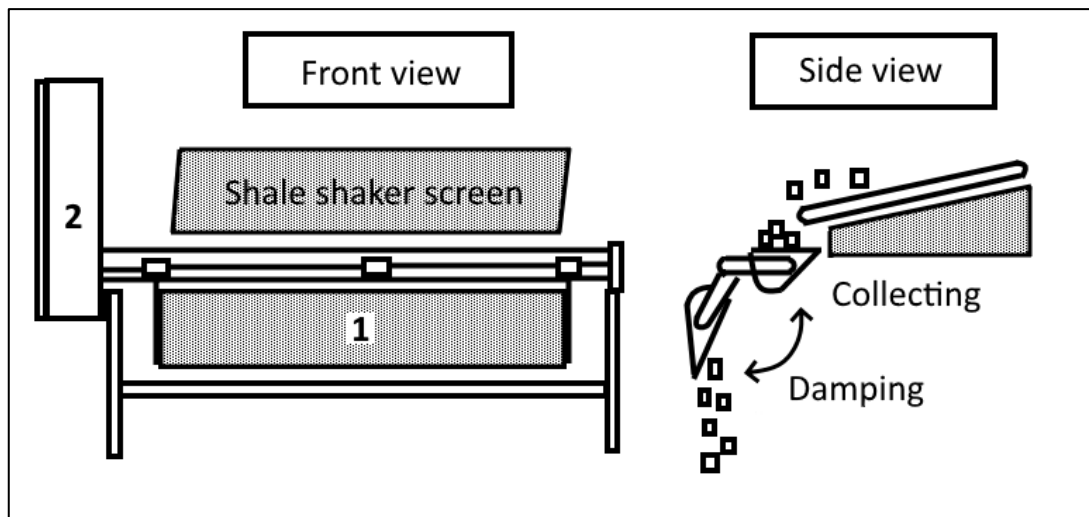


Figure 22: Schematics of the Cuttings Flow Meter (1 – Gutter, 2 – Control Mechanisms in the Protected Enclosure) (modified after Naegel, et al. 1998)

The main parameter, which is acquired from this device, is the mass flow rate derived from the measured mass of the cuttings. This is basically needed to ensure the effectiveness of the cleaning or washing procedures. If there is a decline from the trend, the actions are to be taken. Apart from that, there is a possibility to get the volumetric flow rate from after measuring the mud density, cuttings density, and the density of the cuttings mass in the gutter. It is said that the result seldom varies except with the formation change (Naegel, et al. 1998).

The device was mainly used to confirm or describe such events as:

- Cuttings bed formation
- Cuttings removal during string rotation
- Circulating conditions and hole cleaning efficiency

### 3.2.2 Computer-Based Techniques

There are several technologies, which are based on measuring the physical distance between a target surface and sensor's position. Those techniques are 2D vision, stereo vision, time-of-flight, and structured light (Omland, et al. 2007).

#### 3.2.2.1 2D Machine Vision

2D machine vision is the simplest cost-effective approach, which can perform the following functions: Image acquisition and analysis, the recognition of an object, or objects within object groups (Legutko, Raos and Labudzki 2014).

The required device is a camera regardless of the sensor type or used lens. These elements are chosen depending on the ambient light intensity, distance from an object, desired quality, resolution, etc.

This technique can perform At-Line measurement, which means that the camera can be installed directly at the shaker screens. One of the benefits of this approach is that the cavings do not interact with the device. That way, remoteness is its strong benefit.

The basic working principle is recognized in Figure 23. The scene (or shaker screens in our case) are illuminated by a light source. The optical image is captured by cameras or image sensors, which is digitized into an optical array. Then this data is modified in order to adjust brightness, enhance contrast, conduct image sharpening or smoothing, etc. Thereafter this imaging array is segmented, which is needed to partition an image for leaving only the region of interest. Feature extraction seeks for identifying the specific characteristics, features, or patterns, which are relevant for certain object types. Finally, the image is associated with one of the predetermined classifiers, which were determined manually by the operator or specialist.

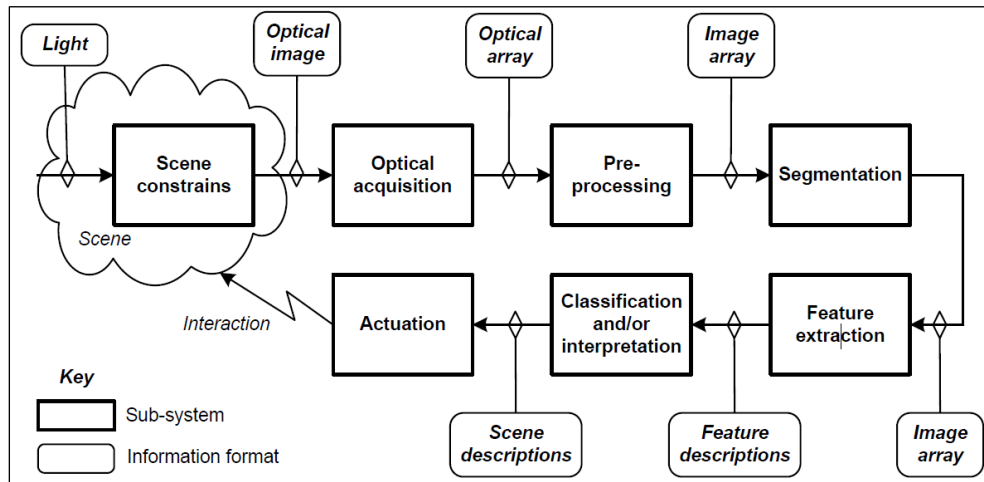


Figure 23: Typical 2D Vision Flowchart (Legutko, Raos and Labudzki 2014)

As long as this system is based on reflected light, the illumination is a very important part of this process. There are three the most widely-used light sources, which are collected in Table 5. As it is seen, LED light sources are desired among others in a sense of their power consumption and efficacy. In addition, they have a more uniform spectrum for the white light, small size, and low-maintenance in terms of exploitation in various thermal conditions.

Table 5: Comparison of Light Sources (Nasrullah and Naeem 2011)

Light source	Examples	Power (W)	Efficiency (%)	Efficacy (Lm/W)	Lifespan (thousands of hours)
Incandescent	Light bulb, halogen lamp	100	1.9 – 2.6	12-20	1
Fluorescent	Tube	18	9-15	70-100	20
	CFL	23	8-11	50-80	10
Solid-state lighting (SSL)	LED lamps	15	20-22	80-150	50

However, even if the illumination is appropriate, the ambient light (e.g. sunlight) might be present, if the installation is located outdoors, as in our case. In addition, fog and rain might occur during the operation process. This might require the installation of the insulation chamber.

### 3.2.2.2 Stereo Vision

The device set for the stereo-vision is similar to the 2D vision system. In the simplest case, this method uses two Charged Coupled Device (CCD) equipped cameras placed horizontally at a small fixed distance from a scanning object. The following assumptions have to be introduced for the simplest stereo-vision system (National Instruments 2012):

- Both cameras have the same focal length
- The cameras are parallel to each other
- The X-axes of the two cameras intersect and align with the baseline
- The origin of the real-world coordinate system coincides with the origin of the left camera coordinate system

There are two variants of cameras placement (Figure 24). The first one is compliant with the demands mentioned above. In the second case, the cameras are located randomly. This variant requires stereo calibration. Calibrating the camera basically done to measure distances in length units, not in pixels. During this process, the real-world coordinates are synchronized with cameras' coordinates.

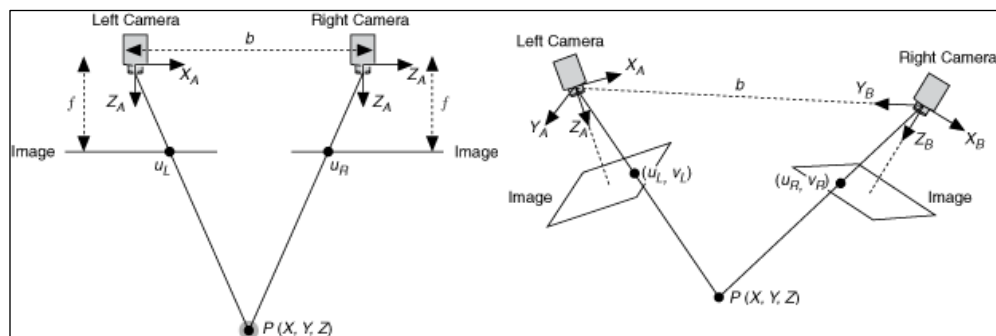


Figure 24: Simplest (Left) and Typical (Right) Stereo Vision Systems (National Instruments 2012)

The working principle is illustrated in Figure 25. The process begins by sending two images to the input. Thereafter the images are processed, the noise is filtered out, the resolution is changed and optionally the colour channels are converted to monochrome. Afterwards, the features have to be extracted. The correspondence problem is quite challenging and is formulated as a question: how to find the same point on a real object from the two images provided from cameras. If the correspondence is not established, depth determination might be inaccurate. Generally, the salient points are chosen, establishing high signal variations. The simplest examples are corners or color patches. When the corresponding points in both images are found, they should be matched, so that each of the points actually has relation to each other. Afterwards, the depth map is built by computing actual coordinates of the points on both images.

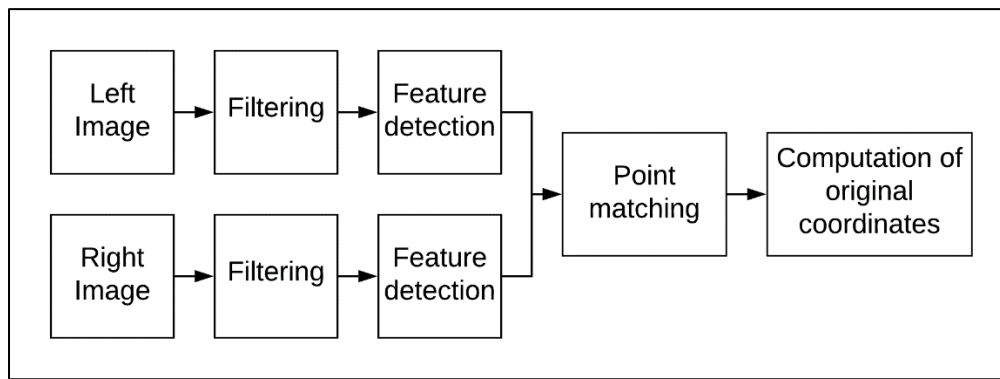


Figure 25: Working Principle of Stereo Vision (modified after Cyganek and Siebert 2009)

The resolution is mainly dependent on the camera's focal length, sensor resolution, and baseline. One of the drawbacks of the stereo vision is the high processing time for comparing two images. The computational demands also increase with the resolution, which makes this technology of best application for scanning objects with low frame rate or simply static objects.

### 3.2.2.3 Structured Light

One principal method of 3D surface imaging is based on the use of "structured light," i.e., active illumination of the scene with specially designed 2D spatially varying intensity pattern. The band of light has a predefined pattern as grey codes, light stripes, sine waves, or speckle patterns (Geng 2011). For the employment of this technique to devices are needed: a camera and a pattern projector. It is possible to use either a single camera or multiple cameras to observe the light pattern (Fofi, Sliwa and Voisin 2004). As long as this technique is a variation of 3D vision, the installation is basically the same. However, the camera's field of view should coincide with the projection area. There are two technique types: multi-shot and single shot.

The multi-shot technique is also called a sequential projection. The principle is illustrated in Figure 26. The series of patterned stripes is projected onto the object. As long as the positions of the image sensor (camera) and the pattern projector are known, it is possible to calculate the depth of each point for every single stripe. However, to achieve a high spatial resolution, a large number of sequential patterns have to be projected. This is why this technique is called a multi-shot. It is of high importance to say that the object has to remain static during one projection sequence.



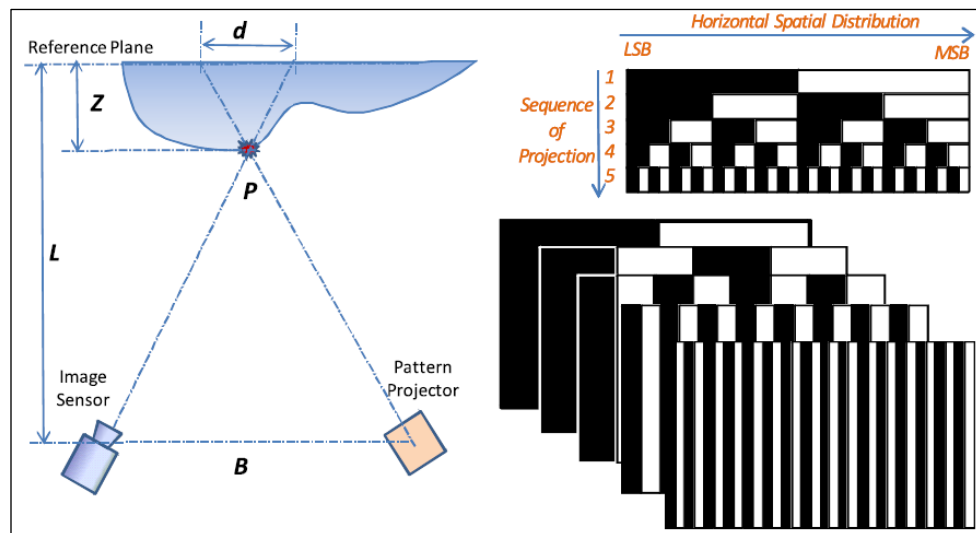


Figure 26: Principle of the Sequential Projection Imaging (Left) and Projected Patterns (Right). LSB and MSB Stand for Least Significant Bit and Most Significant Bit Correspondingly (Geng 2011)

The single-shot technique takes advantage of colour information of a unique encoding scheme in the projection pattern and requires only one captured image of the colour pattern to derive the 3D image with all three coordinates of each visible point. The patterns take the form of the colour-indexed stripes or colour-coded grid (Figure 27). The order, in which pattern is observed is not necessarily the order in which the pattern is projected. This is due to the possibility of stripes missing from the acquired image because of the occlusion of the object's parts.

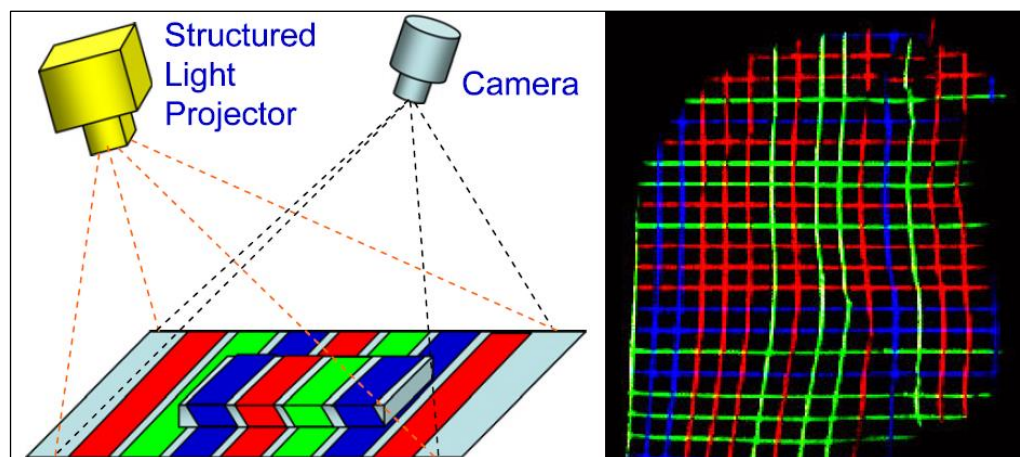


Figure 27: An Example of Single-Shot Techniques: Colour-Indexed Stripes (Left) and Colour-Coded Grids (Right) (Geng 2011)

### 3.2.2.4 Time-of-Flight

The time-of-Flight technique, in contrast to some of the previously mentioned installations, uses a single device is used, which accommodates two tools: light emitter and receiver. Typically, an infra-red-light source (laser or LED) is used. Consequently, the sensor is sensitive only to the frequency range of the emitter. Here it has to be

mentioned that the sensor responds not only to the reflected light but also an ambient component, which is typically sunlight at the rig site (Figure 28). For this reason, the camera, as well as the shaker screens have to be isolated in a separate chamber to ensure the reliability of results. Apart from that, to capture the shape profile of cavings, it has to be installed directly at the shakers in order to capture the size along the two largest spatial dimensions. The time-of-flight camera works by illuminating the object with a modulated light and capturing the reflected light. The measured phase shift is translated as a parameter for object description. To detect phase shifts the emitted light is modulated with a continuous wave, typically with a sinusoid or a square wave (Li 2014).

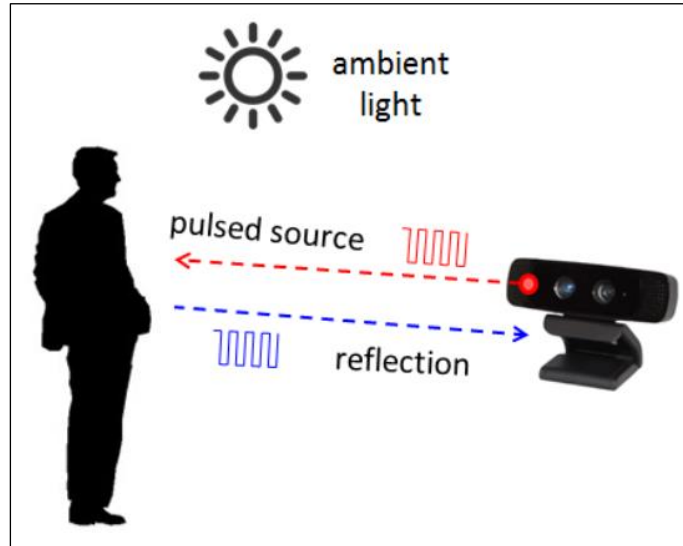


Figure 28: Principles of Time-of-Flight Camera Operation (Li 2014)

Thereafter the distance is measured for each pixel resulting in a depth map, which is a series of 3D points (or voxels). In Figure 29 there is a 2D representation of a depth map, formed from an image of soda cans set. The depth is visualized with a greyscale, where white colour stands for closer voxels, whereas black – for farther. Alternatively, every voxel can be visualized through a 3D point-cloud, where each point would have three possible coordinates.



Figure 29: Input Image (Left) and a Depth Map (Right) (Li 2014)

### 3.2.3 Shortcomings (Automated Method)

The observed methods are gathered in Table 6. They are split according to identified parameters, depth accuracy, scanning speed, distance range, low light performance, outdoor performance software complexity, and material cost. With respect to our demands (cavings size is found within in the range of several cm) and the computing power, 2D computer vision is the best choice among these types of techniques. There is also a CFM device which has the best performance in outdoor and low light conditions, however, as it was also mentioned in the previous subsection, only Image Analysis techniques among listed in Table 6 allow us to analyze each rock piece individually. Despite its simplicity, it gives no opportunity to detect the appearance of cavings on the shakers.

Table 6: Comparison of Automated Measurement Tools (Based on Brading, et al. 2013)

<b>Parameter</b>	<b>CFM</b>	<b>2D Computer Vision</b>	<b>Stereoscopic vision</b>	<b>Structured light</b>	<b>Time of flight</b>
Identified parameters	Mass flow rate	Shape and size	Shape and size	Shape and size	Shape and size
Depth Accuracy	N/A	mm to cm	mm to cm	µm to mm	mm to cm
Scanning speed/Testing frequency	Low	Medium. Limited by software complexity	Medium. Limited by software complexity	Fast/Medium. Limited by camera speed	Fast. Limited by sensor speed
Distance Range	N/A	Mid-Range	Mid-Range	Very short to mid-range. Depends on illumination power	Short to long-range. Depends on laser power and modulation
Low Light Performance	Good	Weak	Weak	Good	Good
Outdoor Performance	Good	Good	Good	Weak/Fair. Depend on illumination power	Fair. Depend on illumination power
Software Complexity	Low	Middle	High	Middle	Low
Material Cost	Middle	Low	Low	Middle	Middle

## 3.3 Field Application of Automated Methods

This section is intended to describe all attempts to build and installation for automated cuttings analysis techniques. Some of the tools used in these services were described in the previous section. A concise description of each technology was provided, as well as specifications for each of them are available in order to register the state of the art.

### 3.3.1 Schlumberger CLEAR Service

CLEAR is a Schlumberger-designed hole cleaning and wellbore risk reduction service, which is intended to monitor hole cleaning effectiveness and wellbores stability. This service allows us to continuously measure the cuttings' weight and volume as the cuttings come off the shale shakers. This is needed for comparing these parameters with theoretical data for proactive reaction to changing borehole stability and hole cleaning issues (Schlumberger 2015).

The CLEAR service is accomplished with a CFM and weighing tray located at the end of the shale shaker so that it would collect the cuttings as they fall off the screen. The measurements are taken periodically, and each period is preset in advance and could be adjusted. When the one is filled, it discharges the collected cuttings by swinging down and returning back to the initial horizontal position. The measured data is the following:

- Cumulative wet and dry weight of cuttings falling from the shakers
- Measured and theoretical dry cuttings volume
- Measured and theoretical (based on ROP) cuttings flowrate
- Volume excess or deficit
- Percentage of cuttings recovery

Subsequently, the obtained data is compared with the drilling parameters, cuttings geology, mud properties, and LWD data. The results are then sent to the dashboard, which is accessible both from the rig site or at the remote offices (Schlumberger 2015). Another benefit is that the software allows us to generate daily reports.

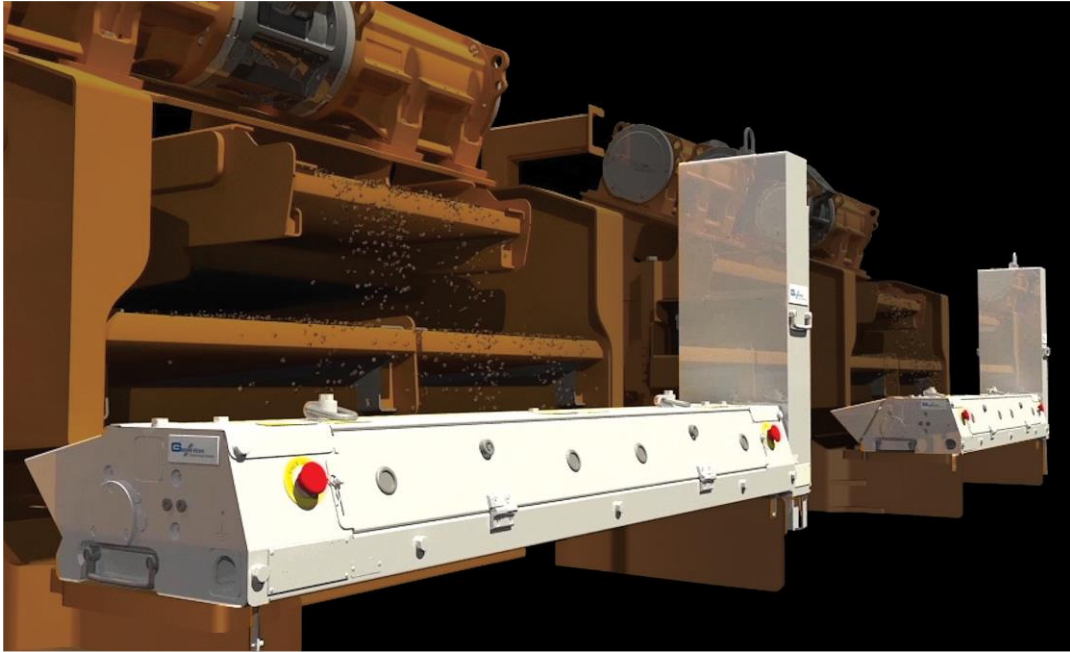


Figure 30: CLEAR Hole Cleaning and Wellbore Risk Reduction Service  
(Schlumberger 2015)

This technology was successfully used during drilling an ERD operation in Southeastern Asia. CLEAR service indicated on the ineffective drilling mud rheology. Having this information in mind, the drilling crew adjusted the fluid rheology, improving hole cleaning. That allowed the company to save 16 rig hours or USD 194000 (Schlumberger 2015).

Another case study was conducted in the Shaybah field, Saudi Arabia. As proposed, CLEAR service provided early detection of inadequate hole cleaning and excess returns resulting in cavings appearance on the shale shakers. Having this support, the mud system was kept in good condition during drilling. As a result, the section was drilled 2.46 days ahead of the plan with a cumulative cutting recovery of 84.4% (Schlumberger 2016).

### 3.3.2 Device for Measuring PSD and Cuttings Analysis

In 2009 an automated device was introduced, which was designed to measure drilling fluid properties and conduct cuttings analysis. Here only the solids control part of this system is covered. The device included the tools for measuring the cuttings Particle Size Distribution (PSD), their concentration, morphology, and mineralogy (Saasen, et al. 2009). This cuttings analysis system is shown in Figure 31.

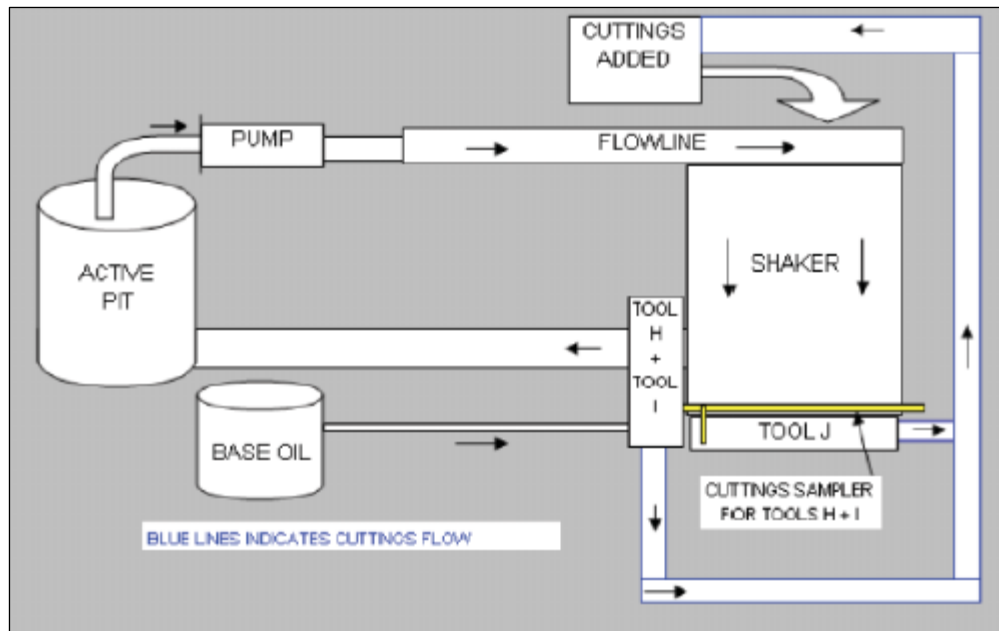


Figure 31: Schematic Diagram for Drilling Cuttings Analysis (Saasen, et al. 2009)

For testing purposes, different rock fragments, such as sands, shales, and carbonates were added to simulate drill cuttings and cavings flow. The materials were added just before the shaker. Then the major part of the cuttings is collected and measured with cuttings flowmeter (Tool J). Right above the tool, a cuttings sampler is placed to determine if there are any cavings in the flow. The cuttings morphology analyzer is equivalent to Tool H. When the measurement is performed, the cuttings are transported to Tool I to measure the cuttings mineralogy with a Raman spectroscope.

This system allows us to proceed with sampling, washing, and drying of cuttings and image analysis. It was reported that the system worked without any problems during the test period. In order to install such a device on the rig site, it would need certain refinements to be done. It is said, that the Raman spectroscope should be broken down automatically into individual mineral and fluid species. This is mainly needed to monitor the mineral phases, not the cuttings' size.

### 3.3.3 Intelligent System for Cuttings Concentration Analysis

The core of this system is a high definition camera installed above the shale shakers, which sends the captured images to a computer with an installed data analysis system. This module is responsible for classifying images obtained from the vibrating shale shaker. If the image doesn't match any of the classifiers, the mud logger is notified to inspect the sample manually (Marana, et al. 2010).

Such a system has two main advantages: high accuracy in identifying anomalies during the drilling operation and is of low cost. In addition, this system is non-intrusive, meaning that it doesn't consume much of the rig space, as the only video camera and the laptop with the software are required (Figure 32).

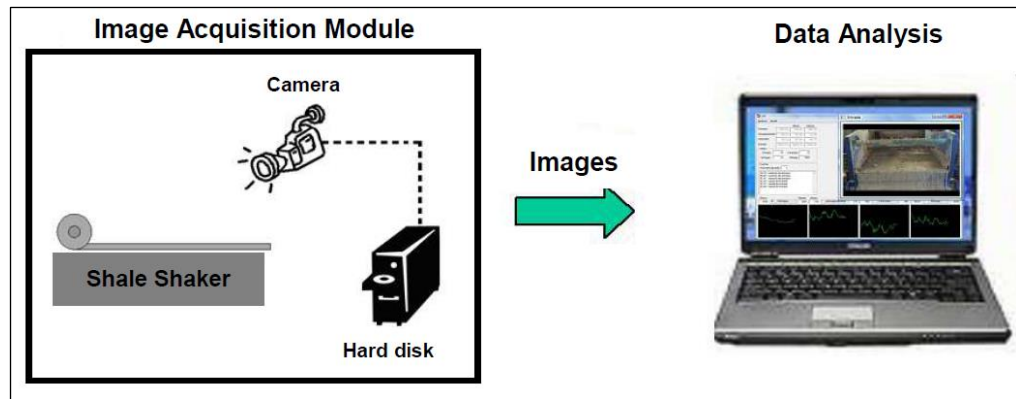


Figure 32: Non-Intrusive Cuttings Analysis System Installation (Marana, et al. 2010)

The machine learning techniques used for the classification purposes were: Optimum-Path Forest (OPF), Artificial Neural Network using Multilayer Perceptions (ANN-MLP), Support Vector Machines (SVM) and Bayesian Classifier (BC).

The experiment on offshore drilling vessels for automatic image analysis was conducted. The system was tested for three cuttings concentrations: None, Low and High, as illustrated in Figure 33. It means that the cuttings were not analyzed individually, but all together by texture analysis. The algorithm training was done with a supervisor; who has selected 20 frames from each class of concentrations and labelled them accordingly, which were used as a test set. Another 60 images were used for the test set, resulting in a 50/50 relationship between training and test sets. The experimental results are gathered in Table 7.



Figure 33: Images Captured by the Camera Placed Above the Shale Shakers: (a) None Concentration, (b) Low Concentration and (c) High Concentration of Cuttings (Marana, et al. 2010)

Table 7: Experimental Results for Different Classifiers (Marana, et al. 2010)

Classifier	Mean Accuracy	Mean execution time
OPF	99.89±0.001	0.0023
ANN-MLP	99.00±1.200	0.0330
SVM	99.25±0.612	1.5314
BC	99.33±0.970	0.0020

Authors concluded that with such low execution time and accuracy the system can detect any anomaly with respect to changes in cuttings volume in real-time, indicating



problems during the drilling process. Importantly, this was the first attempt to develop an image-based system for drilling operations monitoring based on cuttings analysis.

### 3.3.4 Classifying Cuttings Volume via Video Streaming

This approach proposed to analyze the volume of cuttings from a shale shaker also uses video capturing. The model works in real-time and is able to perform classification in relatively good accuracy in contrast to traditional video analysis methods, which take too much of the processing time. The technology consists of two parts: multi-thread engine for decoding, processing, and encoding video streams, as well as Region of Interest (ROI) selector, and Convolutional Neural Network (CNN). This CNN is tested to classify the cuttings volume into four labels: “Extra Heavy”, “Heavy”, “Light” and “None” (Du, et al. 2020).

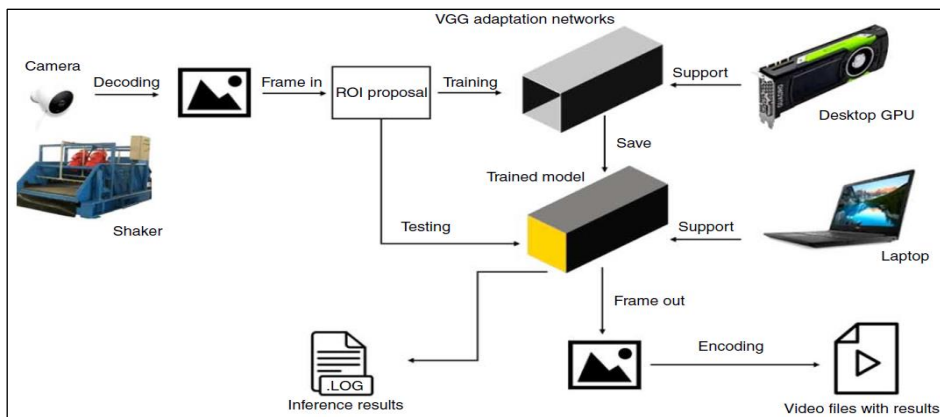


Figure 34: Real-Time Cuttings Volume Monitoring System. VGG Stands for Visual Geometry Group, a Machine Learning Technique (Du, et al. 2020)

As seen from Figure 34, the process starts from capturing an image from the shaker by the camera at the rig. Thereafter the data is streamed to a remote workstation through intrusive rig transmission channels and protocols. Due to bandwidth limitations, the video resolution is comprised. For testing purposes, 10 hours of video were collected and labelled manually. In addition, a fast Graphics Processing Unit (GPU) is needed. Then the model was tested on another set of videos. Testing results were verified by comparing them to manually labelled frames. During the actual process, the videos are labelled in real-time. The video framerate is equal to 5.84 frames/s, the bitrate is 137 Kbps. To guarantee steady interference results, the engineer is required to provide the ROI in which cuttings are moving on the sieves. The ROI can be selected either manually or automatically.



Figure 35: ROI Selected Manually (Left) or Automatically (Right) (Du, et al. 2020)



The testing results indicate that the algorithm easily distinguishes between all the classifiers using the plain VCG-16 network. The results are also dependent on lightning conditions, shooting angles, and distances.

### 3.3.5 Cuttings Shape Acquisition Using 3D Point Cloud Data

This technology provided by (Han, Ashok, et al. 2018) uses plane segmentation, which is a computer vision algorithm, that constructs 3D point cloud data acquired by 3D scanners. The test installation design included the conveyor belt, which was used to simulate the sliding movement of artificially created rock fragments and field cuttings on a ramp. Above the ramp, a 2D high-resolution camera with a 3D laser sensor was installed in order to gain an integrated system. Whereas a camera was used for measuring cuttings moving speed and analyze the size distribution of the cuttings, the sensor was included to build the 3D profile basing on cuttings measurement. Both of them were calibrated for the resolution and scanning frequency.

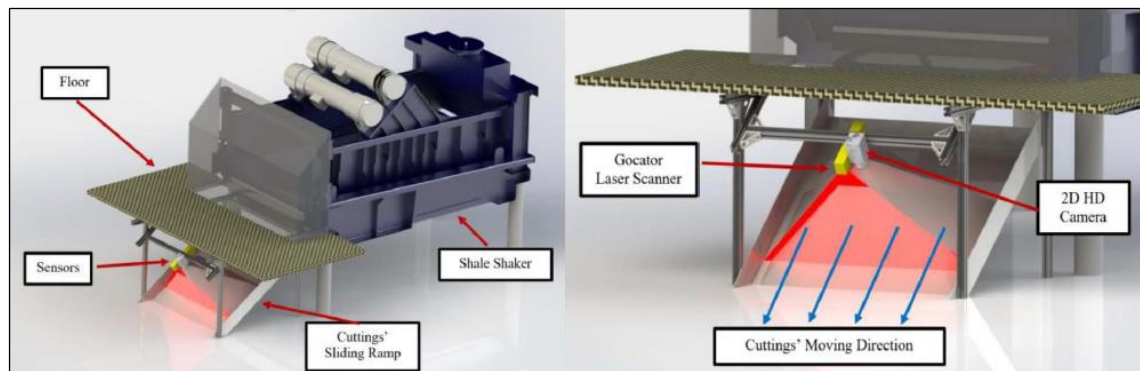


Figure 36: Integrated Cuttings Monitoring Design Setup (Han, Ashok, et al. 2017)

As for the software, Microsoft Visual Studio and C++ were selected as the Integrated Development Environment (IDE) and the programming language respectively. As it is seen from Figure 37, the workflow is the following. The laser sensor and camera are triggered with Visual Studio. Thereafter they start to capture images and pass them to the software via Gigabit Ethernet. The acquired 2D images from the camera allow us to calculate the speed and PDS of the cuttings by comparing the frames. The speed data is coupled with 2D profile depth data from the laser scanner, which results in cuttings volume calculation.

3D depth profile is used further for edge detection and size calculation for each cutting or caving individually. The cavings' shapes are proposed to be split into three categories: tabular, angular, and splintered (Karimi 2013).

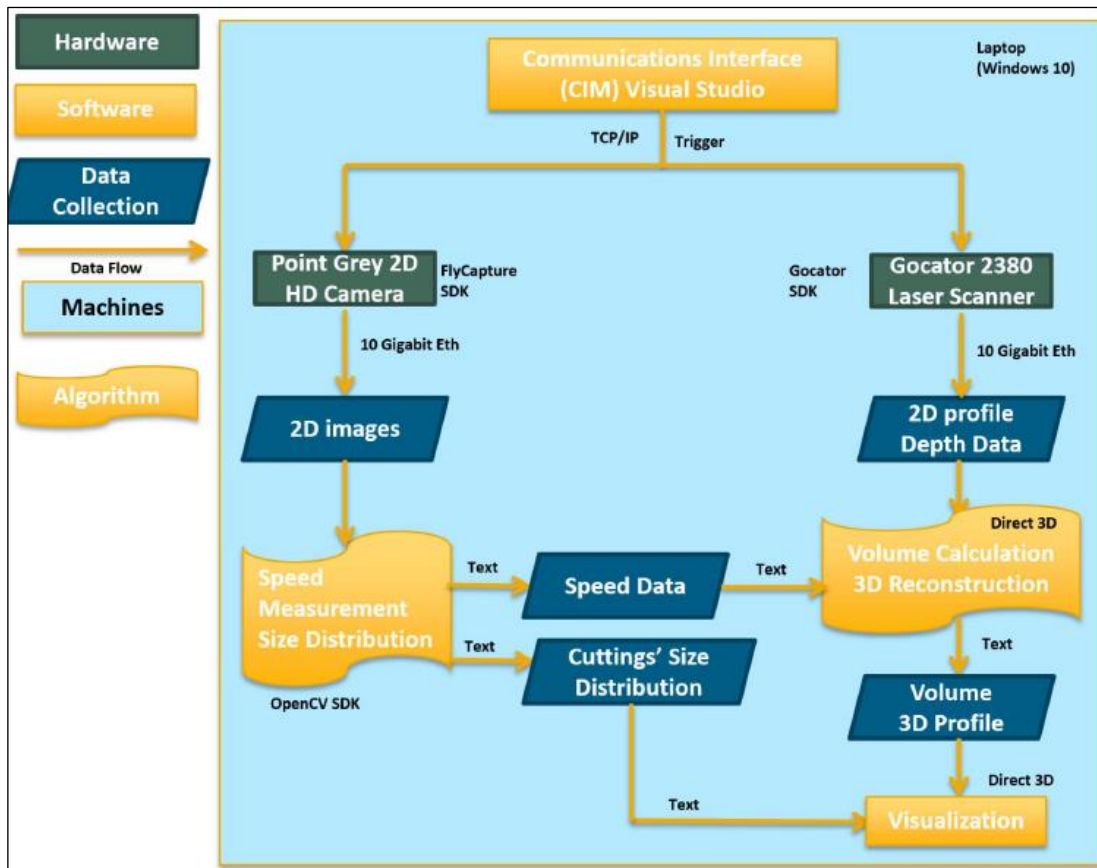


Figure 37: Software Architecture for Measuring Cuttings PSD and Building 3D Profile (Han, Ashok, et al. 2017)

Authors conclude that the suggested technology, thanks to the possibility of 3D profile development, is able to conduct the following:

- PSD estimation
- Return volume calculation
- Caving detection
- Shape profile analysis
- Real-time monitoring
- Guarantee safety

The used hardware specifications are in Table 8 and

Table 9.

Table 8: Gocator 2380 Laser Scanner Specifications (LMI Technologies 2016)

<b>Specification</b>	<b>Information</b>
z-resolution	0.092 – 0,488 mm
x-resolution	0.375 – 1.100 mm
Measurement range	800 mm
Scan rate	5000 Hz

Table 9: Blackfly GigE Camera Specifications (FLIR® Systems 2018)

Specification	Information
Model name	BFLY-PGE-23S6C-C
Frame Rate	41
Resolution	1900 x 1200
Megapixels	2.3
Colours	Yes

### 3.3.6 Lithology Recognition Using Various Machine Learning Techniques

The observed technology gives an overview of the lithology determination from the cuttings images. The paper does not provide any information on the hardware used. However, the data set was acquired from the EAGE Earth-Hack challenge (EAGE 2019). The general idea of the reviewed publication was to use various machine-learning techniques and their combinations, such as Convolutional Neural Network (CNN), Support Vector Machine (SVM), Transfer Learning, and the Ensemble of four CNNs. These models were both trained and tested on this dataset (Kathrada and Adillah 2019). CNN will be discussed in Chapter 4.

The images were depicting the drill cuttings photos, which were further divided into four classes in order to have enough data to train the network (Figure 38).

Four different techniques combinations were used to classify the images (Table 10). One of the most popular networks, which was used is AlexNet (Krizhevsky, Sutskever and Hilton 2012). In the research, it was used together with SVM and Transfer Learning. The main disadvantage of SVM is that it performs relatively poorly on the validation set. In the case of Transfer Learning, it is assumed that CNN is pre-trained and has required filters for edge and contrast detection, and it would require less time for additional training. This technique performed a bit better than a combination with SVM (67% versus 62% on a validation set). Interestingly, the Ensemble of CNNs classified the images worse than an optimized single CNN. This is because the images were quite similar, and it was relatively hard for both machines and humans to distinguish between them. It was concluded, that more initial data is required to train and test the networks.

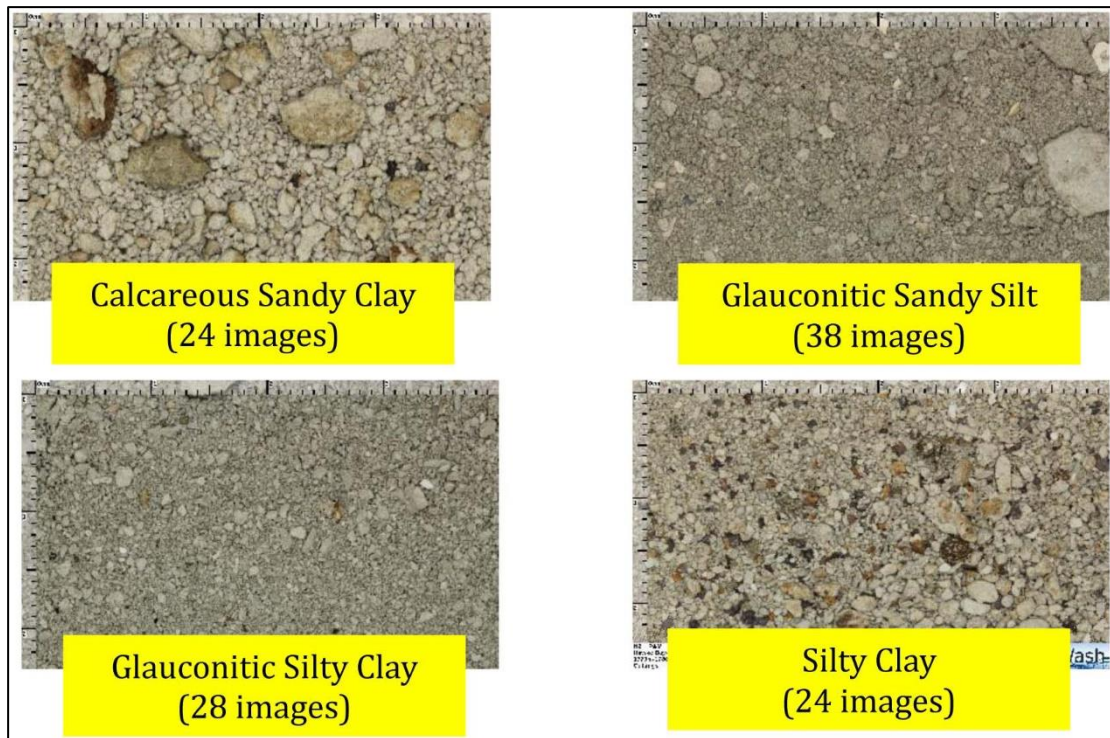


Figure 38: Image Examples for Each Lithology (Kathrada and Adillah 2019)

Table 10: Results for the Tested Methods (Kathrada and Adillah 2019)

Method	Training set	Validation set
AlexNet activations + SVM	100%	62%
Transfer Learning + AlexNet	87%	67%
Bayesian optimized CNN	100%	82%
An ensemble of four CNNs	98%	73.5%

### 3.3.7 Rock Classification with a Deep Convolutional Network

Another methodology for rock types classification utilizing a CNN was developed (Ran, et al. 2019). The technique was not developed to serve for cuttings lithology identification purposes, but for classifying the field images of rocks. The overall workflow, which is depicted in Figure 39, considers the following steps: taking pictures of rocks, cropping the acquired images in order to focus the field of view directly on rock mass, identification and labelling the rocks, model training, and actual application.

After taking the initial pictures of rocks outcrops, each of the images was divided into regions of rocks with the most typical features in order to get the representative dataset. The samples were taken from the mentioned regions so that they have the same resolution. For providing an understanding of dataset sizes, the number of cropped images for training, validation, and test datasets are listed in Table 11.

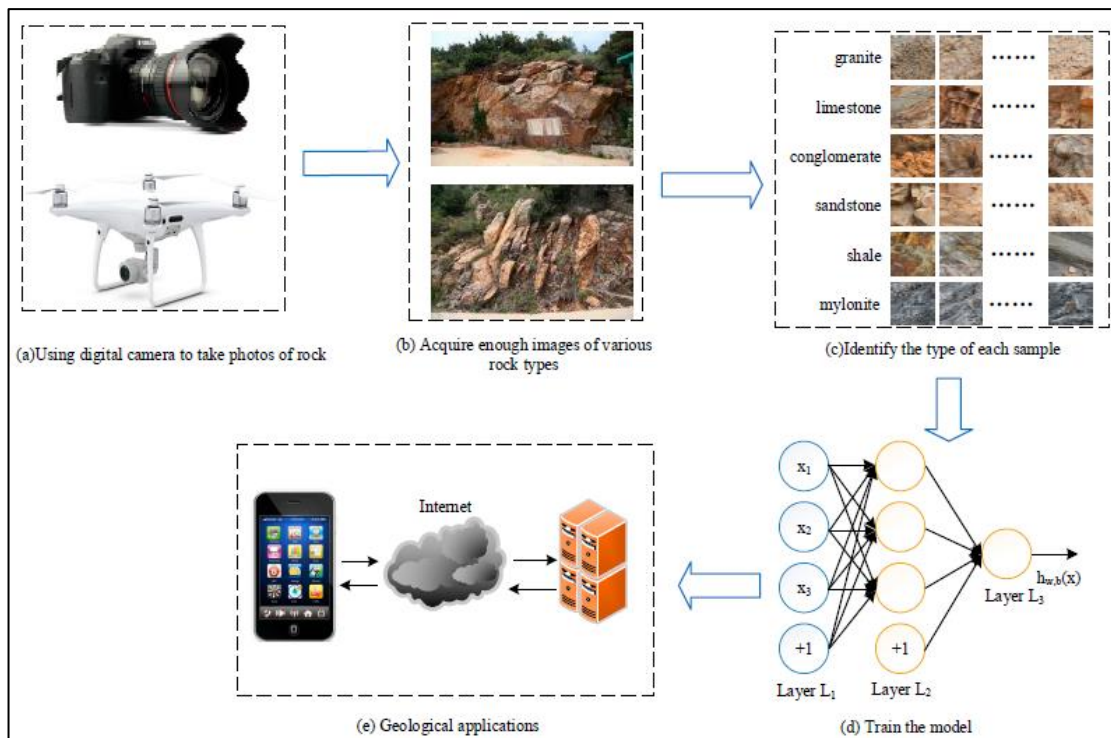


Figure 39: General Flowchart for the Rock Types Identification (Ran, et al. 2019)

Table 11: Datasets for Image Classification of Field Rocks (Ran, et al. 2019)

Type	Training Data	Validation Data	Testing Data
Mylonite	1584	528	528
Granite	3753	1251	1251
Conglomerate	3372	1124	1124
Sandstone	2958	986	986
Shale	1686	562	562
Limestone	1236	412	412
Total	14589	4863	4863

Authors proposed a network with their own architecture in order to decrease computing time and increase accuracy. The architecture is not shown in this section. The main advantage of the proposed CNN is that the training could be carried out on a laptop, with the following specifications including Central Processing Unit and Graphics Processing Unit (CPU and GPU correspondingly) (Table 12).

The effectiveness of classification was tested with different CNNs, including the proposed one. It employs two convolution operations, which is not much in comparison with widely known networks. Apart from the proposed one, other techniques were employed, such as Support Vector Machines (SVM), AlexNet, GoogleLeNet Inception v3, and VGGNet-16 networks. Each of the models was trained in 200 epochs using the batch (number of images in a training iteration) size, which is specified in Table 13. The accuracy and training time is also listed in Table 13.



Table 12: Used Hardware Specifications (modified after Ran, et al. 2019)

Item	Value
Type of the laptop	Dell Inspiron 15-7567-R4645B
CPU	Intel Core i5-7300HQ 2.5 GHz
GPU	NVIDIA GeForce GTX 1050Ti with 4GB RAM
Memory	8 GB
Hard Disk	1 TB
Solid State Disk	120 GB

Table 13: Performance of the Tested Models (modified after Ran, et al. 2019)

Method	Accuracy, %	Batch Size	Training Time
SVM	85,5	200	3:32:20
AlexNet	92,78	128	4:49:28
GoogleLeNet Inception v3	97,1	100	7:12:53
VGGNet-16	94,2	100	5:18:42
Proposed network	97,96	16	4:41:47

As it is seen from Table 13, the proposed network not only has one of the least computing time, but also the highest accuracy among the compared models. In this sense, the authors did not only develop a simpler CNN but also reached a higher performance.

### 3.3.8 Comparison Summary

All existing cuttings analysis technologies are assembled in Table 14. The techniques were compared according to their output parameters, used devices, complexity, cost, reliability, and maintenance. The last four criteria were assessed by qualitative scale consisting of „Low“, „Middle“ and “High” values.

“Low” category implies that there is:

- a little amount of technical or electronic elements in the equipment
- the low complexity of software
- low comparative costs
- absence of repeatable results or low accuracy of output data
- no or little necessity of operating the equipment, meaning that the installation is stand alone

In contrast, “High” category means that there is:

- the overall complexity of either hardware or equipment
- computationally demanding and sophisticated software
- high costs
- repeatable results or high accuracy of output data

## Cuttings Analysis Techniques

- the necessity of frequent equipment maintenance or demand of human presence

Consequently, everything within the “Middle” category did not fall under each of the previously mentioned labels. Therefore, the chosen items tend to have moderate complexity, costs, performance, and self-sustainability.

Table 14: Comparison of Existing Installations for Cuttings Analysis. Green colour shows the best category, red – the worst, and yellow – neutral

Name	Outputs	Device	Complexity	Cost	Reliability	Maintenance
Schlumberger CLEAR	Mass, Volume	CFM	Low	Low	High	Low
Device after (A. Saasen 2009)	PSD, Morphology, Mineralogy	CFM, Raman spectroscope, X-ray	High	Middle	Middle	Middle
Device after (A.N. Marana 2010)	Volume	Camera	Low	Low	High	Low
Device after (Xunsheng Du 2020)	Volume	Camera	Low	High	Middle	Middle
Device after (Han, Ashok, et al. 2017)	PSD, Shape, Volume	Camera and laser scanner	Middle	Middle	Middle	Middle
Model after (Kathrada and Adillah 2019)	Lithology	Camera	Middle	Middle	Middle	Low
Model after (Ran, et al. 2019)	Rock type	Camera	Middle	Middle	High	Low

Mentioned techniques could be distinguished by the output parameters: the most frequently determined were PSD and Volume. Others, such as Mass, Morphology, Mineralogy, and Shape were mentioned only once. This trend could be described by the simplicity of volume determination, as the rocks are analyzed in batches, and not individually. This method is less computationally demanding and therefore is widely used. At the same time, the last described approach is the only one, which is able to give PSD, Shape, and Volume as the output simultaneously. This was achieved by installing a laser scanner, which build the cuttings profile. Here it is to remind that the initial goal



of the authors was to calculate the volume and PSD, whereas shape was calculated as a secondary parameter. It means that the shape could be determined for all the cuttings, and not the cavings only. This is why this algorithm is demanding equipment and processing power. For purposes of cavings analysis, it is not necessary to build a 3D depth profile, which is storage prompting and time-consuming operation.

At the same time, the device after (Du, et al. 2020) could be used as part of the proposed technology in this thesis. Even though it does not deal with shape determination, it might alarm for mud overflow. Under these circumstances, it is not actually possible to determine any cavings. Warning for excessive mud and rock on the screens might save computational powers, as the cavings analysis system should stay in standby mode. In addition, the goal of the thesis is not only to classify the cavings according to their shape and size but also to warn the crew about possible complications, depending on the conditions on the shale shakers. Mud overflow is not what usually reported, so, having a system that notifies about it, could be a benefiting point from a proactivity perspective.

With regard to lithology determination, it is hard to presume in advance, if CNN would actually determine the cavings lithology in real conditions, as none of the discussed above models was tested on real cavings. Another complicating factor is the mud layer and fine particle on the rocks, which seriously affect the measurement accuracy. It means, that the cavings have to be either washed before appearing under the camera field of view, or another means of analysis should be introduced.



# Chapter 4 Convolutional Artificial Neural Network

Artificial neural network (ANN) is a huge family of computing systems designed to perceive the input data basing on the training data set without simple tasks like if-else clauses. In considered case, ANN should be able to recognize cuttings and cavings from the transmitted image data and classify them into predetermined sizes and shapes.

## 4.1 Simplest Artificial Neural Network

Convolutional neural networks are intended for recognizing image data, as their design differs from the simplest ANN. The most general ANN design is illustrated in Figure 40. It consists of an input layer of neurons, which transforms initial information into the hidden layer (there might be several of them). In this layer, each neuron is connected to every neuron in the previous layer. It is important to say that the neurons in the same layer do not share any connections with each other. Being processed, the information is passed to the layer of output neurons, giving the final result.

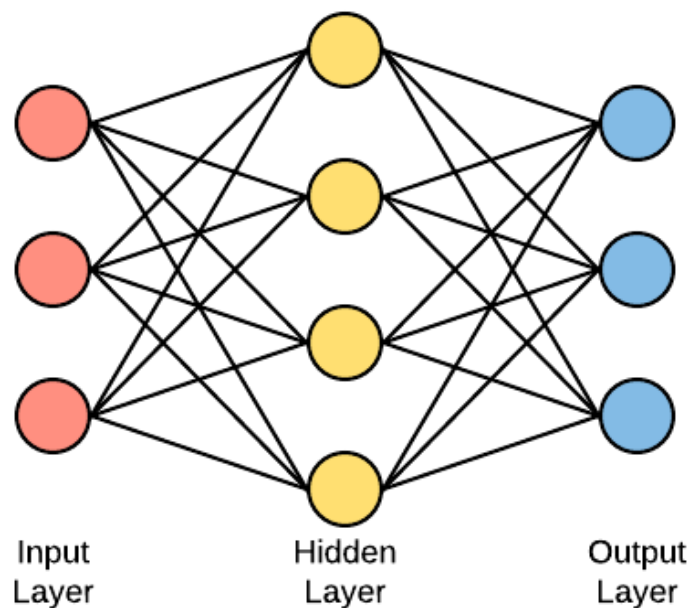


Figure 40: Principle Design of ANN

The single neuron structure is depicted in Figure 41. The neuron takes an array of inputs and multiplies them by weights. Afterwards, all the multiplications are summed together. Here, the bias is also added to the result. It is needed to adjust the results and fit in the given data. The result is further passed to the activation function. There is a high number of different activation functions:

## Convolutional Artificial Neural Network

- Identity function
- Heaviside step function
- Rectifier function
- Gaussian
- Tangent
- Exponential and others

The type of function influences its robustness and the possibility of the neuron to pass the information further or not. If the information gained after the summation function is not enough to overcome the threshold, the neuron will not “fire”. In the end, the output is generated which is either passed to other neurons or gives the actual outcome of the calculation.

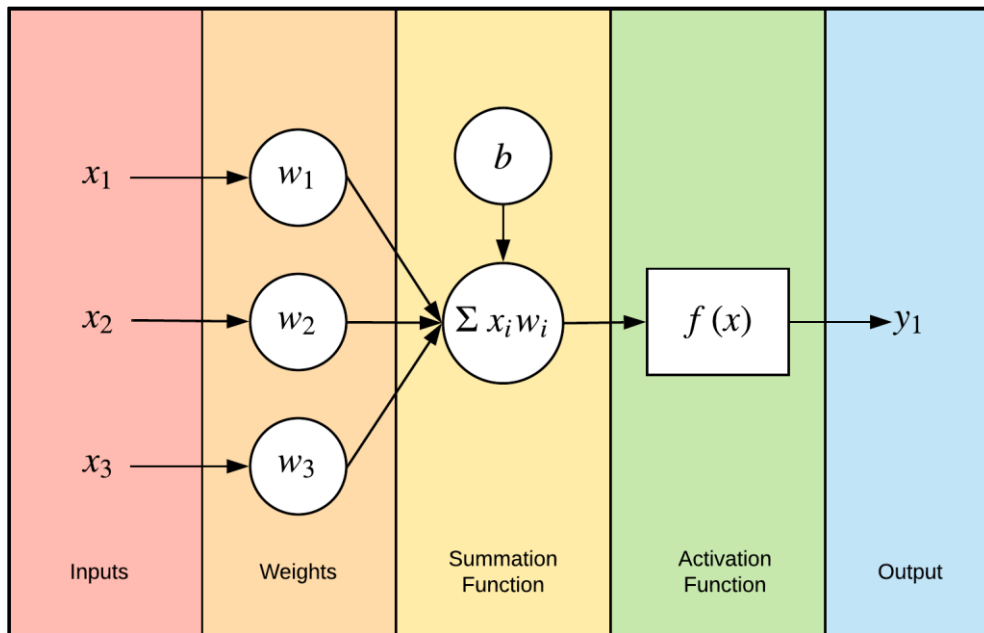


Figure 41: The General Neuron Structure

The operation of the neuron is formulated with the following equation:

$$\hat{y}_1 = \sum_{i=1}^N x_i w_i + b \quad (1)$$

Where  $x_i$  – neuron input;

$\hat{y}_1$  – computed output;

$w_i$  – weight;

$b$  – bias;

$i$  – index of the input;

$N$  – number of inputs.

The main goal of the ANN is to adjust weights so that the neurons would focus on one type of information they get as an input. They might be adjusted either by supervised or non-supervised learning. Supervised learning technique provides the ANN with the

labelled examples, so that the machine “knows”, what it should get. This kind of learning technique is mainly used for bioinformatics, image, and pattern recognition. In the case of unsupervised learning, ANN learns to label the inputs all by itself. Unsupervised learning is needed for anomalies detection, hierarchical clustering, and generating data with given patterns.

## 4.2 Training, Validation, and Testing

Prior to actual employment, the model has to be trained, tested, and validated. For that purpose, the collected data is split into three datasets: training, testing, and validation sets. The essence of these processes and methods of splitting the dataset are discussed in the following subsections.

### 4.2.1 Training

The training dataset consists of the data (images, as in the considered case), which are used to train an algorithm. This data is labelled in advance so that for every existing input there is a corresponding output. The goal of the training session is to adjust the weights in the network. For that reason, some fundamental concepts should be explained.

The first concept to discuss is the cost function, which is determined as Mean Squared Error (MSE):

$$C(w, b) = \frac{1}{2N} \sum_{i=1}^N (\hat{y}_i - y_i)^2 \quad (2)$$

Where  $w$  – weights in the network;

$b$  – biases in the network;

$y_i$  – the target value of the output;

The purpose of the MSE introduction is to compute the error for each layer output between the target value  $y_i$  and calculated value  $\hat{y}_1$  for the given input  $x_i$  and the corresponding set of weights  $w$  and biases  $b$ . From this perspective, there is an objective to decrease MSE in order to obtain valid results.

In order to minimize the error and adjust weights, the backpropagation algorithm should be introduced. Here it will be useful to link the weights and biases to the actual neurons in the network. The weight between neuron  $j$  in layer  $k$  and neuron  $i$  in layer  $k - 1$  will be denoted as  $w_{ij}^k$ , and bias for neuron  $j$  in layer  $k$  will be defined as  $b_j^k$ . Neuron activations in the corresponding layer and input neuron will be denoted as  $a_j^k$  for the outputs and  $a_i^{k-1}$ . Therefore, equation (1) could be updated as follows:

$$a_j^k = \sum_{i=1}^{N_{k-1}} a_i^{k-1} w_{ij}^k + b_j^k \quad (3)$$

Where  $N_{k-1}$  – the number of neurons in level  $k-1$ .

For the simplicity, bias  $b_j^k$  will be defined as  $w_{i0}^k$ . Since the neurons are counted from 1 and not 0, this will not create any computational problems. Consequently, equation (3) can be formulated as follows:

$$a_j^k = \sum_{i=1}^{N_{k-1}} a_i^{k-1} w_{ij}^k + b_j^k = \sum_{i=0}^{N_{k-1}} a_i^{k-1} w_{ij}^k \quad (4)$$

Error minimization is computed by finding the gradients of the cost function with respect to weights and biases:

$$\Delta w_{ij}^k = -\alpha \frac{\partial C}{\partial w_{ij}^k} \quad (5)$$

Where  $\alpha$  – learning rate, which is usually taken in a range of (0,001 ÷ 0.1). It shows, how fast the model should converge to the result.

Here it is needed to apply the chain rule:

$$\frac{\partial C}{\partial w_{ij}^k} = \frac{\partial C}{\partial a_j^k} \frac{\partial a_j^k}{\partial w_{ij}^k} \quad (6)$$

The first term is defined as an error, denoted as:

$$\delta_j^k = \frac{\partial C}{\partial a_j^k} \quad (7)$$

The second term is simplified as follows:

$$\frac{\partial a_j^k}{\partial w_{ij}^k} = \frac{\partial}{\partial w_{ij}^k} \sum_{i=0}^{N_{k-1}} a_i^{k-1} w_{ij}^k = a_i^{k-1} \quad (8)$$

Hence, the partial derivative of the cost function with respect to  $\partial w_{ij}^k$  is equal to:

$$\frac{\partial C}{\partial w_{ij}^k} = \delta_j^k a_i^{k-1} \quad (9)$$

It might be shown that:

$$\delta_j^k = \sigma(a_j^k) \sum_{l=1}^{N_{k+1}} \delta_l^{k+1} w_{jl}^{k+1} \quad (10)$$

Where  $l$  –neuron index on  $k + 1$  level;

$N_{k+1}$  – number of neurons on  $k + 1$  level;

$\sigma(a_j^k)$  – activation function for the  $k$  level.

As a result, the backpropagation is expressed as follows:

$$\frac{\partial C}{\partial w_{ij}^k} = \delta_j^k a_i^{k-1} = \sigma(a_j^k) a_i^{k-1} \sum_{l=1}^{N_{k+1}} \delta_l^{k+1} w_{jl}^{k+1} \quad (11)$$

It is seen that the error  $\delta_j^k$  on the layer  $k$  is computed from the error  $\delta_l^{k+1}$  on the next layer  $k + 1$ , so that the error is propagated backwards. To sum up, when the network is computing the outputs for each neuron, the process is called forward pass, while error

calculation is called a backward pass. As a result, after the whole forward pass up to the final layer, the error is computed, and the weights and biases are adjusted. Afterwards, another forward pass is conducted, but with already adjusted parameters. This process continues until the error reaches its minimum.

On a large scale, when for the selected inputs the weights are adjusted in such manner that the labels are determined correctly, that means that the network is trained.

## 4.2.2 Validation

In order to estimate, how well the network was trained, it is essential to prepare the validation dataset. Again, all the inputs are also labelled in order to obtain the error. The main difference between validation and training phase is that during validation the model weights and biases basically stay unchanged. What could be changed is hyperparameters of the ANN, such as learning rate, number of epochs to train, batch size, or activation function. This combination of hyperparameters basically creates a number of models to choose from. For that reason, the validation error is estimated. After that such set of hyperparameters is selected, which gives the least validation error.

The training error is often compared to a validation error, giving the following combinations:

- Underfitting – validation and training errors are high
- Overfitting – validation error is high, whereas training error is low
- Fitting – low validation and training errors
- Extra research is necessary - validation error is low, and training error is high

Obviously, the desired case is a fitting model, when both errors are low.

## 4.2.3 Testing and Splitting the Dataset

When the network architecture is finally defined and the hyperparameters are tuned, the ANN evaluation is conducted. For that purpose, a test set is compiled. It is not necessary to label the dataset unless to trace the network accuracy. The only demand is that the labels should be the same in training, validation, and testing sets, so that the model has actually learned the full number of classes and also performed on all of them. If the testing phase was successful, the model can be employed in real-life conditions.

Apart from that, validation and testing errors are often compared. For the best case, these errors should not differ within a high range, as overfitting or underfitting are likely to occur.

In order to avoid such problems, the whole dataset should be correctly split. As a rule, validation and testing sets are divided equally. The training set has to be the largest among the three, as the network has to learn as many features as possible. If the initial data is well prepared, and the network had enough data to adjust the weights and biases, then it should perform well on the validation and test sets. The reason, why sets for the last two phases are chosen to be equal is the fact, that during validation and testing the number of layers is not changed. It means that the network basically doesn't change during validation. So, the overall process is the same. However, there might be the case, where validation is conducted together with training on the same set. This is called cross-

validation, and will not be discussed here. Therefore, the only use of the testing phase is to approve and validate the tuned model on the data, which it has never seen before.

### 4.3 Convolutional Artificial Neural Network

In convolutional ANN (or CNN) the input layer is represented by image pixels, which are to be captured and analyzed, whereas on the output layer there are pre-determined classifiers or scores, which are intended to categorize the image (or, as in our case, classify the cuttings, depending on the shape, size, and lithology). The general structure of convolutional ANN is shown in Figure 42. Different types of layers with the help of images from the CIFAR-10 dataset are discussed, which is commonly used for training artificial networks.

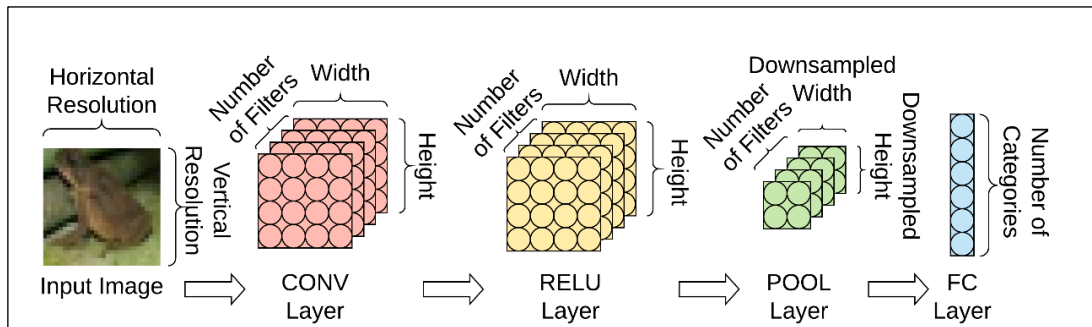


Figure 42: Principle CNN Architecture

#### 4.3.1 Input Layer

The input layer holds the initial image, which is desired to be analyzed. It is represented by raw pixel values of horizontal and vertical position, as well as the number of channels (in our case it is three, which corresponds to RGB). The resolution of the CIFAR-10 image is 32x32 pixels. As a result, there is a 32x32x3 matrix as an input volume (Figure 43).

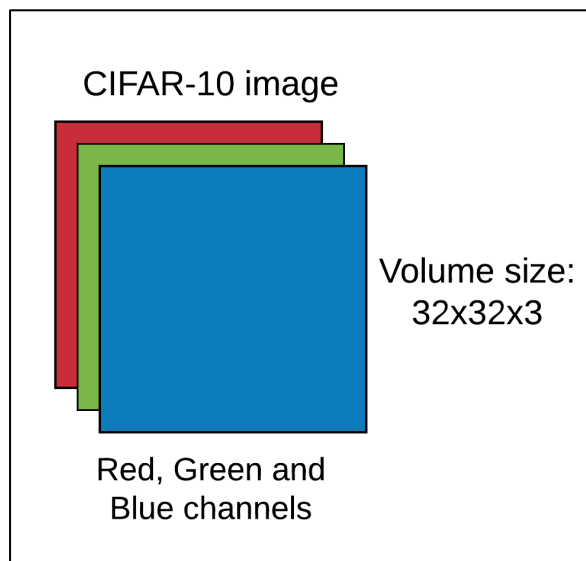


Figure 43: Schematics of the Input Layer



### 4.3.2 Conv Layer

Conv (or convolutional) layer is three-dimensional, as the neurons are packed in stacks. The number of stacks (or depth dimension) is equal to the number of filters needed to actually identify the information from pixels (Figure 44). Within one stack the neurons are aligned spatially into width and height dimensions. In the simplest case, each neuron in a stack is to analyze one single pixel from the image. During forward pass the layer slides (or convolves) along the image width and height and calculates the dot product between the input and filter parameters. This process iterates along the depth dimension, where different filters are applied. Usually, it is more useful to use a neuron to capture not a single, but a certain number of pixels from the image to save processing time.

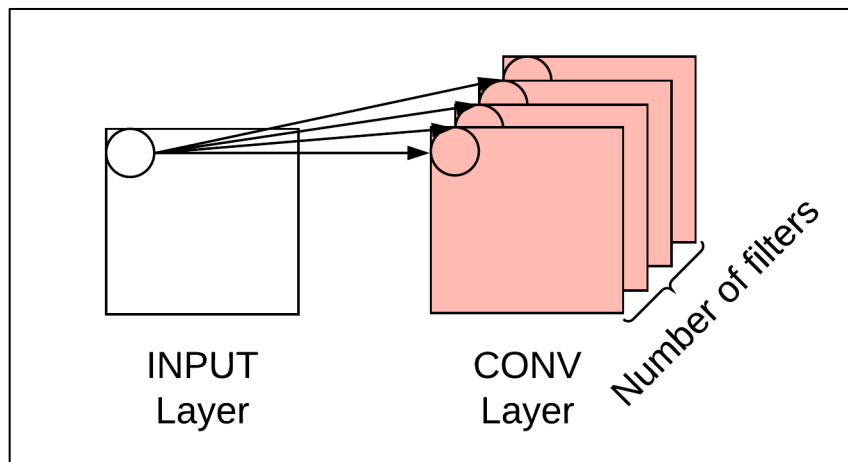


Figure 44: Schematics of the Conv layer

From the mathematical point of view, filters are relatively small matrices, which are filled with certain numbers. When the filter is applied to the array of pixels, it computes the dot product with each corresponding pixel value and then gets the sum of the products. Consequently, the filter produces only one value after projection on one part of the pixel array. In the example in Figure 45 the filter slides along the array, computing the sum of dot products of each of the three steps. As a result, a 5-number array as an input and 3-number array as the output is obtained. Filters generally needed for searching and extracting image features like edges, corners, or colour patterns. Visually, the result looks like changing image contrast, brightness, saturation, etc.

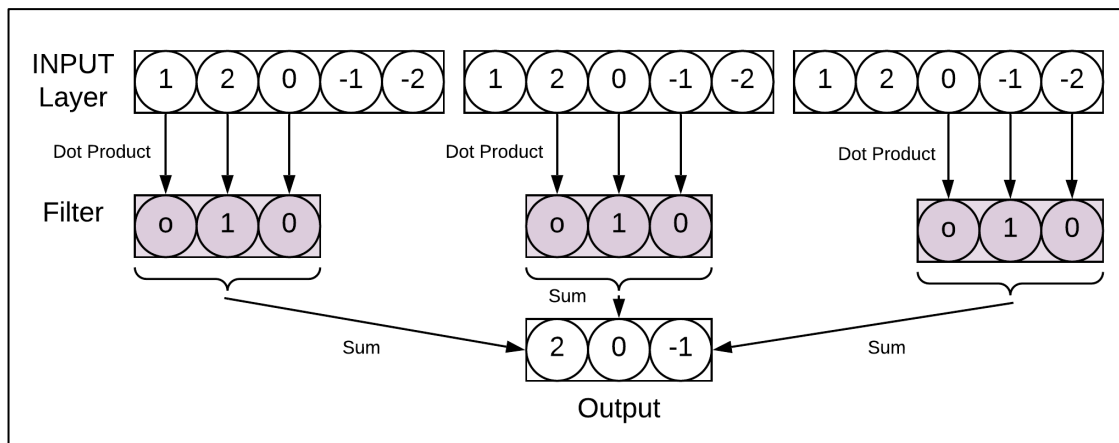


Figure 45: Working Principle of the Filter

As was said above, the output volume of the Conv layer is not necessarily of the same size along spatial dimensions, as the input image. Here it is needed to consider Stride  $S$  and Zero Padding  $P$  parameters.

Stride is defined as the number of pixels, which filter passes through when sliding across the image. For example, when  $S = 1$ , then for each iteration the filter passes through every neighbouring pixel. When  $S = 2$ , it “jumps” over one pixel (Figure 46). Consequently,  $S = 1$  ensures larger output size spatially, however, the number of iterations to count increases.

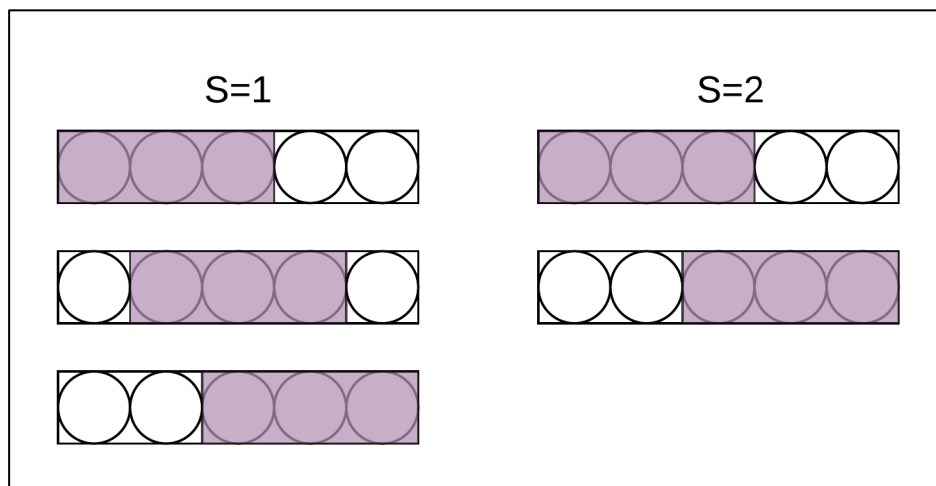


Figure 46: Demonstration of Stride Parameter. Blue Frame Represents a Filter, Which Slides Along the Pixels

Zero-Padding parameter  $P$  basically adds a frame around the image matrix filled with zeros. It is very useful for controlling the spatial output size and fitting the filter with certain  $S$  value. In Figure 47 there is the following example: An input layer of size 5 is convolved with a filter of size 4 with  $S = 3$ . If  $P = 0$ , then there is no place for the filter to fit inside the INPUT layer. However, by adding zeros at the sides of the input layer, the filter will stride and not yield errors. In this case,  $P = 1$ , which means adding one zero on each side.

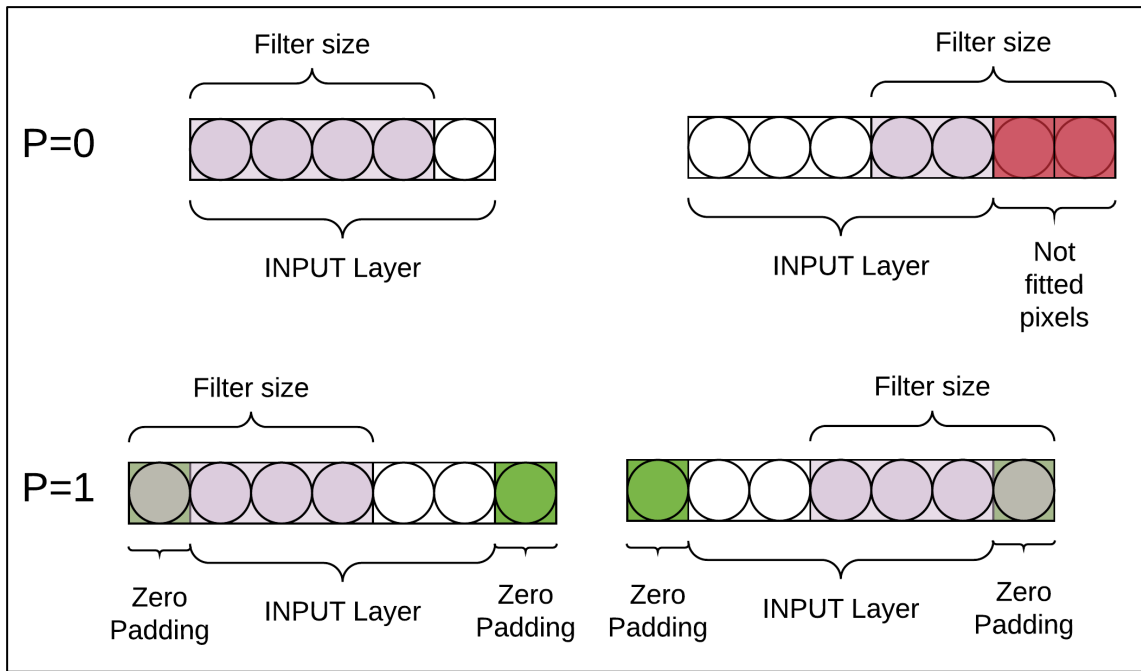


Figure 47: Demonstration of Zero Padding Application

Having the above parameters considered, one gets the following formulas, connecting input size with output size of the Conv layer:

$$W_{out} = \frac{W_{in} - F + 2P}{S} + 1 \quad (12)$$

$$H_{out} = \frac{H_{in} - F + 2P}{S} + 1 \quad (13)$$

$$D_{out} = K \quad (14)$$

Where  $W_{in}$ ,  $W_{out}$  – input and output widths correspondingly;

$H_{in}$ ,  $H_{out}$  – input and output height correspondingly;

$D_{out}$  – output depth;

$F$  – filter size;

$P$  – zero padding;

$S$  – stride;

$K$  – number of filters

### 4.3.3 ReLU Layer

ReLU (or Rectified Linear Unit) layer is designed to apply the activation function. The layer volume is similar to the previous one. Usually, among all activation functions, a rectified linear unit function is used, because it is employed computational simplicity, representativity, and linearity. This function can be described with the equation as follows:

$$f(x) = \max(0, x) \quad (15)$$

Where  $x$  – function argument

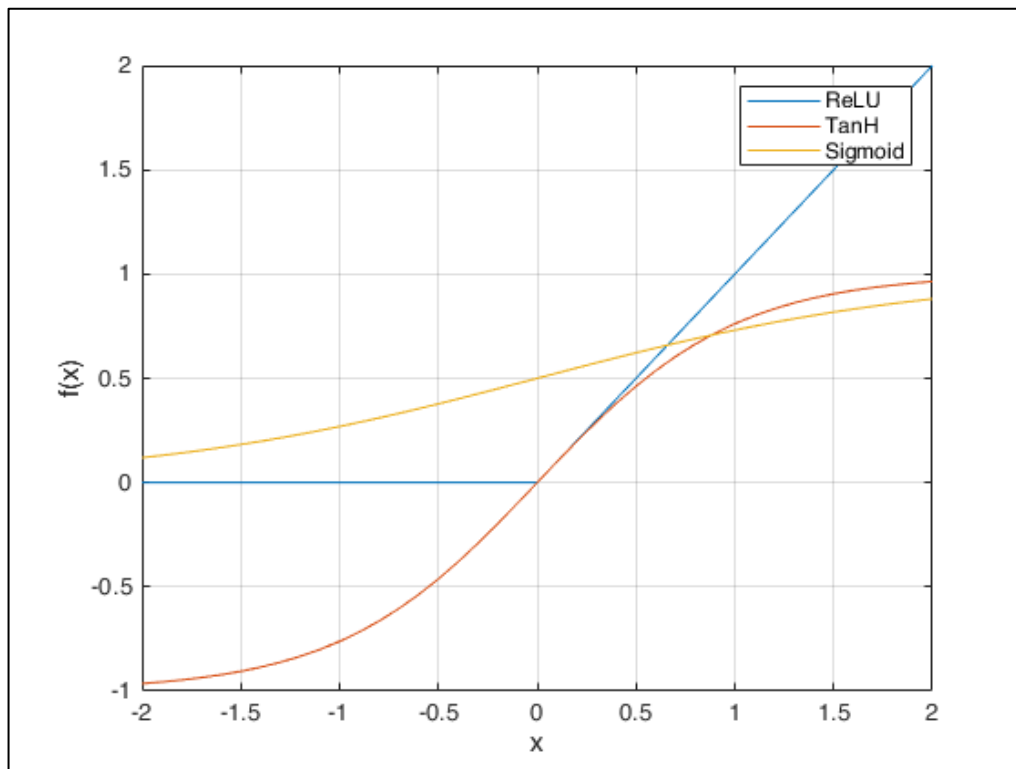


Figure 48: Comparison of ReLU, TanH, and Sigmoid Functions

It means that the function will increase linearly and monotonously on a range of  $(0, \infty)$  and flatten on a range of  $(-\infty, 0]$ . In comparison with other activation functions, as it is seen in Figure 48, TanH and Sigmoid functions are very sensitive to arguments in the vicinity of zero, while having large or small numbers yield more or less the same result. In addition, these functions utilize exponents to calculate the output. They also don't deliver the true zero value. In contrast, ReLU always returns zeros, if the argument is negative, and uses no additional functions to give the output. This saves computational time, which is demanding for training deep networks.

#### 4.3.4 Pool Layer

Pool (or pooling) layer performs the downsampling operation along the width and depth dimensions, which saves the computing power and avoids overfitting. This layer is usually placed between Conv layers. Most commonly the image is upsampled, taking the maximum value among each  $2 \times 2$  region, discarding 75% of neurons. The working principle of this layer is similar to the Conv layer: the filter slides across the matrix, performing certain operations and yielding the result. However, in this case, the filter takes the maximum value out of those, on which the filter is focused on. In Figure 49 there is an example, how the Pool layer works. There is a three-dimensional array as an input and a filter with  $F = 2$  and  $S = 2$ . When the filter slides across the array, it takes every  $2 \times 2$  squares of data, then takes maximum value out of each and outputs exactly two times smaller array in sense of spatial dimensions.

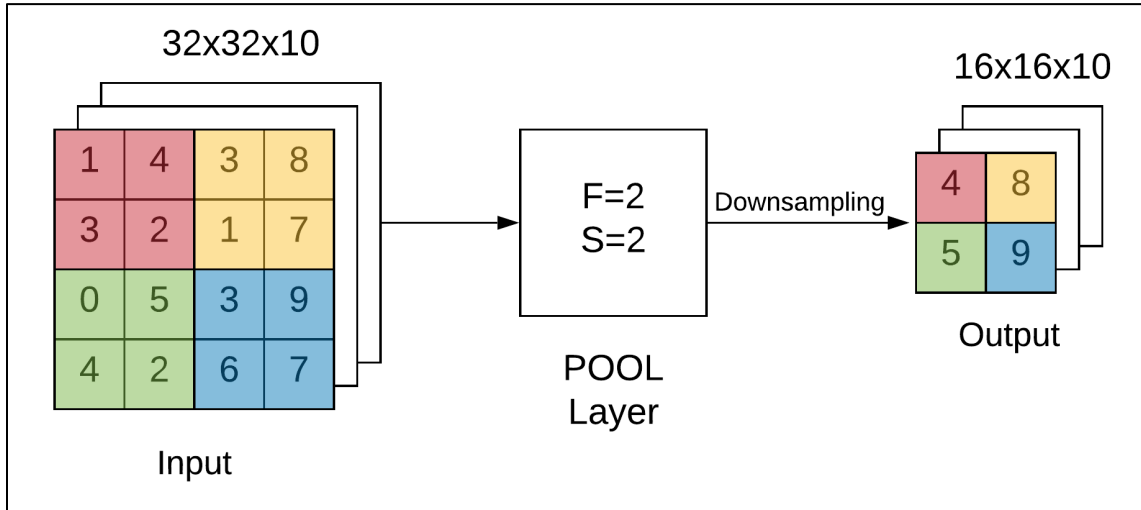


Figure 49: Example of Pool Layer Performance

Similarly, with Conv layer, it is possible to calculate the output size of Pool layer with arbitrary parameters:

$$W_{out} = \frac{W_{in} - F}{S} + 1 \quad (16)$$

$$H_{out} = \frac{H_{in} - F}{S} + 1 \quad (17)$$

$$D_{out} = D_{in} \quad (18)$$

### 4.3.5 FC and Softmax Layers

Fc (Fully connected) layer consists of classifiers, which report the ANN output. This layer is called fully connected, as each neuron from this layer is connected to every neuron from a previous layer, unlike Conv, which is responsible for only a certain amount of Input. In simple terms, the FC layer maps the distributed feature representation to the sample label space. The operations in each neuron are principally the same, as shown in equation (12).

The Softmax layer employs a softmax function, which is also called a normalized exponential function. The intention of this layer is to take the outputs of the fully connected layer and to normalize them into a probability distribution. The highest value of the Softmax layer is considered as the best matching label for the input image.



# Chapter 5 Conceptual Design of the Proposed Technology

## 5.1 Overview

During the discussion in the previous chapters, it was stated that the borehole stability issues are of high importance and should not be overlooked. One of the methods for direct and proactive borehole instability signs identification is cavings analysis. The main benefit of this method results not only in recognizing the instability but also in determining its type and mechanism of generation. In this sense, cavings hold the features, which indicate the complication type. These are basic shapes and sizes. Another cavings feature to consider is lithology, which could link to the unstable interval, giving the information about the possible complication occurrence.

One of the conclusions that were drawn from the previous chapters regarding the conventional cavings analysis methods, is that these methods are time-consuming and require several employees in the workflow to achieve good results. Hence, there is a demand for an automated cavings analysis system, which can overcome the main shortcomings of the conventional methods. The effective automated system should minimally have the following features. Firstly, it should deliver results in real-time, as soon as the cavings appear on the screens. That way the warning signs will be delivered to the mud logger immediately so that the crew would have more time for making a decision. Secondly, it should be completely autonomous, requiring only the installation procedures and initial software or hardware adjustment. Thirdly, the system should yield all the features mentioned above: shape, size, and lithology. For that reason, each of the cavings should be analyzed individually. This creates additional requirements for the associated algorithm, which increases its complexity. Lastly, the results should be accurate and valid. This is the most challenging demand for the algorithm, as shape determination is an uncertain and subjective process. Because of that, the system should be tested in presence of an experienced employee who can give recommendations about algorithm accuracy.

The road map of the proposed system is illustrated in Figure 50. It comes into effect when the rocks appear at the screens. The cavings need to be washed to make it possible to obtain their colour for lithology classification purposes. Afterwards, the image is captured by a video camera, which transfers obtained data to the computer with pre-installed software for cavings classification. As long as the software employs computer vision technology, it will be powered by CNN, which requires training, validation, and testing. These processes were explained in Chapter 4. Here it is to be assumed that the algorithm is already trained. It is not possible to detect the cavings on the screens, the system should also report on mud overflow events or absence of any complications at all. If the cavings are detected, the shape and size are determined. These parameters are reported immediately to the mud logger, notifying about a possible complication. Afterwards, the software attempts to identify the lithology. If the cavings are poorly washed, or there is another reason why the lithology could not be determined, this step

is skipped. Elsewise the lithology is combined with logging data. If there is a match with logs in terms of lithology, each individual caving is associated with the corresponding interval. In addition, obtained data could be placed either with reference to appearance time on the shakers or with correction for the lag time. In this case, not only the borehole instability type is reported, but also the approximate depth range of its occurrence. This data could be used for automatic report generation.

The whole system is formulated with two aspects: hardware and software. The hardware part includes all the equipment, ensuring the cavings’ cleaning and capturing of their image. The software part, in its turn, performs the video frame analysis and delivers the cavings parameters and also alarms the drilling crew, if there is an increasing complications possibility. It is based on CNN, which architecture is discussed in Chapter 4. The software is assumed to be pre-tested on a set of data, and its final version is actually run on a computer at the rig site.

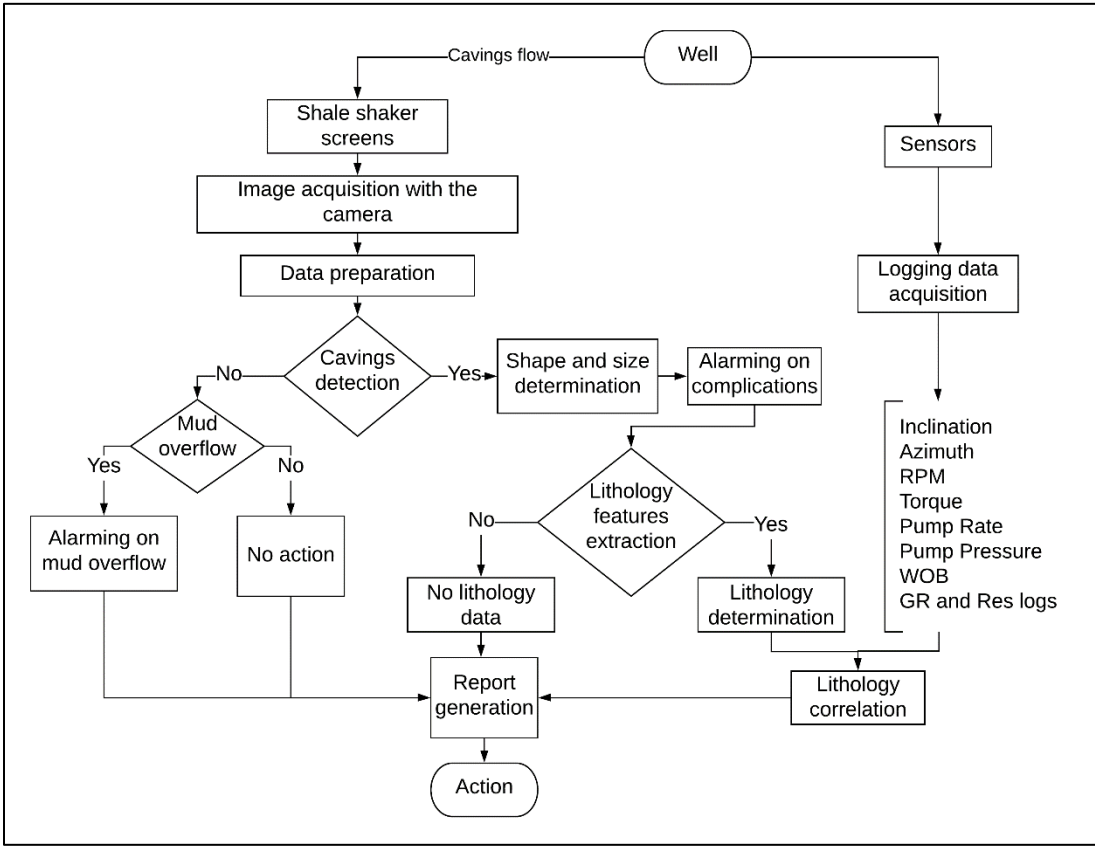


Figure 50: Road Map of the Proposed System

## 5.2 Hardware and equipment

This section includes all the equipment needed for proper system functioning. The exterior design of the installation is shown in Figure 51. As it is seen, the shale shaker and its parts are not changed, however, some modifications are done and a certain amount of equipment is installed. The equipment includes: circulation system and supporting stand with mounted camera, light source, and tent on it.



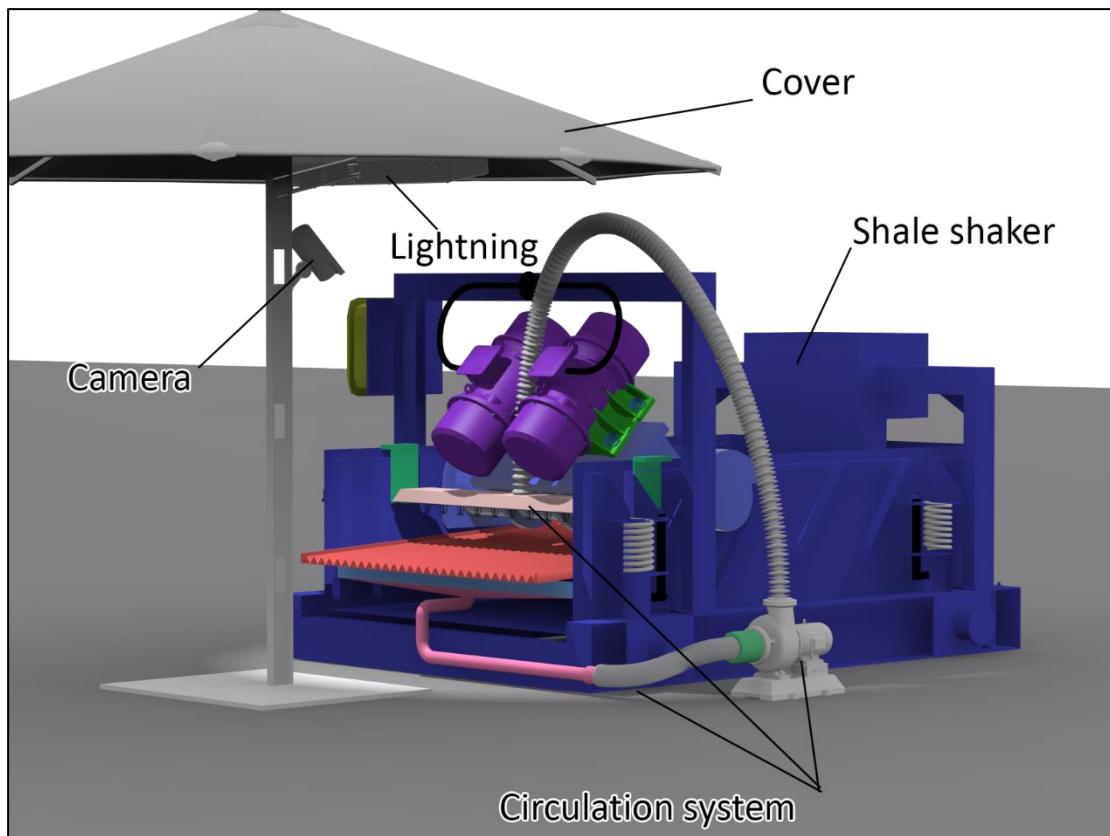


Figure 51: Exterior Design of the Hardware Part of the Proposed System

### 5.2.1 Shale Shaker Modification

As it was discussed, one of the major modification to the shale shaker is the circulation system. The main function of the circulation system is to clean the cavings prior to their appearance in the camera field of view. This is basically needed for lithology determination. If it weren't for cavings washing procedure, they would be covered in remaining mud and finer particles. This system includes the pump, discharge hose, sprinkler head with fixed sprinklers on it, a tray for collection of the base fluid, and filter, as illustrated in Figure 52 and Figure 53. In this section, each of the elements is discussed.

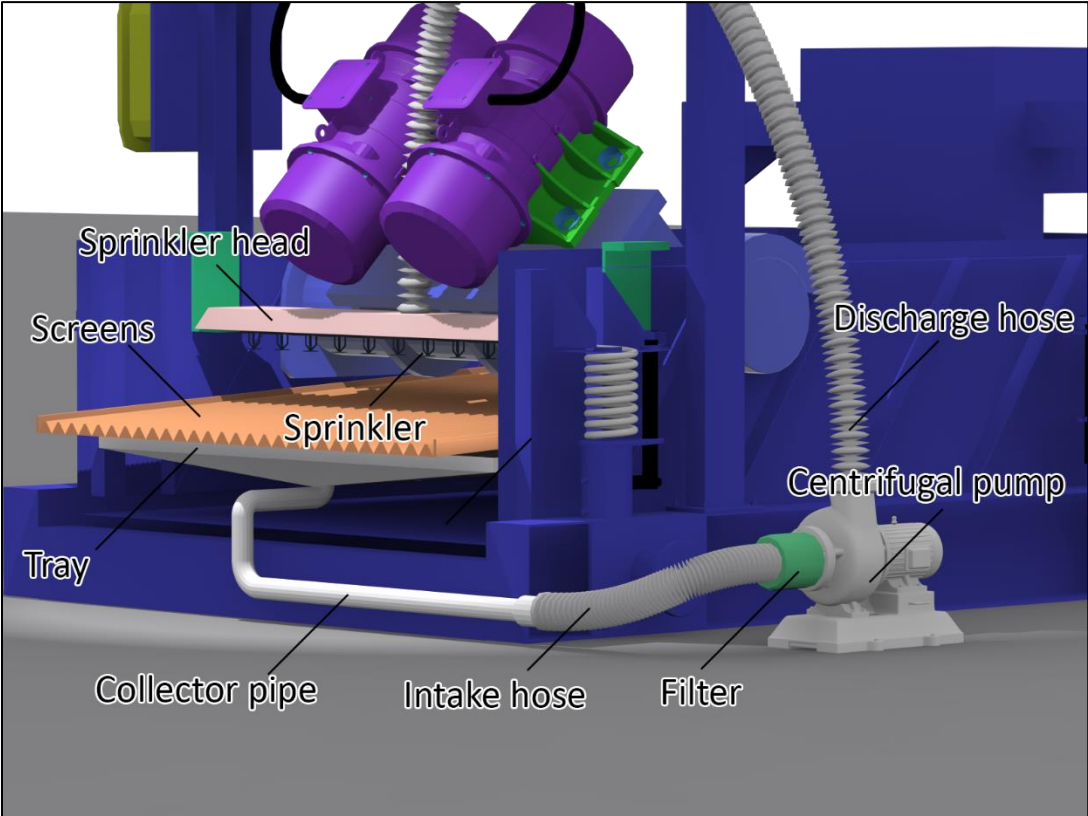


Figure 52: Proposed Modification of the Shale Shaker Design

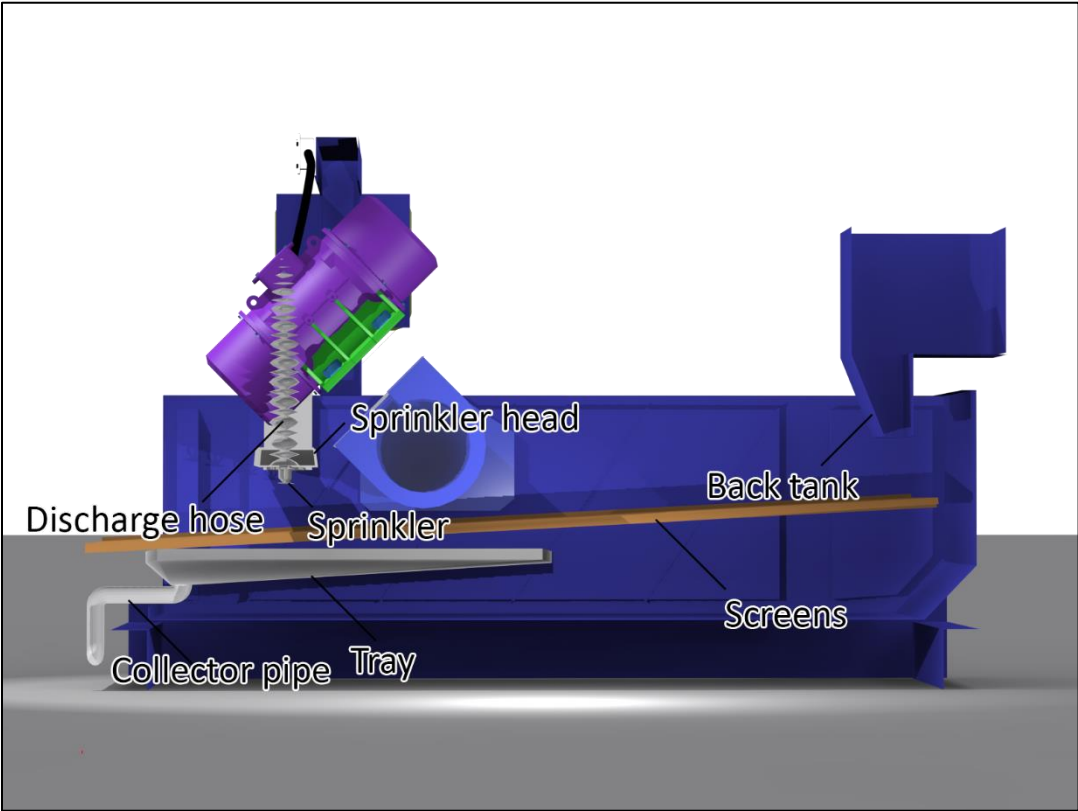


Figure 53: Sideview of the Modified Shale Shaker

### 5.2.1.1 Tray

The functioning of the system begins with the tray, which serves at the same time as a holding tank for all of the base fluid and a discharge place, where the fluid is reflux from the sprinklers. The tray is either screwed to the shaker base to the sides or to the bottom, excluding the transmission of vibrations. Two points should be taken into consideration. The first one is its volume, which should be enough to accommodate the volume of all the pipes, pump itself, the sprinkler head, and some extra volume to maintain continuous circulation without cavitation. The second one is its angle of inclination, which ensures the gravity flow of the base fluid towards the pump intake. Another important point is the location of the sprinkler head. There should be enough time for the cavings before passing it to the camera for image capturing. At the same time, if it is placed too close to the back tank, there is a high possibility of the actual mud appearing on the tray.

### 5.2.1.2 Collector Pipe and Hoses

The most convenient way to allocate the collector pipe, which is attached to the tray bottom, is to pull it out of the shaker's front side. There is likely to be little space for hydraulic communications within the shaker. For that reason, either the pipe or the hose could be used. In a system illustrated in Figure 52, a pipe is used, as it is easier to clean and dismantle it. The possibility of pipe disassembling plays its role when fine particles block the cross-section, and there is a need to unclog the pipe.

At the same time, the collector pipe should be connected to the pump with a hose, as the pump location is not fixed. At the same time, the discharge part of the pump should also be connected with a hose, as shale shaker's vibrations might affect the threads of the connections.

### 5.2.1.3 Filter

As long as the base fluid is sprinkled through the screens, there is a high possibility of fluid contamination with mud and fine particles. This might be a very important issue, as the particles can eventually block the collector pipe. This will lead to fluid loss at the pump intake and its overheating. In addition, fine particles seriously affect the pump performance independently of its type, as they erode the pump's surfaces. For this reason, either a water or an oil filter should be installed at the intake. The filters should be changed during system functioning, and there is the only demand for the intervention of the employee into the operation.

### 5.2.1.4 Pump

For the purposes of fluid circulation, a centrifugal pump is selected. Pumps of this type have the following advantages:

- Simpler construction because of fewer moving parts
- Smaller dimensions
- Availability on the market
- Greater discharging capacity
- Stable flowrate

## Conceptual Design of the Proposed Technology

- Low cost

A lot of centrifugal pumps in the power range of 0,5 to 1,5 horsepower are available on the market, which is enough to circulate the base fluid. There is no need for constant control of discharge pressure, so that the pump may work in standalone mode. The electrical power supply is desired because of lower costs and simplicity of connection. However, the HSE requirements should be met, as shale shaker is located in a zone, in which an explosive atmosphere is likely to occur. For this reason, it should be checked if the pump power supply connections are explosion-proof.

### 5.2.1.5 Sprinkler Head

The sprinkler head is employed with individual sprinklers. The head gets the base fluid from the discharge hose and distributes it between the sprinklers so that the whole screen surface is covered. For the purposes of cavings cleaning, a simple fire protection sprinkler could be used. Their function is to atomize the liquid onto the cavings to clean them from the fine solids, soft clay, and residues of drilling mud. It is important to ensure enough pressure to actually clean the particles and not just cover them with base fluid. For ensuring cavings' cleaning efficiency, the sprinklers should be aligned in the opposite direction of the cavings movement along the screen. The location of the sprinkler head is chosen according to the usual shale shaker design (Figure 54). It is not difficult to notice that the motors for the vibrators are usually located at the top of the basket and relatively close to the gutter. This narrows down the possible positions of the sprinkler head. It is also needed to monitor, at which interval the mud stops appearing above the screens and is fully filtrated. The best place to allocate the sprinklers would be right in front of the motors, hanging on basket walls.



Figure 54: Examples of the Shale Shakers. MONGOOSE PRO (Left) and GN Solids Control GNZS703 (Right) (Schlumberger 2013) (GN Solids Control 2020)

### 5.2.2 Camera Design And Placement

The shale shakers due to their vibrating performance, appear to scatter the waste on the surroundings, which is usually seen as patches of mud and clays on the equipment parts. For this reason, it is rationally to place the camera as far as possible from the screens, but

not too far, so that camera's resolution is enough to capture as much information, as possible.

The weather conditions are another problem to deal with. Rain, fog, and snow might significantly affect camera in a sense of the appearance of water droplets on lenses, blocking the camera's field of view, interfering with shaker screens, creating artefacts in images as a consequence. That means that the camera and its field of view have to be fully isolated from the environment. This could be done cheaply by placing a shelter above the device and the end of shaker screens. In the same way, this shelter shall allow the employees to easily do shaker's maintenance (e.g. repairing, changing screens, checking the cuttings separation conditions). In addition, there shall not be the case, when the sunlight is coming into the camera, so the employee should choose the best place for the camera in order to avoid filming against the sun. The easiest way is to place a small tent above the camera in order to make the measurements as pure as possible.

Another point to consider is explosion protection. Shale shakers' environment is not explosion-proof, as the cuttings and mud could contain hydrocarbon traces. In addition, gas separators are usually present in the vicinity of the shakers, as they are part of the mud treatment system. The zone around shakers is classified as Zone 1 according to ATEX directive as such: a place in which an explosive atmosphere consisting of a mixture with air or flammable substances in the form of gas, vapour or mist is likely to occur in normal operation occasionally. For that reason, explosion-proof enclosures are manufactured. According to ATEX, the housing is labelled as an Ex-d code, meaning that a device would withstand an internal explosion and provide relief of the external pressure via gaps in the construction such as threaded connections or flanges (European Commission 2000). An example of such an enclosure is illustrated in Figure 55. Such enclosure shall also protect the camera lens from contamination.



Figure 55: An Example of Explosion-Proof Enclosure (SAMCON GmbH 2020)

Conceptual Design of the Proposed Technology

The camera itself should be cost-effective, compact, with high enough resolution sensor, having no conflicts with the software, and being able for fast data transmission. For these reasons, the camera from FLIR® Blackfly® S GigE series is used (Figure 56). The cameras range depending on the lens mount type, frame rate, resolution, chroma, etc.



Figure 56: FLIR® Blackfly® S GigE Camera (FLIR® Systems 2018)

Technologies, discussed in Chapter 3, utilize cameras with frame rates not greater than 6 fps. The number of megapixels was around 2. The camera was chosen with regard to these values, as there was no possibility to test and compare the cameras. The chosen camera specifications are listed in Table 15. It is usually possible to change the frame rate, so the initial amount of fps could be reduced.

Table 15: Camera Specifications

Parameter	Value
Serial number	BFSPGE-23S3C-C
Frame Rate	53
Lens Mount	C-mount
Pixel Size	3,45
Resolution	1920 x 1200 px
Sensor Type	CMOS
Sensor Format (Diagonal)	1/2.3" (7.9 mm)
ADC (Analog-to-Digital Converter)	10 bit, 12-bit
Chroma	Colour
Megapixels	2.3
Readout Method	Global shutter
Sensor Name	Sony IMX392

The camera transmits the data via the GigE interface standard, which is developed using the Gigabit Ethernet communication protocol. The standard was introduced intentionally for industrial cameras. Its advantages over other interfaces (like USB 3) are:

- The high bandwidth of 125 MB/s
- Allowable cable length of 100 meters
- Low-cost cables

Having the possibility of using long enough cables, it is reasonable to connect the camera directly to the mud logger unit, where all the other data from sensors is acquired. That would allow us to combine the acquired lithology from cavings with logs, obtained from sensors. It would be reasonable to allocate enough Random-Access Memory (RAM) for the software, because, as it was reviewed in Chapter 3, the software would require up to 8 GB of memory, which is a relatively high amount. Having the computer with an installed software together with a data processing facility in the mud logger unit will allow us to share the data within one framework and ensure faster data transmission. In addition, all the computers will be held in the same place, which enhances convenience for the mud logger.

With regards to the power supply, the camera should plug to the power source with 3.3 V and 120 mA voltage and current load correspondingly. It is also convenient to use the DC-adaptor, located in the mud logger unit.

The camera is manufactured without the lens. Usually, lenses for such cameras have fixed focal length, which depends on the object size, distance from the object, and sensor size. The focal length is calculated as follows:



Conceptual Design of the Proposed Technology

$$\frac{1}{u} + \frac{1}{v} = \frac{1}{f} \quad (19)$$

Or

$$f = \frac{uv}{u + v} \quad (20)$$

Where  $u$  – distance to the object;

$v$  – distance to the image;

$f$  – focal length.

The dimensions are illustrated in Figure 57.

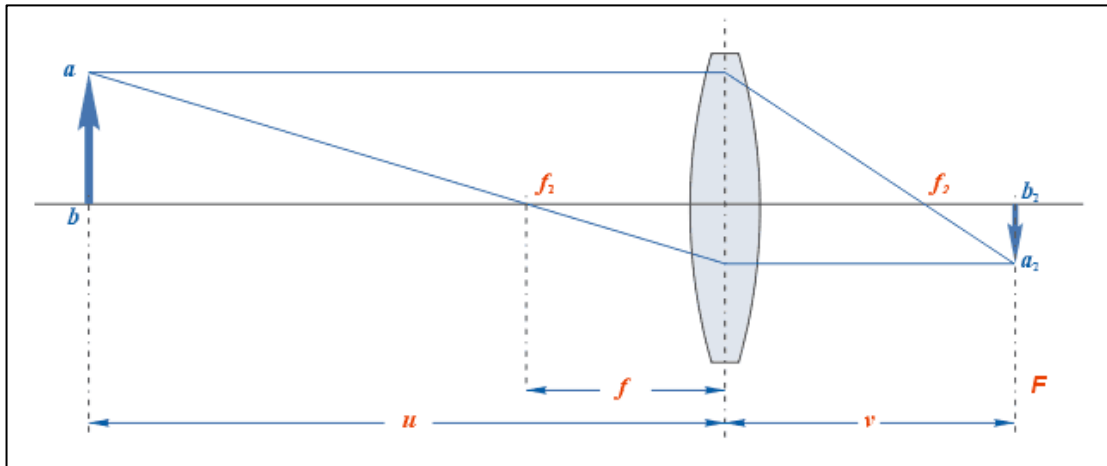


Figure 57: Direction of Beams in a Thin Lens

The simplified diagram for the actual camera is shown in Figure 58 (actual direction of beams is more complicated, in contrast to illustration).

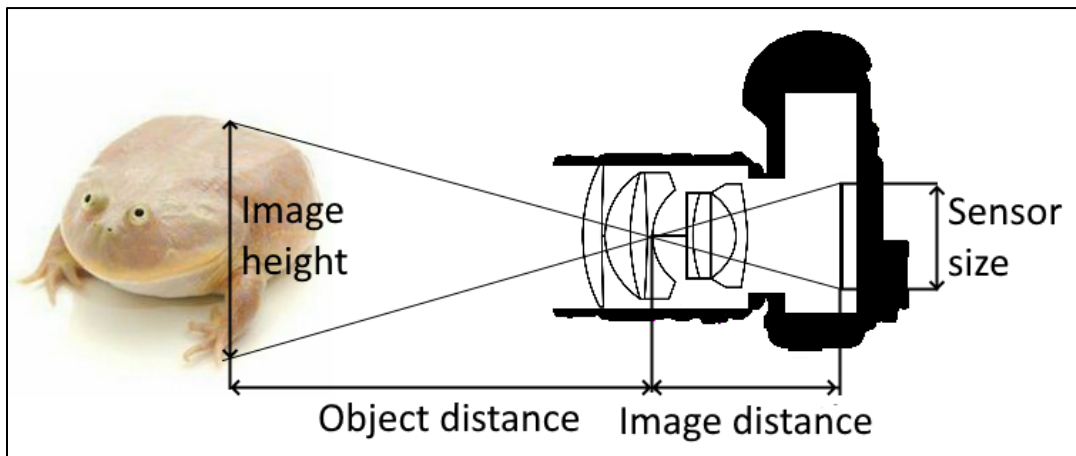


Figure 58: Schematics of Camera Working Principle to Calculate the Focal Length

Constraining the equation for similar triangles:

$$\frac{u}{H} = \frac{v}{S} \quad (21)$$



$$v = \frac{u \cdot S}{H} \quad (22)$$

Where  $S$  – sensor size

$H$  – object's largest dimension (width or height)

After substitution:

$$f = \frac{uv}{u+v} = \frac{u \frac{u \cdot S}{H}}{u + \frac{u \cdot S}{H}} = \frac{uS}{H+S} \quad (23)$$

The typical width of the shaker screens reaches 59.5 inches (1511 mm) (M-I L.L.C 2019). The image sensor size is specified in Table 15. As long as the distance of the camera is uncertain so far, it will be ranged from 1 to 3 m. The results are the following:

$$f = \frac{1000 \cdot 4.5}{1511 + 4.5} = 2.97 \text{ mm} \quad (24)$$

$$f = \frac{3000 \cdot 4.5}{1511 + 4.5} = 8.91 \text{ mm} \quad (25)$$

So, the selected camera will utilize a lens in a range of focal distances from 2.97 mm to 8.91 mm. There is an important fact that lenses designed for smaller sensors are not applicable to larger sensors. As long as the sensor size is 1/2.3", which is not very typical, the lenses were selected in compatibility with sensors with sizes 1/2", 1/1.8", 2/3", 1", etc. However, increasing the sensor increases the crop factor, which determines, how the focal length will change. The most affordable lenses, designed intentionally for machine learning applications are listed in Table 16.

In terms of sensor size, both Fujinon and Edmund Optics lenses would have minimal distortions for our sensor size. These lenses are designed to fit 5MP and 8.8 MP sensors, so this will definitely match the chosen camera. However, lenses manufactured by Edmund Optics, are the cheapest ones. Importantly, Fujinon HF6XA-5M has anti-vibration technology, which speaks well of its installation at the shale shakers. As long as they have the same focal length, it does not matter, which one to choose.

The crop factor for this lens is calculated as follows:

$$k_{cr} = \frac{d_{max}}{d_{used}} = \frac{8 \text{ mm}}{7.9 \text{ mm}} = 1.01 \quad (26)$$

Where  $k_{cr}$  – crop factor

$d_{max}$  – maximal sensor diagonal

$d_{used}$  – used sensor diagonal

That way, the apparent focal distance is decreased times crop factor:

$$f_{apparent} = \frac{f_{actual}}{k_{cr}} = \frac{6}{1.01} \text{ mm} = 5.94 \text{ mm} \quad (27)$$

This means, that having the selected lens on the chosen camera installed, the image will be a bit larger, as there is a smaller value of focal length. The difference is not high so that the distortions are minimal. The resulting focal distance is located in the range of

suggested distances. To calculate the new distance to the object, equation (23) has to be rearranged:

$$u = \frac{f(H + S)}{S} \tag{28}$$

Table 16: List of the Appropriate Lenses for the Suggested Camera (Tamron Europe GmbH) (Fujifilm Corporation) (Edmund Optics Inc.)

Parameter	Tamron M112FM08	Fujinon HF8XA-5M	Fujinon HF6XA-5M	Edmund Optics 6mm UC Series
Sensor size	1/1.2"	1/2"	1/2"	1/2"
Minimum Aperture	F/2.4	F/1.6	F/1.9	F/1.85
Maximum Aperture	F/16	F/16	F/16	F/11
Focal length	8 mm	8 mm	6 mm	6 mm
Horizontal x vertical view angle	70.3° x 54.9° (for 1/1.2" sensor)	58.4° x 44.6° (for 2/3" sensor)	74.7° x 58.1° (for 2/3" sensor)	60° x – (for 1/2" sensor)
Minimum object distance	0.1 m	0.1 m	0.1 m	0.1 m
Megapixel	5 MP	5 MP	5 MP	8.8 MP
Mount	C	C	C	C
Price	279 \$	288 \$	399 \$	210 \$

Substituting the values in (28):

$$u = \frac{5.94 \cdot (1511 + 4.5)}{4.5} = 2000 \text{ mm} = 2\text{m} \tag{29}$$

It means, that it would require two meters to install the camera, which is far enough to protect the lenses from contamination. Considering natural light conditions and the distance of installation, the best way to place the camera would be directly above the end of the screen pointing downwards. Such a way of installation would allow the personnel to operate the shakers without difficulty. In addition, the sun will not shine directly into the camera, while the rain will not fall directly on the lens. For the protection of the camera and screens from weather conditions, a cover above the camera should be placed. Furthermore, the sunshade is recommended, if the lens is designated in such a way. The installation is illustrated in Figure 59.

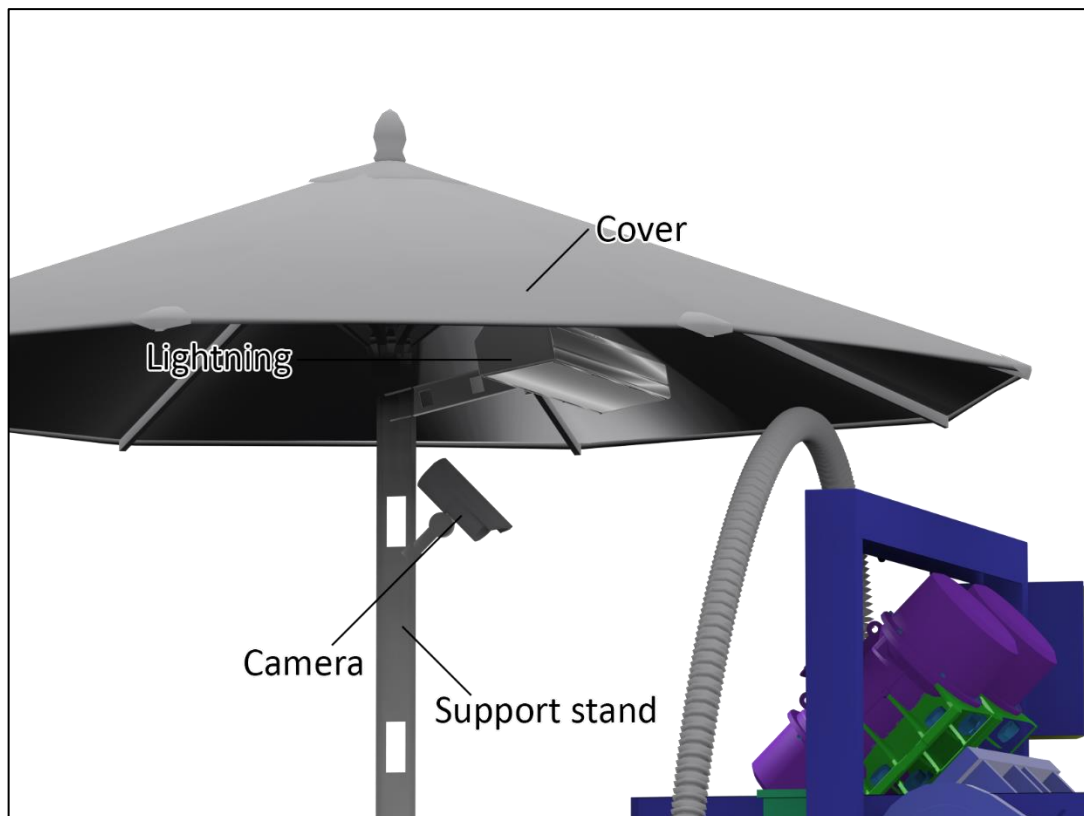


Figure 59: Camera Installation Setup

### 5.2.3 Light Source

As it was mentioned in Chapter 3, the most efficient and economical light source, ensuring uniform spectral distribution, is LED. For the considered case, the lightning should be evenly spread across the screens to exclude the possibility of single spots appearing brighter than others. This could be achieved with LED stripes. There are two varieties of them existing on the market: addressable and non-addressable. Addressable strips are designed in such a way, that each of the LEDs is a part of the array. Each of the diodes fires is controlled individually and addressed in order of precession. These stripes utilize three wires: power, ground, and data input. Non-addressable stripes fire the diodes all together without the possibility to control each of the light sources individually. These stripes may be both single colour or RGB (Red Green Blue). Single colour LED strip consists usually of white diodes having either the same colour temperature or different for the possibility of adjusting the light colour. For the aims of the proposed technology, a white LED strip is the best option. The colour temperature should be maximal, ensuring pure white light and absence of reflected colour distortions.

The strip should be able to perform in outdoor conditions. Even though it is supposed to be installed under the cover, there is also a possibility that humidity, fog, heavy rain, or splashes from the shaker may damage the electronics. For that reason, an IP (International Protection) codes were introduced (International Electrotechnical Commission 2013). The most commonly sold stripes have protection codes IP 40, IP 54,

## Conceptual Design of the Proposed Technology

IP 65, IP 66, IP 67. The first digit shows the solid particle protection, while the second one – liquid ingress protection.



Figure 60: Example of IP 65 Protection. The Strip Is Coated with Polyurethane

For the listed codes there are the following meanings.

First digit:

- 4 – effective against >1 mm particles
- 5 – the ingress of dust is not entirely prevented, but it must not enter in such quantity to interfere with equipment
- 6 – no ingress of dust

Second digit:

- 0 – no protection
- 4 – protection from water splashing
- 5 – protection from water jets (6.3 mm nozzle)
- 6 – protection from water jets (12.5 mm nozzle)
- 7 – no ingress of water in harmful quantity after immersion up to a 1-meter depth

Operating conditions at the rig site definitely anticipate dust appearance, so that dust protection has to be maximal. Considering water protection, it is needed to know that price increases with increased protection. Strong water jets are not expected under such operating conditions so that the fifth level of protection is reasonable. As a result, IP 65 protection should be used in this case (Figure 60).

To prevent light glowing towards the lens, it should be placed behind the camera ensuring that the beams are evenly distributed across the screen surface (Figure 59).

## 5.2.4 Cover

The cover illustrated in Figure 59 is shown for demonstrative purposes. It may vary depending on availability on the market, type, material, and size. It can also be crafted by the drilling crew from a piece of water-resistant material, like nylon or polyamide fabric by stretching it onto the carcass. The cover should be also mounted to the ground with wire ropes to protect it from harsh weather conditions and strong wind in particular. The supporting stand, which it is mounted to, shall also be attached to the ground.

## 5.3 Software

After the images capturing with the camera, the information is streamed to the software input, where it is to be analyzed. In order to get the algorithm working there are two networks to be trained: one for classifying shapes and another one for classifying lithology. Both of the networks belong to the CNN category, as long as they deal with image analysis. When the frame arrives at the input, it is automatically prepared for feature extraction. Afterwards, the first CNN for shape determination is run. If it is impossible to identify any cavings on the screens, there is an additional check for mud overflow conditions. If the cavings are detected successfully, the shape is determined. The shape is automatically reported to mud logger at this stage to warn about complications. Afterwards, size and lithology are detected in parallel. Size is calculated by edge detection algorithms, whereas lithology is found by employing another CNN. There is a chance of no lithology determination, as the cavings could not be cleaned properly. At the output, each of the cavings is assigned with shape, size, and possibly with lithology.

### 5.3.1 Network Building

The first stage is the input data collection. This should not necessarily be done at the rig site, as it does not matter, where to take the pictures. However, to make the scenario more real, the photos could be captured from the same position, as the features like edges and texture is likely to appear the same that way in real conditions. Furthermore, the cavings should be wet, as they are going to appear on the screens already washed by the base fluid. In addition, the photos could be also taken by placing the rocks on the sieves. The set should be split into training, validation, and testing sets. Training and validation sets have to be labelled in advance so that the CNN actually learns the features from given information. It was already mentioned in the literature, that the percentage of samples is taken in the amount of 60%, 20% and 20% for the training, validation and testing sets (Ran, et al. 2019).

After gaining the set for training and validation, the images should be fed into CNN. It is not necessary to build the network from scratch, as there are already researchers (mentioned in Chapter 3), who either used the already built model or designed a new one. The same architecture could be used for both shape and lithology detection. Training should stop when the loss reaches its minimum to avoid overfitting. After that training should take place. If the accuracy of the model is high, then it is to be used at the well site.

### 5.3.2 Algorithm Workflow

The proposed algorithm is illustrated in Figure 61. It starts with the proportional reshaping of the captured frame. Usually, up to six minimized copies of images are used. The point is that the frame is to be scanned with a pre-determined stride by CNN with a fixed size of the scanning matrix. It might be the case when the scanning matrix size is not enough to cover large objects. In this case, the frame dimensions are decreased with keeping the matrix size unchanged, which allows it to accommodate an object. When these transformations are made, each of them is passed into the CNN input.

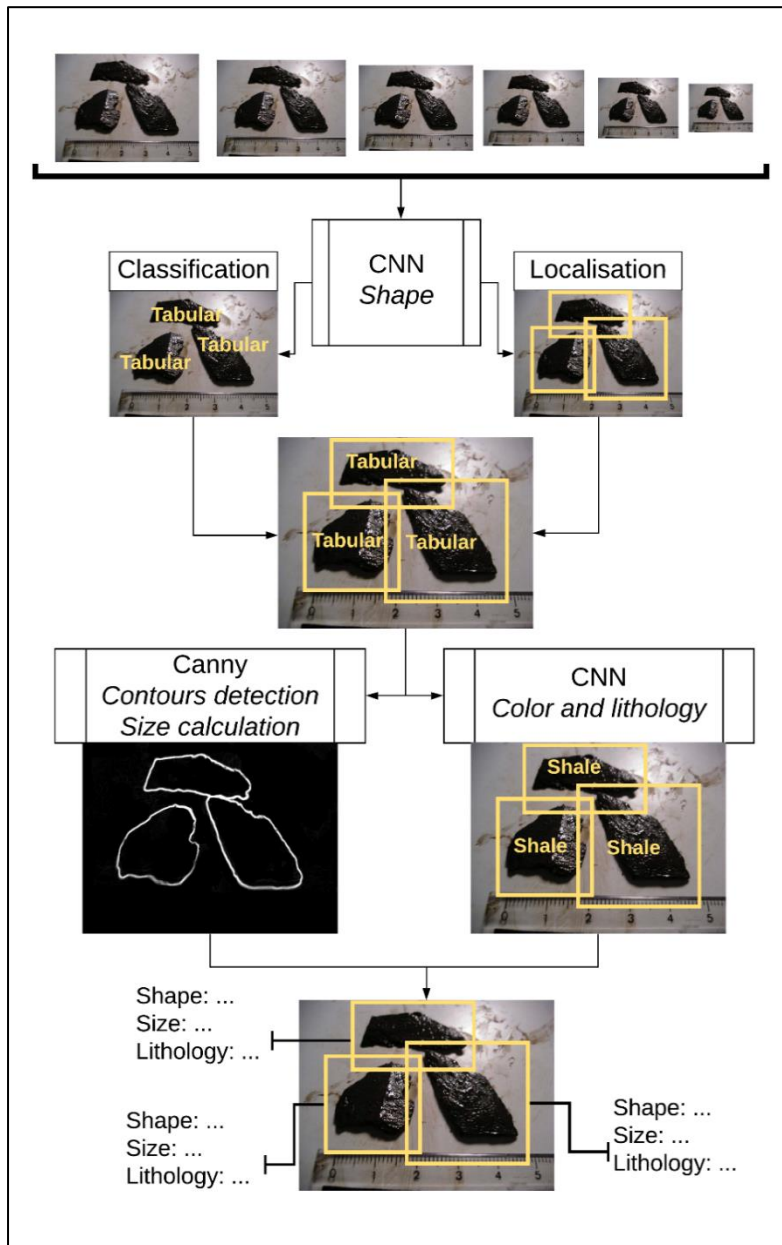


Figure 61: Workflow of the Parameters Detection Algorithm

There are three objectives to solve: detection, localization, and classification. Here it is considered that CNN is already trained and has obtained all the necessary feature maps. As it is seen in Figure 61, the algorithm is split into two directions. The left path goes to

the classification of cavings into shapes, while the right one performs detection and localization. These paths have FC layers and SF classifiers in each of them. The layers are of the same size and work simultaneously, so that feature extraction is synchronized with searching the object location. The detection is, as already was written above, is conducted via scanning each of the frames and looking for similar features, like corners, edges, patches, texture, etc. For each of the scanning steps the probability of the appearance of the searched object is obtained, as well as the coordinates of the bounding box. When the size of the scanning frame perfectly captures the object, the FC layer gives the maximum probability of finding the desired part of the image. As long as the movements inside the CNN are synchronized, for the obtained bounding box coordinates the classified shape is obtained. As a result, there is a labelled object at the output with a certain allocation on the frame.

In addition to shape labels, there could also be two extreme situations: mud overflow and absence of cavings at the shakers. If there were only shapes in the SoftMax layer, the CNN would only deliver shapes with a certain probability as an output, because the neural network always tries to guess the probability of appearance of each label. For that reason, two more labels should be introduced: the absence of cavings, when an only a small amount of rock material appears on the screens, and mud overflow, when the excess of the cuttings is visible. Both of the labels fall within the shape category and will be analyzed by the first CNN.

There are two more parameters, which are to be extracted: size and lithology. The results of previous operations will be used.

To detect the size, the Canny algorithm is applied, which determines the object contours. Afterwards, another bounding box is applied, as it has the ability to rotate. This was not the case with object detection, as the scanning of the image is proceeded by a matrix, which is oriented strictly in a horizontal direction. The newly build bounding box fits along the object's largest dimension. Afterwards, the size of the box is calculated, giving size on the output.

Lithology determination is proceeded inside of each localized objects. It is performed similarly to shape determination: the CNN scans the images for the particular features. Apart from patterns on the cavings surface and their contours, which are essential for shape detection, lithology is determined to base mostly on cavings colour, as well as the texture of the cavings surface. There are two reasons, why a separate network is desired for classifying lithology located at this part of the algorithm. The first one is a distinct group of features. It is not possible to allocate two different classifiers inside one CNN. As long as the intention is to get two classes for each separate caving, there is a need for an additional network. The second reason, why CNN is allocated at this stage is saving computing power. The first CNN gets as input six images, which are to be scanned. And each of these images is to be scanned multiple times. If it was the case, when two CNNs were running in parallel, there would be too many unnecessary calculations. This means that it is much more economically from the processing point of view to place the second CNN sequentially and not in parallel.

Another important point is the detection part of the algorithm. In some cases, object detection could be done not with CNN, but with the Canny algorithm, which detects

edges of the object. The main problem there is the background surface cleanliness and the presence of foreign objects. If the surface is not clean enough, it creates too much noise, as well as any other object appearing in the scene. When all the edges are detected, a threshold is to be applied in order to mask the noise and not desired entities. As long as the shale shaker screen is not a plain and smooth surface, where regular cuttings appear, it will be very difficult for the algorithm to extract only desired information.

### 5.3.3 Decision Support Matrix

A road map was developed to give the concerned person a list of operations to complete in order to deal with complications (Figure 62). A similar tree already exists in literature (Zausa, et al. 1997), and the one described there is partly based on it. However, in this thesis there will be a reference to cavings shapes only, suggesting almost all possible treatment methods which were described in Table 2.

The decision procedure starts with the confirmation of cavings' presence. Whether no cavings are present, but there are poor hole cleaning conditions occurring, there would be a suggestion for hole cleaning improvement or mud weight decrease. Hole cleaning efficiency is determined by mud overflow on screens when the shakers are overloaded with return cuttings. Poor hole cleaning refers to mud overflow, and measures should be taken in order to prevent new cavings from the formation. At the same time, normal drilling conditions require no remedial operations to be performed.

The other branch of the road map refers to the reporting of the cavings shape, which was determined previously by CNN. Here it is needed to specify the number of sequentially appeared cavings, after which the system starts alarming on possible complications. Otherwise, the algorithm will notify about issues after every single caving appeared on the shakers.

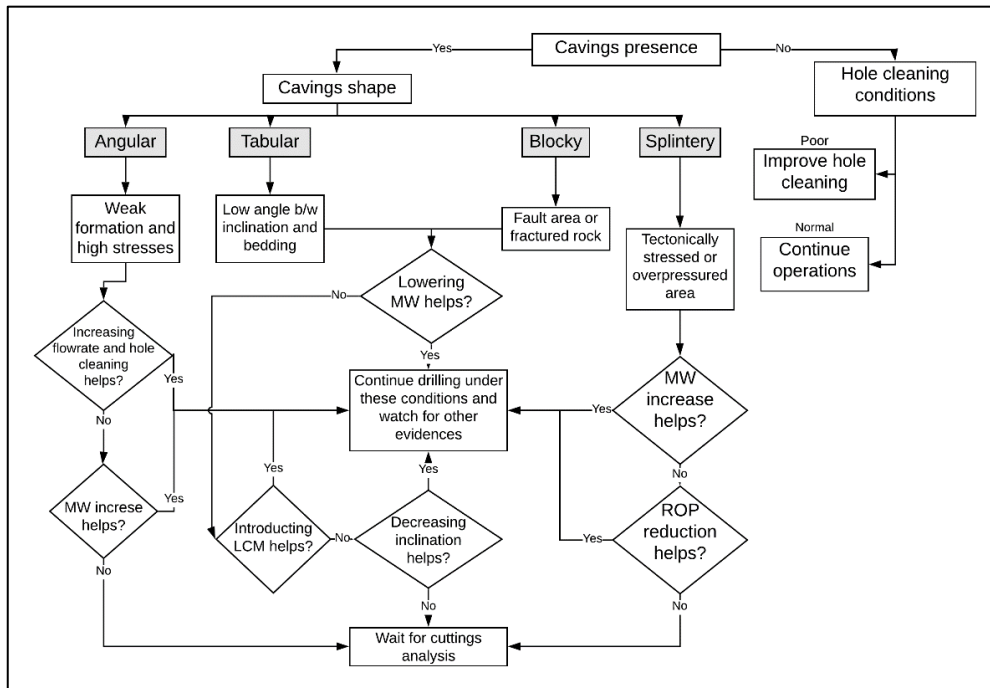


Figure 62: Road Map for Decision Support (based on Table 2)



As it is seen further, the cavings' shape automatically indicates the possible cause of the complication. Afterwards, there is a suggestion on changing the drilling parameters, e.g. changing the mud weight or ROP. A series of such decisions are formed until two outcomes are reached. The first one is quite straightforward and is achieved if one of the changes in drilling parameters actually helped to remedy the situation. When none of the taken actions resulted in successful operation, it would be suggested to consistently wait for the cuttings analysis and possibly perform reaming or washing procedures.

## 5.4 Cost Estimation for Proposed System

The technology cost was estimated by summing the costs of all the included categories of equipment: pump, sprinklers, tray, hoses and pipes, filter, camera, lens, cover, support stand, LED lights, and GPU. The prices were taken from online stores in the corresponding category of items. The costs presented in this section are a rough estimation and the calculation performed here are basic, and the value of the whole system can actually double. In case no other challenges are faced and no extra work is required (installation, mounting, training the CNN, supplying additional computers for the software, etc.), the cost can be close to the estimated one.

Regarding the hardware items, not all of the parts have fixed cost, as such parameters as dimensions, amount of equipment and their performance are uncertain. In addition, there is a tolerance in accordance with price change during time. Furthermore, the same item might be available at different prices, depending on delivery costs and the policy of the store or vendor. Basing on the extracted data, cost distribution for each of the items was taken. Mean values, as well as standard deviation, are were calculated in order to give an impression of the variability of items costs. They are listed in Table 17.

Table 17: Items for the Technology Cost Estimation

Item	Mean, \$	Standard deviation
Pump	333,18	285,76
Sprinkler	34,73	22,46
Tray	64,52	71,86
Hose and pipes	125,09	88,30
Filter	11,75	7,74
Camera	509,00	0,00
Lens	294,00	67,72
Cover	37,42	18,45
Support stand	43,27	22,05
LED	29,75	15,49
GPU	432,18	192,99

## Conceptual Design of the Proposed Technology

In addition, other costs should be included in the technology (Table 18). These are the base fluid costs, installation costs, and maintenance. The base fluid is chosen as diesel to give higher cost expectations. The price is taken as 1,12 \$ per litre. The amount of needed base mud is expected to be 250 litres. Maintenance should include pipe unclogging, filter change, pump inspection, as well as the camera setup and changing light conditions when needed.

Table 18: Additional Cost Categories

<b>Category</b>	<b>Cost, \$</b>
Base fluid (diesel)	280
Installation costs	100
Maintenance	200

Technology cost was determined with the help of Monte Carlo Simulation. For each of the items, the cost was determined, having in mind that the probability of its occurrence was chosen randomly. All the costs were summed up, giving the final cost distribution as an output. This process was conducted one thousand times, giving the distribution of technology costs. This distribution is illustrated in Figure 63.

As it is seen, the mean value is located in the vicinity of 2500 \$. Other parameters, like standard deviation, were calculated and listed in Table 19.

Table 19: Parameters for the Technology Cost Distribution

<b>Parameter</b>	<b>Value</b>
Mean	2495,7
Standard deviation	365,4
Min	1761,8
Max	3707,6
Skewness	0.634
Kurtosis	-0.017

It is seen that skewness is relatively high and positive which says that the distribution tail tends to the larger values. This could be explained by the fact that the prices are not distributed normally and tend to be allocated in the vicinity of a certain value. Furthermore, the higher the price gets, the lower number of items appears on the market. In addition, kurtosis is negative, implying that the data is a little widely distributed than the ideal normal distribution function.

Basing on the distributed values, the Cumulative Distribution Function (CDF) was built in order to determine P10, P50, and P90 costs. The function is illustrated in Figure 64.

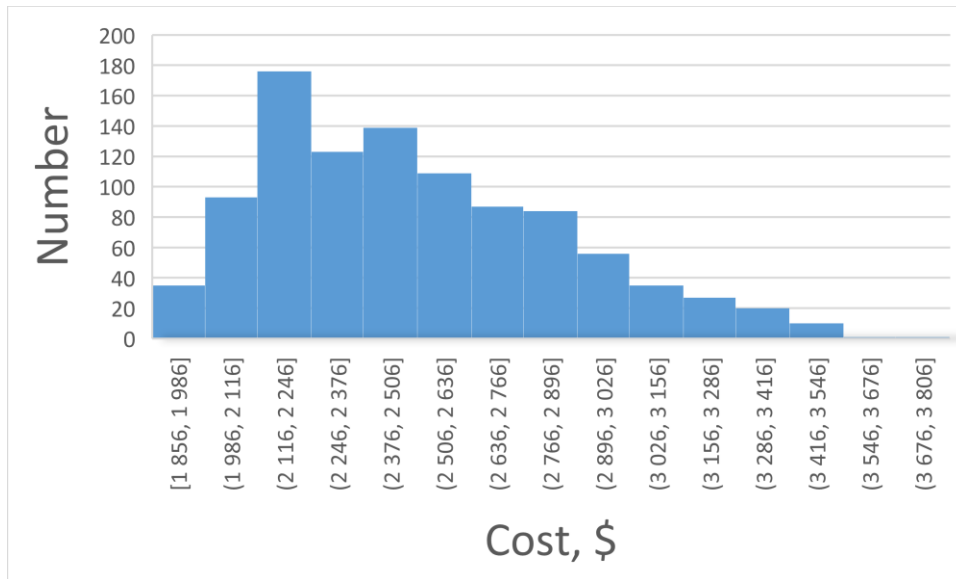


Figure 63: Total Cost Distribution of the Proposed Technology

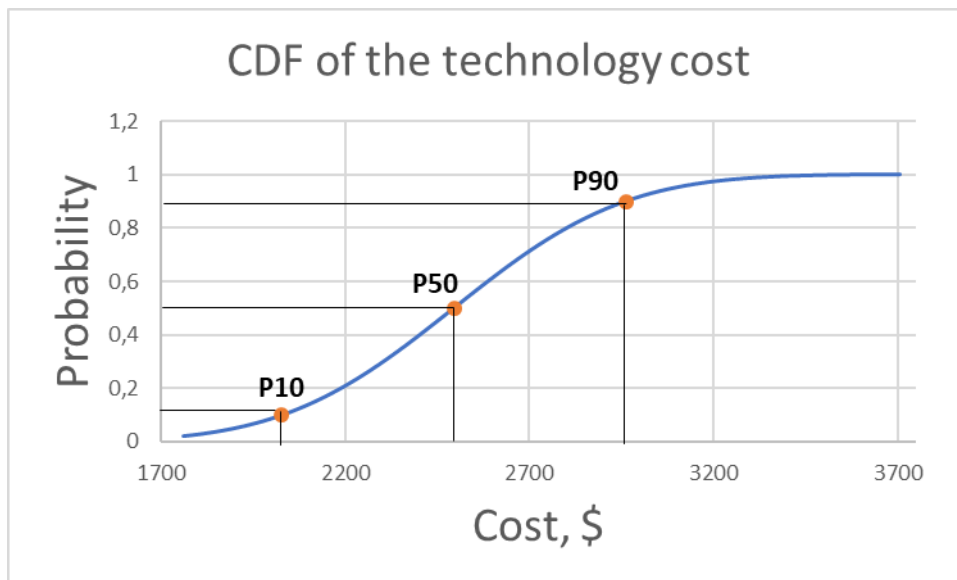


Figure 64: Cumulative Distribution Function (CDF) of the Technology Cost

From this function, it is possible to determine P10, P50, and P90 values, which are defined as 10<sup>th</sup>, 50<sup>th</sup> and 90<sup>th</sup> percentiles correspondingly. Percentile basically means, how much of the data is located below the chosen probability. For example, P50 value in the considered case shows the cost, below which the probability of its likelihood of appearance is below 50 percent. Consequently, P10 shows optimistic results, P90 stands for the pessimistic result, and P50 shows the median value, which is located exactly in the middle position of all the data. The values for P10, P50, and P90 costs are listed in Table 20.

Table 20: P10, P50, and P90 Values

Percentile	Value, \$
P10	2028,09
P50	2496,23
P90	2964,26

The proposed technology consists of quite a large number of items, which prices are widely distributed on market. These items (pipelines, rack, and cover for the camera, etc.) do not significantly affect the technology performance, which means that it is possible to save budget on them. In addition, this gives some extra savings to buy more powerful CPUs and GPUs. In addition, there is also a possibility to take better lenses, which are shake and shock-resistant. It is especially important if the shakers will be having large amplitudes. It might be the case, of the shaker is poorly dampen, and some of the vibrations are transferred through the skid and rack, affecting camera performance.

### 5.5 Limitations

There are a certain number of limitations in the proposed system, regarding mostly the hardware part.

A high number of shale shaker models and manufacturers introduce a certain challenge in the tray installation, as the space between the sieves and the shaker’s body may vary in wide ranges. It implies that it might be not possible to install the circulation system at all for some shakers' models. In another case, the tray volume may also vary.

The main complexity of the sprinkler head installation would be the shaking behaviour of the shaker. To provide the rigidity of the construction, it is important to not only hang the sprinklers on the shaker walls but also attach it with clamps, screw or weld them, if it is necessary. In addition, the ability of a sprinkler head should be actually tested, if the pressure and amount of fluid are enough to clean the cavings from mud and finer particles. It also should be checked, if the tray could be actually located beneath the shakers, as they all vary depending on their design features and dimensions. It is also unclear so far if the base fluid will be contaminated by finer particles, which were washed away. This might require the installation of filters at the pump intake and their change. Otherwise, the sprinklers are likely to be blocked and damaged with time.

There are also challenges in camera installation. In some of the shale shaker models, the screens could be covered with an enclosure. This creates a barrier between the camera and screens, which makes the cavings image capturing impossible. In addition, there is often a series of shaker in the solids control system. They are usually joined with a long gasket for capturing the cuttings, which occupies sufficient space. Here it might be hard to allocate the supporting stand with a camera and lightning facility.

Checks for illuminations should also be done, as it is not clear, how the camera sensor will perform with specks of light, low light conditions at night shift, and whether the

scene will change with alterations of ambient light. From that perspective, a light sensor should be installed to automatically adjust the intensity of the LED.

It also should be checked, if the chosen GPU will actually deliver the results with minimal delay, as it makes no sense if the determination of essential parameters will proceed with too large lag time. As it was already mentioned, the algorithm has to react fast, as time has to be spared.

As was mentioned, the circulation system might not be actually installed due to the original shale shaker design. In this case, the lithology could not be determined properly. Here it should be tested if CNN can actually determine the lithology of the unwashed cavings.



# Chapter 6 Conclusion and Recommendations

## 6.1 Conclusion

For ensuring the trouble-free drilling performance it is important to be aware of possible complications and borehole instability events. For this reason, cavings analysis serves as a powerful methodology in order to identify not only the signs of instability but also its root cause. Conventional implementation of this technique is time-consuming and does not allow to react proactively on changing drilling conditions.

In order to increase the effectiveness of the already existing workflow, a study on the automated cuttings measurement and analysis techniques was conducted. The utilized tools were compared and contrasted. It was decided to focus on computer vision techniques because of their robustness and the possibility of performing remote measurements.

Such tools in the majority of cases are combined with specially designed software, which conducts the image analysis and extracts features from objects. The software often belongs to a large family of algorithms called Convolutional Neural Networks. In this thesis, a review on them is conducted, discussing their working principle, as well as preparation and training procedure.

Basing on the observed analysis techniques, an automated cavings analysis system is proposed with respect to the following criteria:

- Simplicity
- Cost-effectiveness
- The ability of multiple parameters extraction

The heart of the installation is the camera, which performs all the data acquisition. A cover and illumination provided in order to protect the camera from harsh weather conditions and ensure the purity of data capturing. The main benefit of the camera is that it does not disturb the mud separation process. The only modification of shale shakers is the circulation system. This system might be removed if lithology determination is not necessary in the considered case.

Apart from that, the system does not involve expensive sensors and heavy machinery the system would require, however, maintenance costs for the circulation system. From the side, the one-time investment might save hours of NPT and also the money spent on third-party services, fishing equipment, and rig rent.

The final part of the system is the road map to support decision making, which basically gives the recommendations to the involved personnel, based on determined cavings morphology by the CNN ensemble. It was introduced to the associated algorithm because the involved employees are demanding for the validation of their actions. Usually, the actions to mitigate the complications are taken basing only on the experience, and the amount of real-time data is often not enough to take control of the

situation correctly. For that reason, a flowchart is suggested, in which actions are validated by causal reactions between return cavings and the nature of complications.

### 6.2 Recommendations and Future Work

It was already discussed that CNN has to be trained in advance, so it is required to collect a set of proper images to train the network and also label them. This part is the most labour-intensive and time-consuming. Training can be actually done at the rig site and with actual shale shakers. This would ensure that the images are similar during training and testing.

As long as the camera captures quite a lot of visual information, there is also a possibility to extend the network and include some extra features to analyze. As long as there is a freedom of choice in software installations and CNN architectures, the user has alternatives of tools and frameworks to choose from. This is what makes the proposed installation flexible and robust.

In addition, the road map for decision making should be updated and built on real data in order to make it closer to reality. Furthermore, an additional analysis could be conducted, establishing the relationship between cavings features and the least required change to drilling parameters. This would give the employees a range of safe adjustments to drilling parameters.



# Appendix A Cuttings description parameters

## A.1 Shape

The shape is described in Table 21.

Table 21: Cuttings Shape Description (International Logging, Inc. 2001)

Cuttings type	Description
Blocky	Used to describe claystone, marl, limestone in which fractures are developed at approximately right angles, so that small blocks are formed
Subblocky	Commonly used to describe PDC drilled cuttings that are not quite 100% blocky with clean breaks and imperfect right angles
Angular	Used to describe well-lithified formations that break chips with angular surfaces, generally as limestones and siliceous hard formations
Amorphous Irregular	or Cuttings with no distinct shape
Conchoidal	Commonly seen in dense rocks such as chert, argillite, flint, and coal. The term refers to concave and convex surfaces developed on fractures
Elongated	Used to describe rocks, which length is significantly greater than their width
Tabular	The cuttings samples, which were formed by breaking along the bedding plane
Flaky	The rock fractured into small flakes or chips. Common in some marls and occasionally in metamorphic rocks
Platy	Flaky, but used mostly with shales
Fissile	Rock is which is capable of being split or divided in the direction of the grain or along natural planes of cleavage; a characteristic of shales
Splintery	Used to describe shales in which the fissility is not strongly developed, but exists sufficiently to cause irregular surfaces and edges; mostly used to describe some carbonates coals and shales.

## A.2 Roundness and Sphericity

Cuttings grains are described according to their roundness and sphericity. This is very important, that only the grains are inspected in the discussed way, and not the cuttings or cavings themselves. However, the presented description method (or its analogue) might be used to distinguish cavings.

Roundness refers to the roughness of the surface. Sphericity refers to the grain shape in comparison with a sphere of the same volume as the inspected grain.

Basically, two most-frequently scales are present nowadays, presented by (Krumbein and Sloss 1951) and (Powers 1953), which are illustrated in Figure 65 and Figure 66.

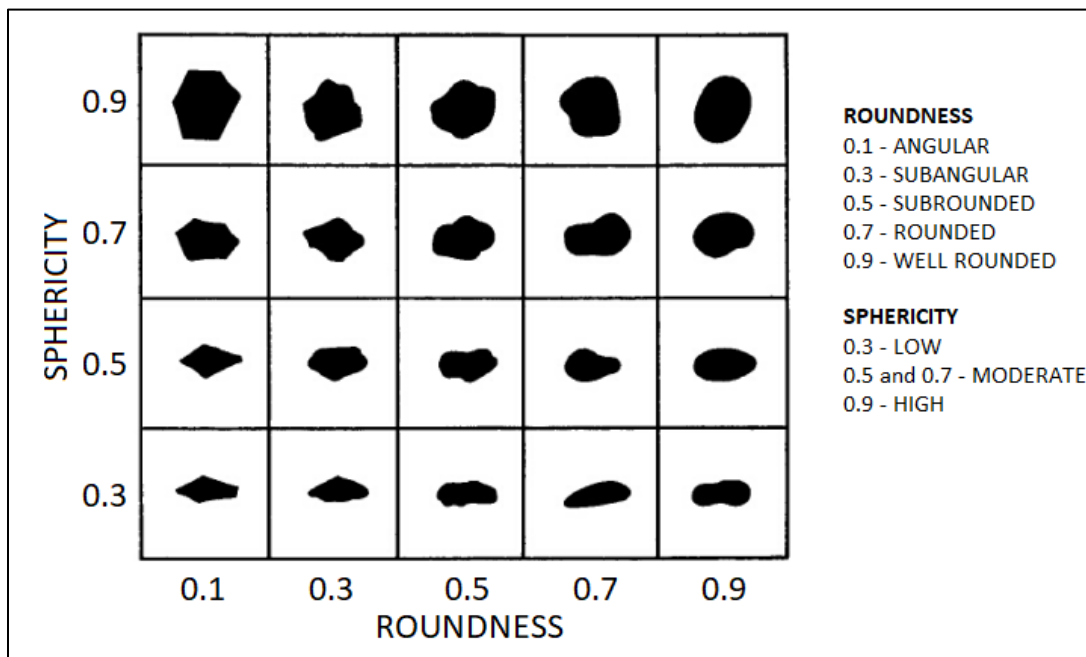


Figure 65: Chart for Roundness and Sphericity Estimation (Krumbein and Sloss 1951)

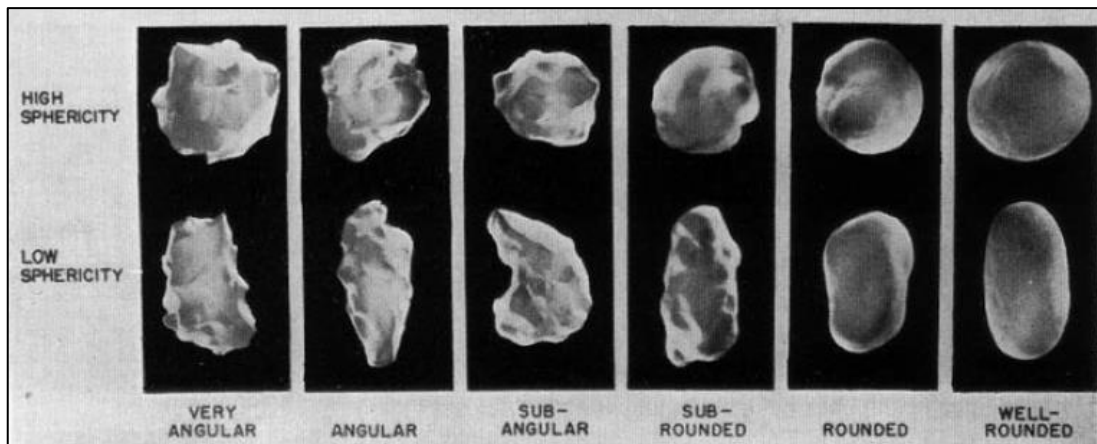


Figure 66: Roundness and Sphericity (Powers 1953)

In these comparative charts Sphericity and roundness are expressed with the following formulas:

$$R = \frac{\sum_{i=1}^N r_i / N}{r_{ins}} \quad (30)$$

$$S = \frac{d_2}{d_1} \quad (31)$$

where  $R$  – roundness;

$S$  – sphericity;

$r_i$  – radii of the inscribed circumferences;

$N$  – number of circumferences;

$d_1$  and  $d_2$  – length and width of the sample.

All the dimensions are illustrated in Figure 67.

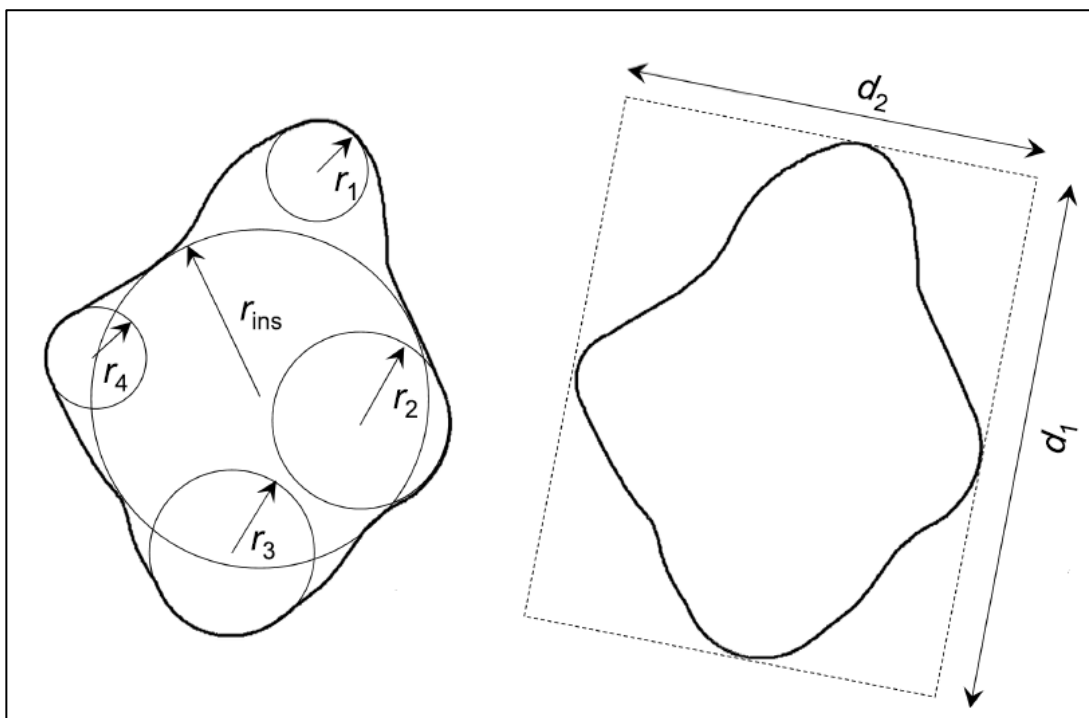


Figure 67: Parameters Used in Roundness (Left) and Sphericity (Right) Calculation (Hryciw, Zheng and Shetler 2016)

### A.3 Colour

The colour of the single rock piece takes effect of the constituent grains and cement. The colours might appear in various patterns, such as mottled, banded, spotted, variegated, etc. It is recommended to observe wet samples with ten-power magnification if it is done manually. In addition, the light source is of high importance, which shall be consistent during all the time of observation. It is also needed to know that the colour might be altered by oxidation, which might take place when storing samples in a damp place, as

## Cuttings description parameters

well as insufficient drying after washing or overheating. In addition, bit or pipe fragments can rust and influence the rock colour. Mud additives cause staining as well (Swanson 1981). A Geological Society of America (GSA) rock chart exists as a reference point for the colour description. All the colours used are coded and may describe the most frequently appearing rocks. An example of this palette is shown in Figure 68.

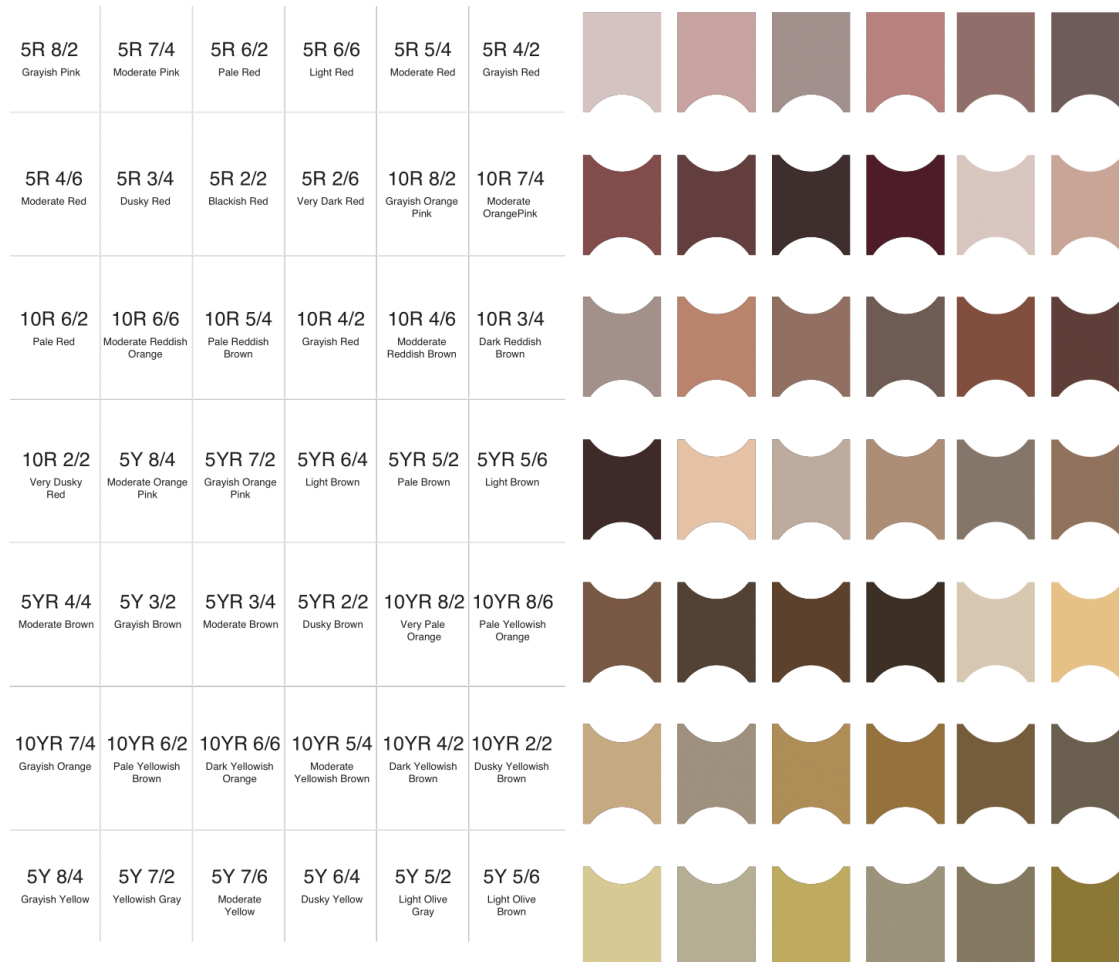


Figure 68: An Example of the Palette (GSA 2009)

# Bibliography

- Aldred, W., D. Plumb, I. Bradford, L. Cousins, J. Fuller, S. Goraya, and D. Toker. 1999. "Oilfield Review - Managing Drilling Risk." *Schlumberger*.
- Bowes, Colin, and Ray Procter. 1997. *Drillers Stuck pipe Handbook*. Ballater, Scotland: Procter & Collins Ltd.
- Bradford, I. D. R., W. A. Aldred, J. M. Cook, E. F. M. Elewaut, J. A. Fuller, T. G. Kristiansen, and T. R. Walsgrove. 2000. "When Rock Mechanics Met Drilling: Effective Implementation of Real-Time Wellbore Stability Control." *IADC/SPE Drilling Conference*. New Orleans: SPE.
- Brading, Michael, Kenneth Salsman, Manjunath Somayaji, Brian Dipert, Tim Droz, Daniël Van Nieuwenhove, and Pedro Gelabert. 2013. "3-D Sensors Bring Depth Discernment to Embedded Vision Designs." *Embedded Vision Alliance*. July 12. Accessed April 15, 2020. <https://www.edge-ai-vision.com/2013/07/3-d-sensors-bring-depth-discernment-to-embedded-vision-designs/>.
- Carr, Russell, Lance Yarbrough, Nicholas Lentz, Kathleen Neset, Brian Lucero, and Tim Kirst. 2014. "On-Site XRF Analysis of Drill Cuttings in the Williston Basin." *SPE/AAPG/SEG Unconventional Resources Technology Conference*. Denver, Colorado: Unconventional Resources Technology Conference.
- Cyganek, Bogusław, and Paul J. Siebert. 2009. *An Introduction to 3D Computer Vision Techniques and Algorithms*. West Sussex, United Kingdom: John Wiley & Sons, Ltd.
- Du, Xunsheng, Yuchen Jin, Xuqing Wu, Yu Liu, Xianping Wu, Omar Awan, Joey Roth, et al. 2020. "Classifying Cutting Volume at Shale Shakers in Real-Time Via Video Streaming Using Deep-Learning Techniques." *SPE Drilling and Completion* (Society of Petroleum Engineers). doi:<https://doi.org/10.2118/194084-PA>.
- EAGE. 2019. *EAGE Earth-Hack*. February. Accessed April 28, 2020. [https://students.eage.org/sitecore/content/events/home/2019/big-data-and-machine-learning/eage-earth-hack?sc\\_lang=en](https://students.eage.org/sitecore/content/events/home/2019/big-data-and-machine-learning/eage-earth-hack?sc_lang=en).
- Edmund Optics Inc. n.d. *6mm UC Series Fixed Focal Length Lens*. Accessed May 28, 2020. <https://www.edmundoptics.com/p/6mm-uc-series-fixed-focal-length-lens/2967/>.
- European Commission. 2000. "DIRECTIVE 1999/92/EC OF THE EUROPEAN PARLIAMENT AND OF THE COUNCIL." *Official Journal of the European Communities* 57-64.
- FLIR® Systems. 2018. *BlackFly GigE | FLIR Systems*. Accessed April 20, 2020. <https://www.flir.com/products/blackfly-gige/>.
- . 2018. *Blackfly S GigE | FLIR Systems*. Accessed May 27, 2020. <https://www.flir.com/products/blackfly-s-gige/?model=BFS-PGE-23S3C-C>.

## Bibliography

- Fofi, David, Tadeusz Sliwa, and Yvon Voisin. 2004. "A comparative survey on invisible structured light." Accessed April 15, 2020. <http://www.le2i.cnrs.fr/IMG/publications/fofi04a.pdf>.
- Forta Corporation. 1997. "FORTA® Super-Sweep® Video." *YouTube*. Accessed May 27, 2020. <https://www.youtube.com/watch?v=68cvNYizCf0>.
- Fujifilm Corporation. n.d. *HF-XA-5M series*. Accessed May 28, 2020. <http://mvlens.fujifilm.com/en/product/hfxa5m.html>.
- Gallant, C., J. Zhang, C. A. Wolfe, J. Freeman, T. M. Al-Bazali, and M. Reese. 2007. "Wellbore Stability Considerations for Drilling High-Angle Wells Through Finely Laminated Shale: A Case Study from Terra Nova." *SPE Annual Technical Conference and Exhibition*. Anaheim, California: Society of Petroleum Engineers.
- Geng, J. 2011. "Structured-light 3D surface imaging: a tutorial." *Advances in Optics and Photonics* 128-160.
- GN Solids Control. 2020. *Shale shaker, linear motion shaker - GN Solids Control*. Accessed May 27, 2020. <https://www.gnsolidscontrol.com/shale-shaker>.
- GSA. 2009. *Geological Rock-Color Chart*. Munsell Color.
- Han, Runqi, Pradeepkumar Ashok, Mitchell Pryor, and Eric van Oort. 2018. "Real-Time 3D Computer Vision Shape Analysis of Cuttings and Cavings." *SPE Annual Technical Conference and Exhibition*. Dallas, Texas: Society of Petroleum Engineers.
- Han, Runqi, Pradeepkumar Ashok, Mitchell Pryor, Eric van Oort, Paul Scott, and Isaac Reese and Kyle Hampton. 2017. "Real-Time Borehole Condition Monitoring using Novel 3D Cuttings Sensing Technology." *SPE/IADC Drilling Conference and Exhibition*. The Hague, Netherlands: Society of Petroleum Engineers.
- Hryciw, Roman D., Junxing Zheng, and Kristen Shetler. 2016. "Particle Roundness and Sphericity from Images of Assemblies by Chart Estimates and Computer Methods." *Journal of Geotechnical and Geoenvironmental Engineering* 142 (9). doi:10.1061/(ASCE)GT.1943-5606.0001485.
- International Electrotechnical Commission. 2013. *IEC 60529 Degrees of protection provided by enclosures (IP Code)*. Geneva.
- International Logging, Inc. 2001. *Basic Mud Logging*. Singapore.
- Karimi, Moji. 2013. "Drill-Cuttings Analysis for Real-Time Problem Diagnosis and Drilling Performance Optimization." *SPE Asia Pacific Oil & Gas Conference and Exhibition*. Jakarta, Indonesia: Society of Petroleum Engineers.
- Kathrada, Muhammad, and Benjamin Jacob Adillah. 2019. "Visual Recognition of Drill Cuttings Lithologies Using Convolutional Neural Networks to Aid Reservoir Characterisation." *SPE Reservoir Characterisation and Simulation Conference and Exhibition*. Abu Dhabi: Society of Petroleum Engineers.
- Kristiansen, Tron Golder. 2004. "Drilling Wellbore Stability in the Compacting and Subsiding Valhall Field." *IADC/SPE Drilling Conference*. Dallas, Texas: SPE.

- Krizhevsky, Alex, Ilya Sutskever, and Geoffrey E. Hilton. 2012. "ImageNet Classification with Deep Convolutional Neural Networks." *Advances in Neural Information Processing Systems* 1097-1105.
- Krumbein, W. C., and L. L. Sloss. 1951. *Stratigraphy and Sedimentation*. San Francisco: Freeman & Co.
- Kumar, D., S. Ansari, S. Wang, J. YiMing, S. Ahmed, M. Povstyanova, and B. Tichelaar. 2012. "Real-time Wellbore Stability Analysis: An Observation from Cavings at Shale Shakers." *AAPG International Convention and Exhibition*. Singapore.
- Legutko, Stanislaw, Pero Raos, and Remigiusz Labudzki. 2014. "The essence and applications of machine vision." *Tehnicki Vjesnik* 903-909.
- Li, Larry. 2014. "Time-of-Flight Camera - An Introduction." *Texas Instruments*. May. Accessed April 14, 2020. <http://www.ti.com/lit/wp/sloa190b/sloa190b.pdf>.
- LMI Technologies. 2016. *Gocator 2380 | LMI3D*. Accessed April 20, 2020. <https://lmi3d.com/gocator-2380>.
- Malvern Instruments. n.d. *Mastersizer 2000*. Accessed May 5, 2020. <https://www.malvernpanalytical.com/en/support/product-support/mastersizer-range/mastersizer-2000/#manuals>.
- Marana, A.N., I.R. Guilherme, J.P. Papa, M.V.D. Ferreira, K. Miura, and F.A.C. Torres. 2010. "An Intelligent System to Detect Drilling Problems Through Drilled Cuttings Return Analysis." *IADC/SPE Drilling Conference and Exhibition*. New Orleans, Louisiana: Society of Petroleum Engineers.
- M-I L.L.C. 2019. "Solid Control, Cuttings Management and Fluids Processing." *Schlumberger*. Accessed May 28, 2020. <https://www.slb.com/-/media/files/mi/catalog/solids-control-cuttings-management-fluids-processing-catalog.ashx>.
- Naegel, M., E. Pradie, T. Delahaye, C. Mabile, and G. Roussiaux. 1998. "Cuttings Flow Meters Monitor Hole Cleaning in Extended Reach Wells." *European Petroleum Conference*. The Hague, Netherland: Society of Petroleum Engineers. 401-408. doi:<https://doi.org/10.2118/50677-MS>.
- Nasrullah, K., and A. K. Naem. 2011. "Comparative study of energy saving light sources." *Renewable and Sustainable Energy Reviews* 15: 296-309. doi:DOI: 10.1016/j.rser.2010.07.072.
- National Instruments. 2012. *Parts o a Stereo Vision System*. June. Accessed April 14, 2020. <https://zone.ni.com/reference/en-XX/help/372916M-01/nivisionconcepts dita/guid-cb42607e-f256-40f5-ab6e-28ec3a33bcda/>.
- Olympus. 2019. *Field Portable XRD and XRF for Shale Gas Drilling Efficiency*. Accessed May 12, 2020. <https://www.olympus-ims.com/en/applications/field-portable-xrf-shale-gas/>.
- Omland, T.H., A. Saasen, K. Taugbøl, B. Dahl, T. Jørgensen, F. Reinholt, N. Scholz, et al. 2007. "Improved Drilling-Process Control Through Continuous Particle and

## Bibliography

- Cuttings Monitoring." *SPE Digital Energy Conference*. Houston, Texas: Society of Petroleum Engineers.
- Pandalaneni, Karthik. 2016. "Focused beam reflectance measurement as a tool for in situ monitoring of the lactose crystallization process." *Journal of Dairy Science* 99 (7): 5244-5253. doi:<http://dx.doi.org/10.3168/jds.2015-10643>.
- Pankewitz, Axel, and Helmut Geers. 2020. *In-Line Crystal Size Distribution analysis in industrial crystallization processes by Ultrasonic Extinction*. Sampatec GmbH.
- Pašić, B., N. Gaurina-Međimurec, and D. Matanović. 2007. "Wellbore instability: Causes and Consequences." *Rudarsko-geološko-naftni zbornik* 19: 87-98.
- Powers, M. C. 1953. "A New Roundness Scale for Sedimentary Basins." *Journal of Sedimentary Particles* 23 (2): 117-119.
- Ran, Xiangjin, Linfu Xue, Yanyan Zhang, Zeyu Liu, Xuejia Sang, and Jinxin He. 2019. "Rock Classification from Field Image Patches Analyzed Using a Deep Convolutional Neural Network." *Mathematics*.
- Ruessink, B.H., and D.G. Harville. 1992. "Quantitative Analysis of Bulk Mineralogy: The Applicability and Performance of XRD and FTIR." *SPE Inti. Symposium on Formation Damage Control*. Lafayette, Louisiana: Society of Petroleum Engineers. 533-546.
- Saasen, A, T.H. Omland, S. Ekrene, J. Brévière, E. Villard, N. Kaageson-Loe, A. Tehrani, et al. 2009. "Automatic Measurement of Drilling Fluid and Drill-Cuttings Properties." *SPE Drilling & Completion* (Society of Petroleum Engineers) 24 (04): 611-625. doi:<https://doi.org/10.2118/112687-PA>.
- SAMCON GmbH. 2020. *Ex-d camera enclosures*. Accessed June 18, 2020. <https://www.samcon.eu/en/products/ex-d-camera-enclosures/>.
- Schlumberger. 2015. "CLEAR Hole cleaning and wellbore risk reduction service." *Schlumberger*. Accessed April 11, 2020. <https://www.slb.com/-/media/files/geoservices/product-sheet/clear-ps.ashx>.
- . 2015. "CLEAR Hole cleaning and wellbore risk reduction service brochure." *Schlumberger*. Accessed April 11, 2020. <https://www.slb.com/-/media/files/drilling/brochure/clear-brochure-br.ashx>.
- . 2016. "Integrated Drilling Approach Achieves Single-Run Lateral to Save 2.5 Days and USD 148,000 off AFE." *Schlumberger*. Accessed April 11, 2020. <https://www.slb.com/-/media/files/geoservices/case-study/clear-middle-east-cs.ashx>.
- . 2013. *MONGOOSE PRO Shale Shaker* | *Schlumberger*. Accessed May 27, 2020. <https://www.slb.com/drilling/drilling-fluids-and-well-cementing/solids-control/shale-shakers/mongoose-pro-shale-shaker>.
- . 2015. "Operator Saves 16 Rig Hours and USD 194,000 Using CLEAR Service." *Schlumberger*. Accessed April 11, 2020. <https://www.slb.com/-/media/files/geoservices/case-study/clear-indonesia-cs.ashx>.



- . 2019. "X-Ray Diffraction While Drilling." *Schlumberger*. Accessed May 5, 2020. <https://www.slb.com/-/media/files/drilling/product-sheet/ecoflex-x-ray-diffraction-ps.ashx>.
- Schlumberger. 2019. "X-Ray Fluorescence While Drilling." *Schlumberger*. Accessed May 4, 2020. <https://www.slb.com/-/media/files/drilling/product-sheet/ecoflex-lithoflex-x-ray-fluorescence-ps.ashx>.
- Skea, Christopher, Alireza Rezagholilou, Pouria Behnoudfar, Raouf Gholami, and Mohammad Sarmadivleh. 2018. "An approach for wellbore failure analysis using rock cavings and image processing." *Journal of Rock Mechanics and Geotechnical Engineering*. doi:<https://doi.org/10.1016/j.jrmge.2018.04.011>.
- Swanson, R. G. 1981. *Sample Examination Manual*. Tulsa, Oklahoma: The American Association of Petroleum Geologists.
- Sympatec GmbH. 2017. *NIMBUS | Particle size and concentration analysis in laboratory*. Accessed May 12, 2020. <https://www.sympatec.com/en/particle-measurement/sensors/ultrasonic-extinction/nimbus/>.
- Tamron Europe GmbH. n.d. *Machine Vision / FA / ITS Lenses*. Accessed May 5, 2020. <https://www.tamron.eu/industrial-optics/products/mega-pixel-machine-vision-fa-its-lenses/#M112FM08>.
- TR Solids Control. 2016. "Shale Shaker for Horizontal Directional Drilling." *YouTube*. December 20. Accessed May 27, 2020. [https://www.youtube.com/watch?v=aS5r\\_PM9DQA](https://www.youtube.com/watch?v=aS5r_PM9DQA).
- van Oort, Eric, and Besmir Buranaj Hoxha. 2016. "Automated Drilling Fluid Analysis using Advanced Particle Size Analyzers." *IADC/SPE Drilling Conference and Exhibition*. Fort Worth, Texas: IADC/SPE.
- Zausa, F., L. Civolani, M. Brignoli, and F.J. Santarelli. 1997. "Real-Time Wellbore Stability Analysis at the Rig-Site." *SPE/IADC Drilling Conference*. Amsterdam: Society of Petroleum Engineers. 837-846.
- Zoback, M.D., C.A. Barton, M. Brudy, D.A. Castillo, T. Finkbeiner, B.R. Grollmund, D.B. Moos, P. Peska, C.D. Ward, and D.J. Wiprut. 2003. "Determination of stress orientation and magnitude in deep wells." *International Journal of Rock Mechanics and Mining Sciences* 1049-1076.
- Zoback, Mark. 2007. *Reservoir Geomechanics*. Cambridge: Cambridge University Press.

Bibliography

# Acronyms

<i>ADC</i>	Analog-to-Digital Converter
<i>ANN</i>	Artificial Neural Network
<i>BC</i>	Bayesian Classifier
<i>CDF</i>	Cumulative Distribution Function
<i>CNN</i>	Convolutional Neural Network
<i>CFL</i>	Compact Fluorescent Lamp
<i>CFM</i>	Cuttings Flow Meter
<i>CNN</i>	Convolutional Neural Network
<i>CPU</i>	Central Processing Unit
<i>ERD</i>	Extended Reach Drilling
<i>GPU</i>	Graphics Processing Unit
<i>IDE</i>	Integrated Development Environment
<i>IP</i>	International Protection
<i>LCM</i>	Lost Circulation Material
<i>LED</i>	Light-Emitting Diode
<i>LPA</i>	Liquid particle Analyzer
<i>LSB</i>	Least Significant Bit
<i>MLP</i>	Multilayer Perception
<i>MSB</i>	Most Significant Bit
<i>MSE</i>	Mean Squared Error
<i>OPF</i>	Optimum Path Forest
<i>PDC</i>	Polycrystalline Diamond Composite
<i>PSD</i>	Particle Size Distribution
<i>RGB</i>	Red Green Blue
<i>RAM</i>	Random-Access Memory
<i>ReLU</i>	Rectified Linear Unit
<i>ROI</i>	Region of Interest
<i>ROP</i>	Rate of Penetration
<i>SDK</i>	Software Development Kit
<i>SSL</i>	Solid-state Lightning

## Acronyms

<i>SVM</i>	Support Vector Machines
<i>VGG</i>	Visual Geometry Group
<i>XRD</i>	X-ray Diffraction
<i>XRF</i>	X-ray Fluorescence

# Symbols

$\hat{y}$	computed input	-
$y$	target value	-
$x$	neuron input	-
$w$	weight	-
$b$	bias	-
$i$	index	-
$N$	number of elements	-
$C$	cost function	-
$\delta$	error	-
$\sigma$	activation function	-
$W$	array width	-
$H$	array height	-
$D$	array depth	-
$F$	filter size	-
$P$	zero padding	-
$S$	stride	-
$K$	number of filters	-
$u$	distance to the object	mm
$v$	distance to the image	mm
$f$	focal length	mm
$S_s$	sensor size	mm
$H_o$	object's largest dimension	mm
$k_{cr}$	crop factor	-
$d_{max}$	maximal sensor diagonal	mm
$d_{used}$	used sensor diagonal	mm



# List of Figures

Figure 1: NPT Breakdown by Root Cause .....	2
Figure 2: Reported Consumption of Fluids and Additives In 2019 By OMV .....	3
Figure 3: TelevIEWER Image Logs of a Well With Wellbore Breakouts (Dark Paths in South-East and North-West Directions) (Zoback, Barton, et al. 2003) .....	9
Figure 4: (a) Breakout, Showing Growth Deeper Inside the Formation. (b) Washout Grows All Around the Wellbore, Increasing Its Instability (modified after M. Zoback 2007).....	9
Figure 5: Example of an Angular Caving (Bradford, et al. 2000) .....	11
Figure 6: Example of a Tabular Caving. The Flat Surface of Bedding Plane Is Visible (Kristiansen 2004) .....	11
Figure 7: Large Tabular Caving Formed as a Result of Failure Along the Bedding Plane (Gallant, et al. 2007) .....	12
Figure 8: Example of a Blocky Caving from a Naturally Fractured Reservoir (Aldred, et al. 1999) .....	12
Figure 9: Example of a Splintery Caving (Kumar, et al. 2012) .....	13
Figure 10: Mud Overflow After Addition of the Fibrous Material to Suspend Cuttings and Clean the Well (Forta Corporation 1997).....	14
Figure 11: Excessive Clay Appearance on the Screens (TR Solids Control 2016).....	14
Figure 12: Conventional Cavings Analysis Workflow .....	18
Figure 13: Cuttings Taken From the Possum Belly (Left) and at the End of the Shaker Screens (Right) (Karimi 2013).....	19
Figure 14: Taking the Cuttings from the Sample Catcher (International Logging, Inc. 2001).....	19
Figure 15: Cavings Collected in a Coarse Sieve (International Logging, Inc. 2001).....	20
Figure 16: Sieve Analysis Procedure (Left) and Cumulative Curve of PSD (Right) (Karimi 2013) .....	22
Figure 17: Laser Diffraction Device (courtesy of Malvern Instruments) .....	22
Figure 18: LPA and Examples of Images; 1 – Sample Mixing Tank, 2 – Camera, 3 – Flow Cell, 4 – Light Source (Saasen, et al. 2009).....	23
Figure 19: FBRM Measurement Workflow (Pandalaneni 2016) .....	24
Figure 20: Measurement Principle of USE (Pankewitz and Geers 2020) .....	25
Figure 21: The Elements, Which Might Be Quantified From the X-Ray Fluorescence Analysis (Schumberger 2019).....	26
Figure 22: Schematics of the Cuttings Flow Meter (1 – Gutter, 2 – Control Mechanisms in the Protected Enclosure) (modified after Naegel, et al. 1998).....	31
Figure 23: Typical 2D Vision Flowchart (Legutko, Raos and Labudzki 2014) .....	32
Figure 24: Simplest (Left) and Typical (Right) Stereo Vision Systems (National Instruments 2012) .....	33
Figure 25: Working Principle of Stereo Vision (modified after Cyganek and Siebert 2009).....	34
Figure 26: Principle of the Sequential Projection Imaging (Left) and Projected Patterns (Right). LSB and MSB Stand for Least Significant Bit and Most Significant Bit Correspondingly (Geng 2011).....	35
Figure 27: An Example of Single-Shot Techniques: Colour-Indexed Stripes (Left) and Colour-Coded Grids (Right) (Geng 2011).....	35
Figure 28: Principles of Time-of-Flight Camera Operation (Li 2014).....	36
Figure 29: Input Image (Left) and a Depth Map (Right) (Li 2014) .....	36
Figure 30: CLEAR Hole Cleaning and Wellbore Risk Reduction Service (Schlumberger 2015)..	39
Figure 31: Schematic Diagram for Drilling Cuttings Analysis (Saasen, et al. 2009).....	40
Figure 32: Non-Intrusive Cuttings Analysis System Installation (Marana, et al. 2010) .....	41

## List of Figures

Figure 33: Images Captured by the Camera Placed Above the Shale Shakers: (a) None Concentration, (b) Low Concentration and (c) High Concentration of Cuttings (Marana, et al. 2010) .....	41
Figure 34: Real-Time Cuttings Volume Monitoring System. VGG Stands for Visual Geometry Group, a Machine Learning Technique (Du, et al. 2020).....	42
Figure 35: ROI Selected Manually (Left) or Automatically (Right) (Du, et al. 2020).....	42
Figure 36: Integrated Cuttings Monitoring Design Setup (Han, Ashok, et al. 2017) .....	43
Figure 37: Software Architecture for Measuring Cuttings PSD and Building 3D Profile (Han, Ashok, et al. 2017).....	44
Figure 38: Image Examples for Each Lithology (Kathrada and Adillah 2019) .....	47
Figure 39: General Flowchart for the Rock Types Identification (Ran, et al. 2019) .....	48
Figure 40: Principle Design of ANN.....	53
Figure 41: The General Neuron Structure.....	54
Figure 42: Principle CNN Architecture.....	58
Figure 43: Schematics of the Input Layer .....	58
Figure 44: Schematics of the Conv layer .....	59
Figure 45: Working Principle of the Filter .....	60
Figure 46: Demonstration of Stride Parameter. Blue Frame Represents a Filter, Which Slides Along the Pixels .....	60
Figure 47: Demonstration of Zero Padding Application .....	61
Figure 48: Comparison of ReLU, TanH, and Sigmoid Functions .....	62
Figure 49: Example of Pool Layer Performance.....	63
Figure 50: Road Map of the Proposed System .....	66
Figure 51: Exterior Design of the Hardware Part of the Proposed System .....	67
Figure 52: Proposed Modification of the Shale Shaker Design.....	68
Figure 53: Sideview of the Modified Shale Shaker .....	68
Figure 54: Examples of the Shale Shakers. MONGOOSE PRO (Left) and GN Solids Control GNZS703 (Right) (Schlumberger 2013) (GN Solids Control 2020) .....	70
Figure 55: An Example of Explosion-Proof Enclosure (SAMCON GmbH 2020) .....	71
Figure 56: FLIR® Blackfly® S GigE Camera (FLIR® Systems 2018).....	72
Figure 57: Direction of Beams in a Thin Lens.....	74
Figure 58: Schematics of Camera Working Principle to Calculate the Focal Length.....	74
Figure 59: Camera Installation Setup .....	77
Figure 60: Example of IP 65 Protection. The Strip Is Coated with Polyurethane .....	78
Figure 61: Workflow of the Parameters Detection Algorithm .....	80
Figure 62: Road Map for Decision Support (based on Table 2) .....	82
Figure 63: Total Cost Distribution of the Proposed Technology .....	85
Figure 64: Cumulative Distribution Function (CDF) of the Technology Cost.....	85
Figure 65: Chart for Roundness and Sphericity Estimation (Krumbein and Sloss 1951) .....	92
Figure 66: Roundness and Sphericity (Powers 1953) .....	92
Figure 67: Parameters Used in Roundness (Left) and Sphericity (Right) Calculation (Hryciw, Zheng and Shetler 2016) .....	93
Figure 68: An Example of the Palette (GSA 2009).....	94



# List of Tables

Table 1: Total NPT For the Considered Cases.....	2
Table 2: Cavings Description, Causes, Consequences and Their Treatment (Kristiansen 2004) (Bowes and Procter 1997) (Gallant, et al. 2007) (Kumar, et al. 2012) .....	15
Table 3: Advantages and Disadvantages of Conventional Cavings Analysis.....	27
Table 4: Comparison of Manual Measurement Tools (after Karimi 2013) .....	29
Table 5: Comparison of Light Sources (Nasrullah and Naeem 2011) .....	32
Table 6: Comparison of Automated Measurement Tools (Based on Brading, et al. 2013).....	37
Table 7: Experimental Results for Different Classifiers (Marana, et al. 2010).....	41
Table 8: Gocator 2380 Laser Scanner Specifications (LMI Technologies 2016).....	45
Table 9: Blackfly GigE Camera Specifications (FLIR® Systems 2018) .....	46
Table 10: Results for the Tested Methods (Kathrada and Adillah 2019) .....	47
Table 11: Datasets for Image Classification of Field Rocks (Ran, et al. 2019) .....	48
Table 12: Used Hardware Specifications (modified after Ran, et al. 2019) .....	49
Table 13: Performance of the Tested Models (modified after Ran, et al. 2019).....	49
Table 14: Comparison of Existing Installations for Cuttings Analysis. Green colour shows the best category, red – the worst, and yellow – neutral.....	50
Table 15: Camera Specifications.....	73
Table 16: List of the Appropriate Lenses for the Suggested Camera (Tamron Europe GmbH) (Fujifilm Corporation) (Edmund Optics Inc.).....	76
Table 17: Items for the Technology Cost Estimation.....	83
Table 18: Additional Cost Categories.....	84
Table 19: Parameters for the Technology Cost Distribution .....	84
Table 20: P10, P50, and P90 Values.....	86
Table 21: Cuttings Shape Description (International Logging, Inc. 2001) .....	91